TÉCNICO LISBOA

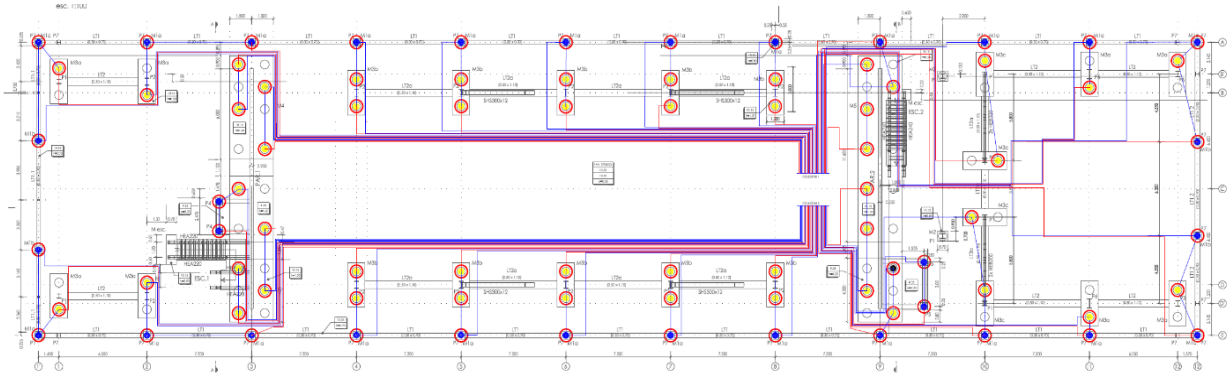

Energy Efficiency Evaluation in Thermo-Active Structures

João Miguel Ventura Sequeira

Dissertação para obtenção do grau de mestre em Engenharia Civil

Mestrado Integrado em Engenharia Civil

Orientadores

Professora Doutora Ana Maria Carvalho Pinheiro Vieira

Professora Doutora Maria Rafaela Pinheiro Cardoso

Júri

Presidente: Professor Doutor Albano Luís rebelo da Silva das Neves e Sousa (DECivil)

Orientador: Professora Doutora Ana Maria Carvalho Pinheiro Vieira (LNEC)

Vogal: Professora Doutora Teresa Maria Bodas de Araújo Freitas (DECivil)

Novembro de 2017

Dissertação elaborada no âmbito Laboratório Nacional de Engenharia Civil para obtenção do grau de mestre em engenharia civil pelo Instituto Superior Técnico no âmbito do protocolo de cooperação entre IST e LNEC

Acknowledgments

I would first like to thank my advisor professor Ana Vieria from LNEC and also professor Rafaela Cardoso from IST for providing unconditional help and motivation in order to try and achieve the high standards that they represent.

I would also like to show my appreciation for Laboratório Nacional de Engenharia Civil for all the resources that were made available for me, including a place for me to develop my work and also access to the geotechnical laboratory.

I also want to thank the investigation program from FCT (reference PTCDT/ECM-GEO/0728/2014) for allowing me to work on this exciting and promising area.

Furthermore, I want to express my gratitude to the kindhearted people of Universidade de Aveiro, including professor José Lapa and professor António Figueiredo. Without them, I would have been working in the dark.

To my friends and family, because I honestly couldn't have done it without them.

To my mother, an apology for the distresses this work caused between us and a thank you for never giving up on me.

Finally, to you Catarina, for lifting me from the dirt and carry me on your shoulders so I could see the light. You are everything.

Abstract

A numerical study was performed for evaluating the geothermal potential of foundation piles used as heat exchangers with the ground, for seasonal heat storage. It is based in a case-study of a building in Aveiro Campus University, equipped with a shallow geothermal heat pump system (GSHP) designed to support most part of the energy demands for the building's acclimatization.

The modeling of a single pile (60 cm diameter and 10 m length) was performed using FLAC, an explicit Lagrangian finite difference software. The influence of the soil thermal properties and location of the water table level were investigated regarding the efficiency of the system. The influence of the building's slab on the thermal performance of the pile was investigated as well. The soil conductivity was obtained by means of empirical relations and through laboratory characterization tests. Different thermal loading conditions on the energy pile and foundation soil were examined. They correspond, respectively, to thermal loads from the building service operation and from estimates based on local climate. In turn, climate data records concerning temperature from different sources in the city of Aveiro were considered. Data from the simulation of those scenarios is discussed considering how these aspects must be taken into account for assessing the ground thermal fluxes and how they influence the energy efficiency of the system.

In general, when the water table is considered closest to the surface, the GSHP performs better than if considered at lowest point. Overall, considering a slab as a temperature boundary between soil and building hinders the efficiency of the thermo-active pile, reversing the direction of the heat flux in the soil, if a long term analysis is considered (5 years)

Keywords

Geothermal, Shallow geothermal, Thermal energy, Efficiency, Energy structures, Thermo-active pile, numerical

Resumo

Um estudo numérico foi desenvolvido para avaliar o potencial geotérmico de um conjunto de estacas utilizadas como permutadores de calor com o solo, utilizando-o como deposito seasonal de energia térmica. É baseado no caso de estudo de um edifício localizado no campus da Universidade de Aveiro, equipado com sistema superficial de bomba de calor geotérmica, dimensionado para comportar a maiora da energia necessária para a aclimatização do edifício.

Foi modelada uma estaca (60cm de diametro e 10m de comprimento) utilizando um software de diferenças finitas denominado FLAC. A influência das propriedades do solo e da localização do nível freático foram investigadas. A influência da laje do edifício no desempenho térmico do sistema foi igualmente investigada. As conductividades térmicas do solo foram obtidas por meio de relações empíricas e por caracterização em laboratório. Diferentes condições de carregamento témico na estaca e no solo de fundação foram examinados. Estas foram, respectivamente, as necessidades térmicas do edifício e a acção climática. Nesse sentido diversas fontes de dados climáticos para a cidade de Aveiro foram consideradas. A informação utilizada na modelação numérica para os diferentes cenários é discutida nesta dissertação, tendo em vista uma análise dos fluxos de calor geotérmicos no solo e a sua influência global no sistema.

Em geral, quando o nível freático é considerado o mais próximo possível da superfície, o solo responde melhor à acção da estaca termo-activa do que quando é considerado no seu ponto mais baixo. Globalmente, considerar a laje de fundo do edifício como uma condição de fronteira entre o solo e o edifício, prejudica a eficiência da estaca termo-activa, revertendo a direcção do fluxo de calor no solo, se for considerada uma análise longa (5 anos).

Palavras-chave

Geotermia, Geotermia superficial, eficiência energética, Estruturas termoactivas, numérica

Table of Contents

Chapter Page

List of Tables

Table Page

List of Figures

Figure Page

List of Symbols

ACRONYMS

$erfc$ – accumulated error function
ASHRAE – American Society of Heating, Refrigeration and Air Conditioning Engineers
CICFANO – Complexo Interdisciplinar de Ciências Físicas Aplicadas à Nanotecnologia e Oceanografia;
CCCI – Complexo das Ciências da Comunicação e Imagem
COP – Coefficient of Performance
GSHP – Ground source heat pump
HVAC – Heat, Ventilation and Air Conditioning
HFMA – Heat Flow Meter Apparatus
HWM – Hot Wired Method
EER – Energy Efficiency Ratio
LNEC – Laboratório Nacional de Engenharia Civil
SI – International system of units
SF – Sizing Factor
SPF – Seasonal Performance Facot
TRT – Thermal Response Test
UTES – Underground Thermal Energy Storage
VDI – Verein Deutcher Ingenieure

SYMBOLS

c – Specific heat
d – thickness of the sample for a HFMA test
e_h – heat flux imposed on a TRT
e_0 – Initial void ratio
f – Calibration factor for the heat flux meter
i – Gridpoint coordinate in the horizontal direction
j – Gridpoint coordinate in the horizontal direction
q – heat flux
q_i – Heat flux along the direction i
r – radial distance to the axis
t – Time
v – Flow velocity
z – Shape factor for particles and voids

A – Area

A_{ij} – Area of a single element of the grid

C – Heat capacity

D – Diameter

H – Height

L – Lenght

Q – Heat generated

Sr – Saturation Degree;

T – Temperature

T_1 – Upper face temperature on a HFMA

T_2 – Lower face temperature on a HFMA

T_{avg} – Average temperature

T_{ref} – Reference temperature

T_h – Heating Temperature

T_c – Coolong Temperature

U – Internal Energy

V – Volume

V_t – Total Volume

V_v – Void volume

α – Thermal diffusivity

γ – Volumetric weight

γ_d – dry volumetric weight

γ_w – Water volumetric weight;

λ – Thermal conductivity

λ_{eff} – effective thermal conductivity

$\boldsymbol{\lambda}_{\mathrm{sat}}$ – Saturated thermal conductivity

$\boldsymbol{\lambda}_{\mathrm{dry}}$ – Dry thermal conductivity

$\boldsymbol{\lambda}_{\mathrm{s}}$ – Soil thermal conductivity

$\boldsymbol{\lambda}_{\mathrm{w}}$ – Water thermal conductivity at 20ºC

$\boldsymbol{\lambda}_{\mathrm{a}}$ – Air thernal conductivity at 20ºC

ρ – volumetric mass density

υ – Viscosity

χ – Porosity

1. Introduction

1.1. General overview

The consumption of fossil fuels is the biggest responsible for greenhouse gas emissions and it is the largest world source of primary energy (about 86%) (Rubio-Maya C. et al, 2015). The growth of fossil fuels consumption poses a serious threat to the environment and also has impact in the financial balance for many countries in the world, and in Europe in particular. At the moment, the statistical trend is showing that world greenhouse gas emissions would rise 55% by 2030 and that the dependence of fossil fuels would dramatically increase (COM 545, 2006). In order to address this issue, the commission for the European union proposed an energy efficiency action plan with specific goals, establishing as a priority to reduce by 20% the global primary energy consumption by the year 2020 (COM 1, 2007), as well as to reduce greenhouse emissions by 20% in the same time frame. Combining renewable energies with energy efficiency is a proven alternative solution for our planet's environmental sustainability (Omer AM, 2008).

When tracing back how energy is used around the globe, statistics have shown that the building sector consumes about 35% of global energy, and accounts for 50% of worldwide electricity demand, being the largest consuming sector in the world. The sources of primary energy for electricity generation along with electricity's demand by sectors is represented in figure 1.1. Furthermore, in Europe and other temperate/cold climate regions, the main end-use for energy consumption is space heating and cooling, accounting for 50% (IEA, 2013). From the considerations above it is clear that improving the energy efficiency and supporting renewable sources for heating and cooling systems is of utmost importance.

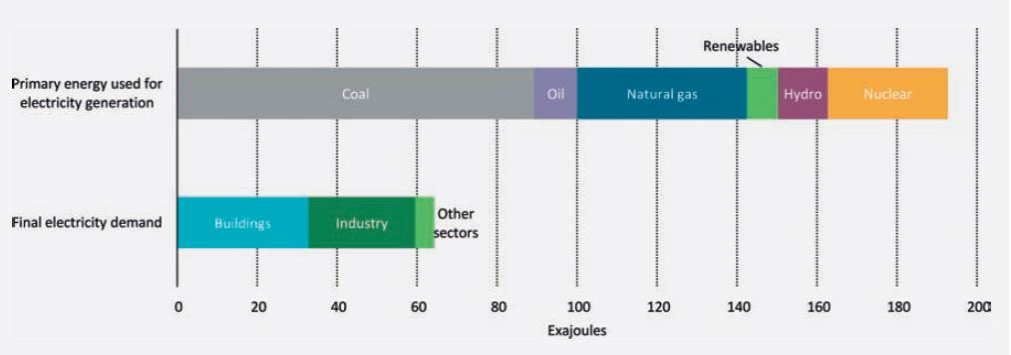

Figure 1.1 Energy use for power generation and total final electricity demand, 2010 (IEA, 2013)

Heat pumps are a mature technology that allow the transport of thermal energy from a heat source to a heat sink by means of an electrical compressor. This technology may provide efficient cooling/heating by using small amounts of energy to ensure adequate acclimatization. Among all types of heat pumps available, ground source heat pumps (GSHP) are the most cost-effective, reaching point-of-use energy efficiencies of 500% and over, as shown in figure 1.2 (IEA, 2013). Furthermore, GSHP have shown to reduce greenhouse gas emissions by more than 66% and use up to less than 75% of the electricity used

by conventional heating and cooling systems (Omer AM, 2008). In the beginning of the XXI century, GSHP was already utilized in 30 countries, but mostly in USA, Sweden, Germany, Switzerland, Canada and Austria. Since 2004, the number of these systems have been growing at an approximate rate of 10% per year (Self S. et al, 2013).

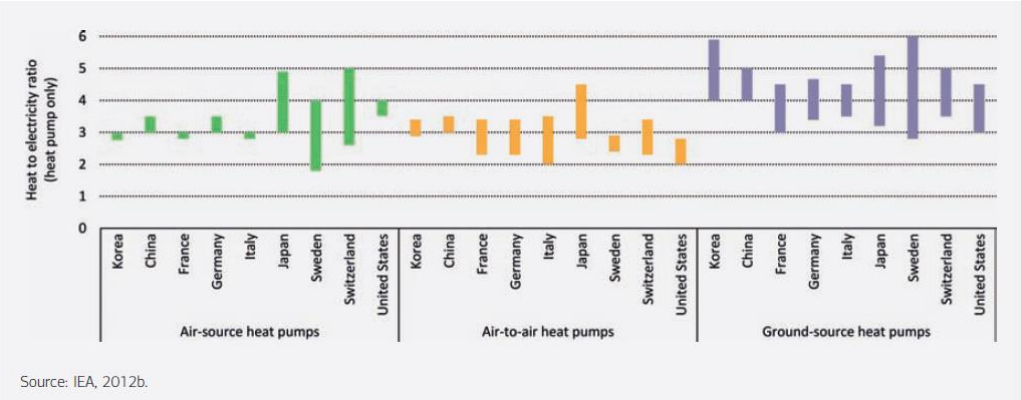

Figure 1.2. Typical operating efficiency ranges for heat pumps in heating and cooling modes by technology (IEA, 2013)

Although Portugal has been making efforts to embrace sustainable energy technologies (official statistics regarding 2013, show that 14.3% of all energy consumption was from renewable sources), low enthalpy geothermal energy production is still in its early stages (PORDATA, 2105). This resource represents a great opportunity for Portugal to meet the goals set by the European Energy Plan for 2020, which states that the country's renewable energy should account for 31% of the consumption (COM 1, 2007).

GSHP are proven effective solutions for heating and cooling in buildings, but it has yet to emerge as the top notch solution it should be. *Hughes* establishes a number of barriers that are hindering its implementation (by order of importance, being 1 the most important barrier) (Hughes P, 2008):

1. High first cost of GSHP systems to consumers
2. Lack of consumer and policymaker knowledge and/or trust in GSHP system benefits
3. Limitations of GSHP design and business planning infrastructure
4. Limitations of GSHP installation infrastructure
5. Lack of new technologies and techniques to improve GSHP cost-effectiveness

In recent years, energy foundations have been the subject of investigation as a different solution of GSHP. These solutions reduce the installation cost of such systems by being installed in the early construction stages of a building. Instead of drilling expensive boreholes/shafts solely for the purpose of installing the heat exchanger primary circuits, this approach takes advantage of the concrete foundation structures, such as piles and retaining walls, predicted in the project. Attaching heat exchanger pipes to the reinforcement steel mesh makes the whole system more robust and facilitates its setup. Furthermore, the heat exchanger pipes encased inside the foundation reinforced concrete

have less maintenance costs and longer durability. Finally, the thermal properties of concrete improve the heat transfer process in comparison with most soils (Brandl H, 2006).

However, new challenges arise regarding energy foundations. Understanding thermal response of such systems, as well as the thermal interaction between soil, foundation and heat exchanger is one of them. Another challenge is to properly investigate thermo-mechanical behaviour of these structural elements, since continuous thermal cycles (loading/unloading) are an inherent consequence of the GSHP *modus operandis.*

1.2. Goals

The first goal to be met consists on investigating and outlining the different aspects that affect the performance of an actual ground source heat pump (GSHP) system working since 2013, in an academic building located in Aveiro, Northwest of Portugal. The GSHP was installed to partially account for the building's heating and cooling demand. The performance of such system depends not only on the solution itself, but also on other aspects such as:

- Climate
- Ground conditions
- System's features
- Building's energy demand

The ultimate objective of this master thesis is to make a preliminary assessment of the thermal behaviour of the mentioned shallow geothermal heat pump system. This analysis will be done under an efficiency perspective, by evaluating how well can the soil transfer heat in different conditions and what is the thermal response of that soil under the thermal load imposed by the SGHP. For this purpose, a numerical simulation using software *FLAC 2D* will be performed

1.3. Thesis framework

This thesis is comprised of a total of five chapters, including this first introductory section. In the second chapter, entitled "Shallow Geothermal Energy", an overview of heat transfer in soils is presented, followed by a description of the current heat pump systems that allow heat to be mobilized to/from the soil for acclimatization purposes. The third chapter presents the case study, in which several inferences will be carefully made about the external and internal aspects of the GSHPsystem in study. This chapter will serve as a premise for the numerical simulation, outlining all the important input data for that purpose. In the fourth chapter, a simple numerical model will be built in order to replicate the behaviour of a single pile under certain thermal loads. Different soil conditions will be tested, including saturated and dry states. The influence of the building's slab on the thermal response of the system will also be subject of analysis. After the discussion of the results obtained, Chapter 5 presents the conclusions and the future work perspectives for this specific case.

2. Shallow Geothermal Energy

2.1. The different uses for geothermal energy

Geothermal resources refer to the thermal energy found underneath the earth's surface. From a molecular point of view, heat is the result from the decay of natural radioisotopes, and then it is stored in the earth's constituent materials. Global terrestrial heat flow is about 40 million MW, which alone would take 10^9 years to exhaust the earth's immense heat capacity (~1013 EJ). Therefore, geothermal energy can be classified has a renewable resource, since the pace at which it is replenished by the radioisotope decay process is similar to the pace at which it is removed, in accordance with current society and technology standards. (Rybach, 2006)

Mankind has been using geothermal energy for more than 10.000 years. Paleolithic tribes from South America used it for bathing, cleaning and cooking. For thousands of years, many civilizations around the world continued to use geothermal energy for direct uses. However, after the beginning of the XX century, some remarkable technological advances took place, including the invention of the first geothermal electric power plant in 1904, by Italian scientist Piero Conti. The oil crisis of 1973 showed how severe was oil dependency and it encouraged governments to develop and invest in energy sustainable strategies for their countries, including taking a chance on renewable sources. As a result, by the 1980's, geothermal energy was already a viable solution in many countries, either for electricity production through high capacity power plants, or for indirect heating using geothermal heat pumps. Climate change has also played an important part in the development of sustainable energy sources such as geothermal. In 1997, the Kyoto Protocol was signed, making 184 countries accountable for their environmental footprint on the planet.

Geothermal energy can be sorted into three different categories based on the temperature level of the source. High enthalpy resources comprises temperatures higher than 150ºC and are the consequence of the ascending of molten core materials. For temperatures between 100ºC and 150ºC, resources are classified as medium enthalpy. Finally, soils under 100ºC are considered low enthalpy resources. These different derivations of thermal energy can be exploited for three main purposes: electricity production, direct heating and indirect heating. Each of these types of resources is associated with a different activity. In high enthalpy regions, electricity generation is the most appropriate process. With medium enthalpy resources, thermal energy is used for direct heating. Low enthalpy resources may be used for heating purposes as well, but with the help of geothermal heat pumps. (Self et al, 2013) (Rubio-Maya et al, 2015)

Table 1- Geothermal resources differentiation

Type of Resource	Resource Denomination	Temperature Range	Related Activity
High Enthalpy	Deep Geothermal	>150ºC	Electricity Generation
Medium Enthalpy		100ºC - 150ºC	Direct Heating
Low Enthalpy	Shallow Geothermal	<100º	Indirect Heating

Medium and high enthalpy resources are restricted to small areas of the globe (tectonic conflicting areas), and since their high temperatures originate in the earth's mantle, they are known as deep geothermal resources. On the other hand, low enthalpy geothermal energy can be exploited in most regions, relying only on the energy provided by solar irradiation. Contrary to high enthalpy, low enthalpy is associated with shallow geothermal resources. This master thesis focuses only on shallow geothermal resources, which will be thoroughly described.

Solar irradiation varies its intensity constantly in a daily, seasonally and yearly fashion. This reason is responsible for changes in air temperature. However, soil and other materials show resistance to thermal energy penetration. Therefore, temperature gradients tend to homogenize with increasing depth. In fact, bellow 5-10 meters of depth, temperatures remain practically constant and equal to the yearly average air temperature, as shown in figure 2.1. In Europe these temperatures are found to be between 5ºC and 20ºC. The constant, near ambient temperature is what makes low enthalpy energy such a reliable source. (Brandl, 2006)(Self et al, 2013)

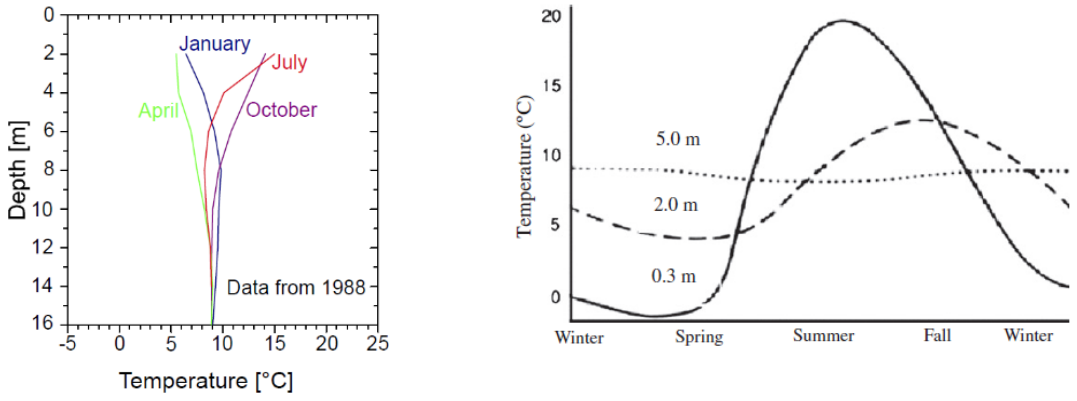

Figure 2.1. Underground temperatures from a borehole south of Wetzlar (left) (Mands & Sanner, 2007) and Otawa, Canada (right) (Self et al, 2013)

The concept behind shallow geothermal energy utilization states that one may harness or dump thermal energy from and to the soil, respectively. In the Winter, thermal energy would be gathered from shallow soil and transported to a building in order to heat the colder air. The opposite occurs in the Summer season, where soil works as a deposit for the thermal energy retrieved from a building's usable space. This becomes an advantage for countries with moderate climate and others. In many countries, including

Portugal, temperatures rise to values of more than 30ºC in the summer, and may come down to less than 0ºC in winter. Therefore, the thermal energy of shallow soils may be used both for heating and cooling, depending on the energy needs of a building.

However, as mentioned before, shallow geothermal resources cannot be used directly for acclimatization purposes. Indirect heating and cooling processes requires the support of certain machines called heat pumps. Heat pumps use the same principle as a refrigerator, moving heat from one place to another, with the help of a little electrical energy input. These devices will be described further in section 2.3. Heat pumps associated to shallow geothermal resources are called ground-source (GSHP), shallow geothermal (SGHP), or even just geothermal heat pumps (GHP).

The installed capacity of ground-source heat pumps increased from an estimated 1.9GW_{th} in 1995 to 50 GW_{th} in 2015, which represents an average annual growth of 18% in those 20 years, as can be seen in figure 2.2. Regardless of this growth in thermal capacity, 2015 showed a market contraction in the sector's sales of about 13%.Up to that year, market had been growing consistently at 3% rate per year (Renewables 2016, Global Status Report).

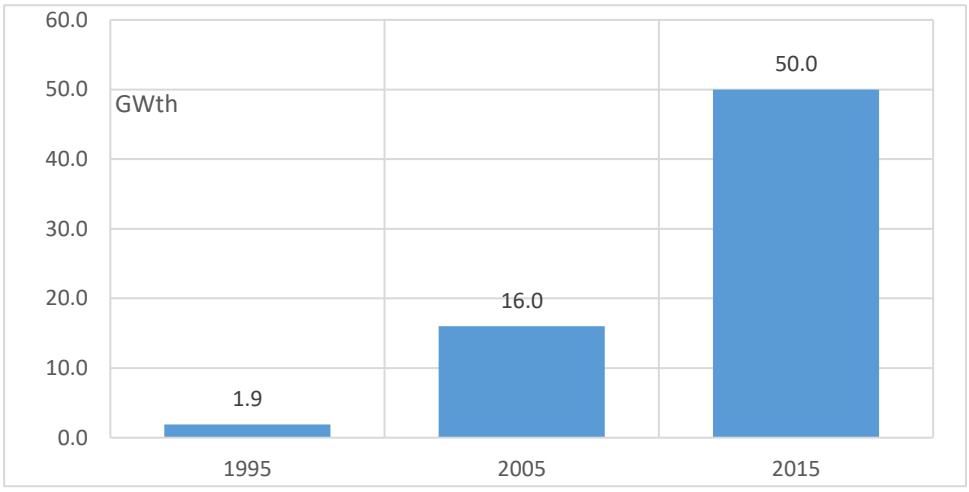

Figure 2.2. Worldwide annual incremental growth of shallow geothermal capacity (adapted from Renewables 2016, Global Status Report)

In Portugal, legislation is far from being clear on the recommendations regarding shallow geothermal systems. There is however the obligation of using renewable sources for the acclimatization of buildings (Figueira and Vieira, 2016). So far, the only two government infrastructures in Portugal that use shallow geothermal energy for acclimatization purposes are located in Aveiro's University and comprise a thermal capacity of a few dozen kilowatts. One of those buildings will be analyzed in this thesis.

2.2. Heat transfer in soils

2.2.1. Modes of heat transfer in soils

When studying geothermal energy systems, the paradigm lies within the complexity of heat transfer. The rate at which thermal energy moves and the mechanisms responsible for it are the subject of this chapter. In nature, there are three modes of heat transfer (Al-Khoury, 2011):

i) Convection
ii) Conduction
iii) Radiation

In most soils and in shallow geothermal energy systems, convection and conduction are the only relevant modes of heat transfer, relegating radiation to a negligible role. Conduction heat results from the random spread of heated particles that occurs when a higher energy region contacts with a lower energy region, or in other words, heat diffusion. This phenomenon always takes place from a higher temperature region to a lower temperature region. Convective heat transfer combines diffusion with the transport of heated particles by the motion of a fluid, which is what defines advection (Al-Khoury, 2011). Summarizing, advection and diffusion are the physical phenomena that, combined, describe the motion of the heat inherent to conduction and convection.

Radiation is related to the heat transfer across vacuum or a transparent medium by propagation of electromagnetic waves. The effects of radiation may vary greatly with soil type. For instance, sands have shown a poor response when transferring heat through radiation (less than 1% of overall heat transfer), while in some types of gravel, the same process may have an importance of 10% (Rees et al, 2011). Most natural soils are not influenced by radiation heat transfer at ambient temperature and therefore they won't be further detailed in this thesis.

In order to one or more modes of heat transfer occur, the phenomenon must be triggered by imposing a thermal disturbance within the energy system. *In extremis*, if all the molecules in a system have the same amount of energy and the system boundaries prevent interferences with the outside, neither conduction or convection will occur. However, this is not the case with shallow geothermal systems because they are dynamic thermal systems, not only among its several components, but also dynamic with the surrounding environment.

Some of this thermal triggers were described by Brandl (2006) as others are the natural consequence of the GSHP features and location. Altogether, the most important heat transfer triggers are summarized as follows:

i) Vaporisation-condensation and Freezing-Thawing processes

Changes of phase of a certain material (i.e. water) are either endothermic or exothermic reactions. Therefore, heat is absorbed or released to the nearby environment during these processes. Freezing and thawing are exothermic and endothermic chemical reactions, respectively. The same goes for condensation and vaporization. After heat is released to the surroundings, it will be transferred by convection or conduction as described above. While freezing-thawing is not expected to occur in normal conditions below the surface, the latent heat of vaporization may take a relatively significant part when dry conditions prevail (Brandl, 2006) (Rees et al, 2011).

ii) Ion unbalance

Ion exchanges generates heat by promoting particle movement between two regions that have different concentrations of positive cations and negative anions. In those situations, the electrically charged particles will attract each other. This phenomenon plays a negligible part in most soils, being more relevant in saturated clays with significant organic matter.

iii) Earth molten core and solar irradiation

Solar irradiation and the earth molten core are obviously the most important heat sources in geothermal energy systems, in the sense that without them it wouldn't be possible to apply this technology. They are further away from the earth's crust than any other thermal energy source, and yet they represent a huge impact on a GSHP. How do they work and why they impact soil temperature was already exposed in section 2.1.

iv) Underground water flow

Underground water flow occurs in many soils, mainly in regions close to rivers or oceans. Besides location, soil properties like porosity will also help determine the intensity of water flow. Underground water flow works through advection, by transporting water molecules from one place to another. The constant process of gathering/damping heat to the soil may, with time, cause a reduction in the efficiency of the system because soil temperature will decrease/increase with time. Advection by ground water flow is important to renew and maintain natural ground temperature, as shown in several studies. (Brandl, 2006)

v) Heat Exchangers

At last, but not the least, heat exchangers are an engineering tool designed to retrieve or damp heat into the soil mass. With the help of a thermal heat pump, heat exchangers cause a thermal disturbance in the system by working as a heat source.

When modeling heat transfer in a certain soil volume, all the phenomena described above must be taken into account, if necessary, either by imposing initial conditions or by carefully establishing boundary conditions. Figure 2.3 displays the main processes that are responsible for heat transfer in soils.

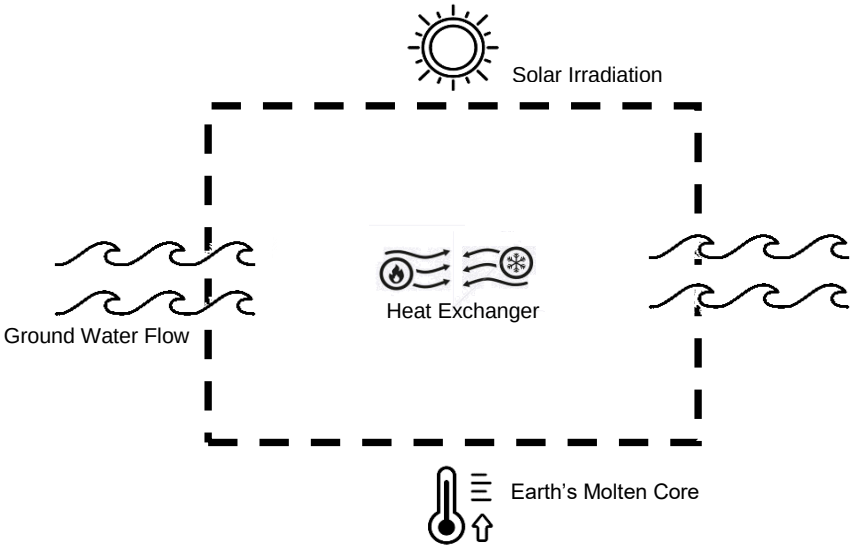

Figure 2.3. Physical processes involved in heat transfer in soils

2.2.2. Thermal properties of soils

Soils are heterogeneous materials with several different constituents. Each constituent has a different thermal behavior, which is explained by two thermal properties: thermal conductivity (λ) and Heat capacity (C). Besides thermal properties, other physical properties play an important role in heat transfer problems, including porosity (η) and hydraulic properties like viscosity (υ) and flow velocity (v) (Al-Khoury, 2011).

The internal energy a material can store is directly related to the specific heat capacity (c) (SI units J/Kg.K). For a better understanding of this property, it may be described as the energy necessary to raise the temperature by 1ºC on a 1 Kilogram mass. Heat capacity can be written in the form $C = \rho . c$ and is described as the energy necessary to increase 1ºC in $1m^3$ of a certain material. This property is especially relevant while soil is gaining or losing heat, instead of just transmitting it (Farouki, 1981).

On the other hand, if temperatures are not changing with elapsing time, then it means molecules are purely transmitting energy. In this case, the ruling property is thermal conductivity (λ). This property may be described as the amount of heat passing in unit time through a unit cross-sectional area of the soil, under a temperature gradient (SI units W/mK) (LoRusso et al, 2009).

In current geothermal problems, both situations occur, and therefore both variables are relevant. Therefore, another concept is introduced by the variable $\alpha = \frac{\lambda}{\rho c}$ (SI m^2/s) known as thermal diffusivity, which is a conjugation of both properties mentioned above. It describes the speed at which a material changes temperature. For instance, a material with very high thermal conductivity and low volumetric heat capacity will change its temperature very quickly when subject to a temperature differential.

These parameters are not temperature independent. Relationships of the following type should be taken in consideration (Al-Khoury, 2011):

$$\lambda = \lambda_0\left[1 + a(T - T_{ref})\right] \tag{2.1}$$

$$c = c_0\left[1 + b(T - T_{ref})\right] \tag{2.2}$$

where λ_0 and c_0 are the values of conductivity and specific heat at the reference temperature T_{ref}, while a and b are material constants determined experimentally. However, for small temperature gradients like the ones observed in shallow geothermal energy systems, such variations are negligible and a constant value can be assumed. For instance, the specific heat of water changes only 1% when raising its temperature from 0ºC to 50ºC. On the other hand, for the same temperature variation, thermal conductivity of water raises only 13%. Compared to water, solid materials suffer even less changes in their properties (Rohsenow et al, McGraw-Hill 1998).

Porosity is defined as the ratio of the volume of pores (voids) within the total volume of the material:

$$\eta = \frac{V_v}{V_t} \tag{2.3}$$

Where V_v is the volume of the pores and V_t the total volume. As will be shown later on, porosity plays a major role in determining other parameters like the effective thermal conductivity λ_{eff}.

Viscosity (υ) (SI units m^2/s) is a measure of a fluid's resistance to movement. It may be described as an internal friction force exerted between the fluid's molecules. Ultimately, viscosity affects flow velocity, which affects the convective behavior of a geothermal system.

Convective heat by means of advection requires the understanding of flow and fluid behavior. Other thermo-hydraulic parameters that help characterize such behavior are: Reynolds Number, Prandtl number, Peclet number and Nusslet number. These parameters relate the geometry of the percolation medium with the flow speed and also with the conductive properties of the fluid (Al-Khoury, 2011). Characterization of the convective parameters is a rather complex subject and difficult to determine accurately, and such complexity will not be the subject of analysis in this master thesis.

Table 2. Thermo-physical properties of typical geothermal materials (Al-Khoury, 2011)

Material	λ (W/m · K)	ρ (kg/m^3)	c (kJ/kg · K)	n	υ (m^2/s)
Ground material					
Limestone	1.2–2.15	2300–2500	0.8–0.9	0–0.2	
Sandstone	1.8–2.9	2160–2300	0.7–0.8	0.05–0.3	
Sand	0.15–4	1280–2150	0.8–1.48	0.2–0.6	
Clay	0.15–2.5	1070–1600	0.92–2.2	0.33–0.6	
Soil	0.4–0.6	1600–2050	1.8–1.9	0.3–0.5	
Pipe material and fluid					
Polyethylene	0.33	960	2.1		
Grout	0.8–1.5	1100–1400	2–2.2		
Water	0.56	1000	4.18		1.006E–6
Water + 25% Ethylene glycol	0.5	1050	3.795		4.95E–6

Every soil behaves differently, due to its different microstructure and composition, however, countries from the north of Europe have been using the GSHP technology for many years. This experience is translated in guidelines that allow easy consulting of typical values. For instance, the VDI 4640 is a German guideline compilation for planning and dimensioning of such systems. In VDI 4640 there is a number of recommendations regarding soil parameters. In annex B there is part of the information that can be found in those guidelines. The United States have also a designer code for Geothermal Systems in a document called ASHRAE Handbook-HVAC Applications. The recommended values for soil parameters are in the same range of those from VDI 4640. If a more precise approach is required, it might be necessary to estimate thermal parameters. In the following chapter, a number of methods for determining those parameters will be presented.

2.2.3. Determining Thermal Parameters in Porous Media

Soils are heterogeneous materials, which comprise three different phases: solid, liquid (mainly water) and gas (mainly air, assumed dried). The solid phase usually is made from many different minerals, each one with an individual thermal behavior. This variability poses a challenge when trying to determine thermal properties of a specific soil. There are three ways of estimating these properties: empirical methods, laboratory testing and field testing (Figueira and Vieira, 2016).

Empyrical methods

Many empirical methods were proposed along the years since the second half of the 20th Century. De Vries (1952) was the first who proposed a calculation of an effective thermal conductivity λ_{eff}, which is based on the individual thermal conductivities of the multiphase constituents ($\lambda_s, \lambda_w, \lambda_a$, respectively solids, water and air). This method was based both on volumetric percentages (χ) of the soil's constituents and the shape of the particles and voids (z), resulting in the following:

$$\lambda_{eff} = \frac{\chi_w . z_w . \lambda_w + \chi_a . z_a . \lambda_a + \sum_i (\chi_{s,i} . z_{s,i} . \lambda_{s,i})}{\chi_w . z_w + \chi_a . z_a + \sum_i (\chi_{s,i} . z_{s,i})} \quad (2.4)$$

Other authors attempt to determine the effective conductivity considering aspects like the percentage of clay (Makawski et al. 1957) or bulk density of the solid particles (Johansen 1975), or even the value of the heat flow affecting the soil mass (Gori et al. 2013).

However, literature suggests that for shallow geothermal behaviour it is often satisfactory to consider a Pythagorean average of the soil's volumetric constituents, depending on the material disposition related to the heat flow direction, as shown in figure 2.4 (Rees et al, 2011). Some authors also add that, in such systems, the temperature gradients are small and, as such, a simple pithagorean average will suffice to provide an adequate thermal conductivity (Al-Khoury, 2011).

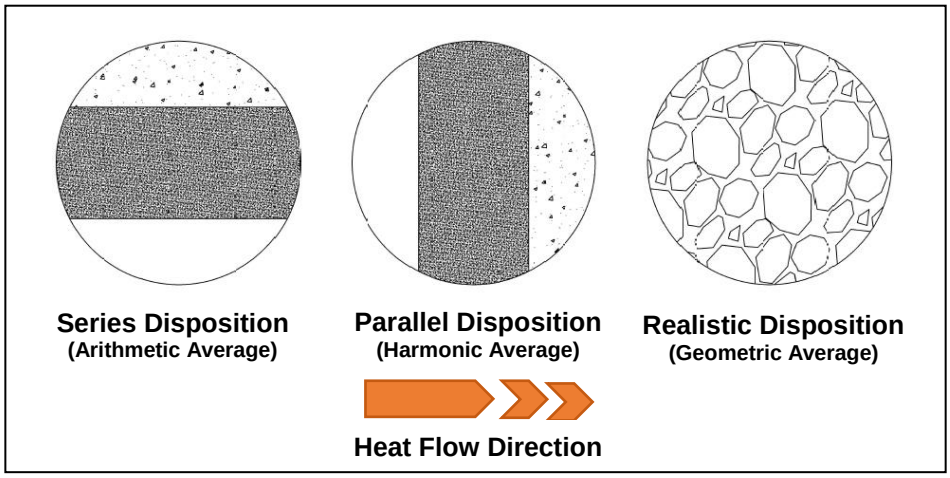

Figure 2.4. Three possible material dispositions and their correspondent Pythagorean averages

The most common Pythagorean means are the weighed arithmetic mean, the weighed harmonic mean and the weighed geometric mean. Mathematically, for any given variable (n) they may be written has the following:

Weighed Arithmetic Average

$$\bar{n} = \chi_1.n_1 + \chi_2.n_2 + \chi_3.n_3$$

Weighed Harmonic Average

$$\bar{n} = \frac{n_1.n_2.n_3}{\chi_1.n_2.n_3 + \chi_2.n_3.n_1 + \chi_3.n_1.n_2}$$

Weighed Geometric Average

$$\bar{n} = n_1^{\chi_1}.n_2^{\chi_2}.n_3^{\chi_3}$$

For soils, χ_1, χ_2 and χ_3 represent the volume fractions of the three constituents of soil and may be defined using the porosity (η) and degree of saturation (S). On the other hand, n_1, n_2 and n_3 are either c_s , c_w , c_a or λ_s , λ_w , λ_a depending on which thermal propertie is being determined. Furthermore, the solid fraction may be sub-divided into their mineralogic fractions.

$$\chi_1 = \chi_s = (1 - \eta) \quad (2.5)$$

$$\chi_2 = \chi_w = \eta.S \quad (2.6)$$

$$\chi_3 = \chi_a = \eta.(1 - S) \quad (2.7)$$

All three averages are valid methods but they provide very different results. As an example, calculations were performed for a soil (95% quartz minerals and 5% clay minerals) exhibiting a void ratio e = 0.53 and different saturation levels. Figure 2.5 presents the results of that analysis. The series and parallel arrangements provide extreme estimations which, according to literature, are unadequate approximations for soils. Since real soils are arranged somewhere in the middle of those two hipotesis, the geometric average is usually the prefered method (Al-Khoury, 2011).

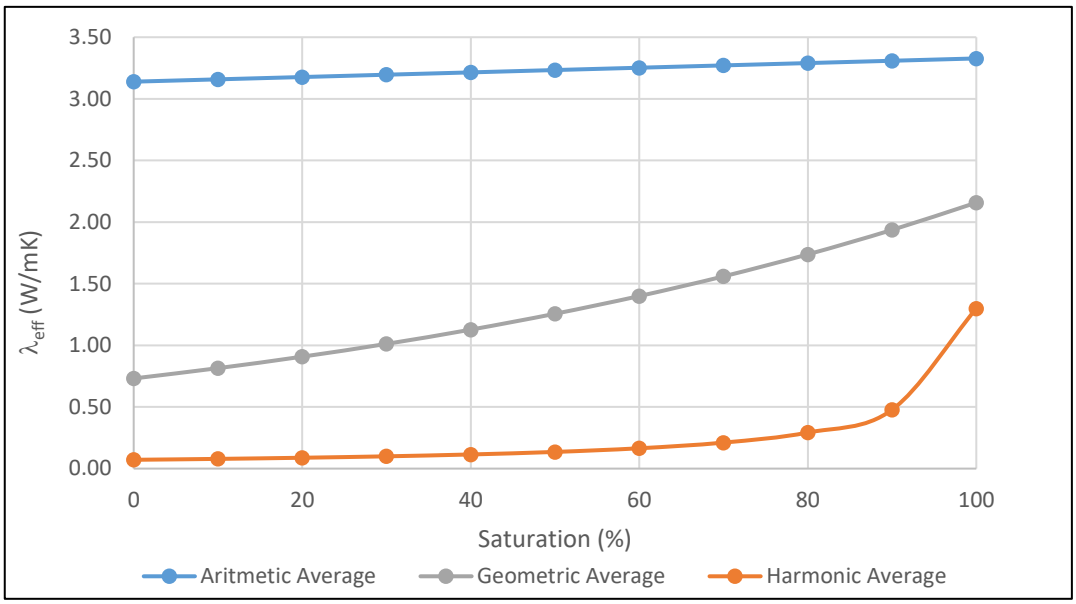

Figure 2.5. Change in thermal conductivity with the level of saturation

For saturated soils, where there are only two phases, literature provides several formulations that estimate the effective thermal conductivity of the material. For instance, Krupiczka (1967) suggests

$$\lambda_{eff} = \lambda_w \left(\frac{\lambda_s}{\lambda_w}\right)^{0.28-0.757\log(\eta)-0.057\log(\lambda_s/\lambda_w)} \tag{2.8}$$

While Bromberg and Shirtliffe (1978) proposed the relationship

$$\lambda_{eff} = \lambda_s \left(1 + 4\frac{\eta S_w \rho_w}{(1-\eta)\rho_s}\right) \tag{2.9}$$

Laboratory Tests

Laboratory methods may also be usefull for determining thermal parameters. Unlike empirical methods, laboratory tests don't require previous knowledge of the geotechnical and geological properties of the soil. There are two groups of laboratorial tests in which heat flow is applied: stationary regimen and variable regimen.

In stationary methods, both heat flux and temperature of the sample remains constant throughout the duration of the test. The most commonly used methods are the Guarded Hot plate (GHP), the Heat Flow Meter Apparatus (HFMA) and the Guarded-Comparative-Longitudinal Heat Flow Technique (GCLHFT). All this techniques are based on Fourier's law of conduction. For instance, in HFMA thermal conductivity is obtained through the following equation:

$$\lambda = \frac{f e_h d}{(T_1 - T_2)} \tag{2.10}$$

Where d is the thickness of the sample, $T_1 - T_2$ is the difference between the temperatures in the upper face and lower face of the sample, f is the calibration factor of the heat flux meter and e_h is the imposed heat flux.

Dynamic methods register changes in temperatures across the probe and the soil during the duration of the test. One of the most commonly used methods is the Hot Wire Method (HWM) which determines thermal conductivity based on the line source model. In this model, an infinitely long source of heat with infinitely small diameter generates a radial heat flux. Other methods include the Transient Plane Source (TPS) and the Laser Flash Method (LFM). Dynamic methods are more adequate to measure thermal diffusivity (α) since they monitor temperatures in the transient phase of the heat transfer (Vieira & Figueira, 2017). For instance, the HWM typical results are in accordance with figure 2.6. The timeframe for accurate conductivity measurements must be after transient state is over and before boundary effects of the sample occur:

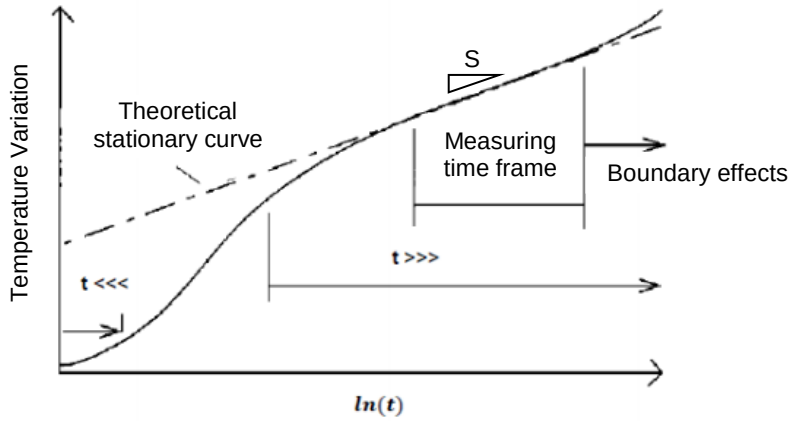

Figure 2.6. Typical curve obtained in a HWM test, adapted from (Vieira & Figueira, 2017)

After the measurement is performed, conductivity may be simple determined by

$$\lambda = \frac{\dot{q}}{4\pi S} \tag{2.11}$$

Where $\dot{q}$ is the imposed heat flux and S is the inclination of the theoretical line in figure 2.6.

Field Tests

Field tests may also be very usefull tools, since they may potentially reproduce the real thermal behaviour of the soil. Usually field tests are performed in the future location of a GSHP system. At the moment the only method which is widely accepted and performed is the Thermal Response Test (TRT).

A typical TRT measures the temperature change in a heat carrier fluid, which is located inside a borehole. The boreholes depth may vary between 10 and 100 meters, while the diameter is usually between 120mm and 200mm. It is recommended that the test should run for more than 50 hours (Sanner et al, 2005). The typical display and results of a TRT can be seen in figure 2.7.

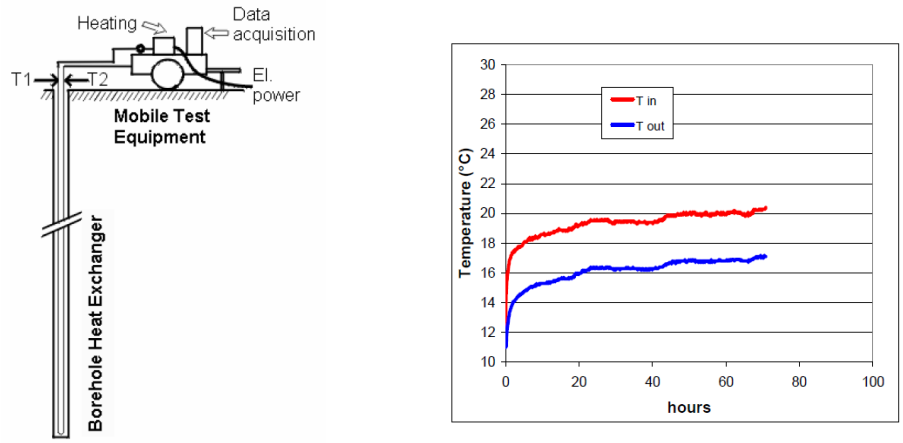

Figure 2.7. Typical display (left) and results(right) of a TRT (Sanner et al, 2005)

To determine the effective thermal conductivity of the soil, the typical approach requires the application of the following formula (Gehlin 1996):

$$\lambda_{eff} = \frac{Q}{4\pi Hk} \tag{2.12}$$

Where Q is the ammount of heat injected, H is the length of the borehole and k is the linear corelation between temperature change (ΔT) and time elapsed (log(t)). To assure realistic results, climate interferencces and excessive ground water flow must be avoided (Sanner et al, 2005).

2.2.4. Mathematical description of the heat transfer modes

As described in the chapters above, in a shallow geothermal energy system, conduction and convection are the main modes of heat transfer. In this master thesis, convection will not be considered in the numerical modelling. Therefore, the following explanation refers only to the conduction mechanism.

Heat transfer in a solid body can be explained by Fourier's law of conduction and by the first law of thermodynamics. The conservation of energy principle applied to thermal conditions can be written as equation 2.1, and figure 2.8 represents it in a unitary control volume.

$$\{Heat\ Flow\ in\} + \{Energy\ Generation\} = \{Heat\ Flow\ out\} + \{Energy\ stored\} \tag{2.13}$$

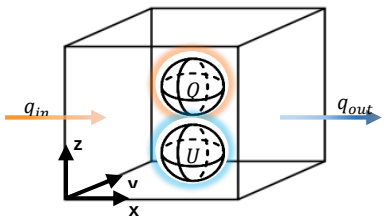

Figure 2.8. Control Volume (dx,dy,dz)

In the first place, the conductive mode of heat transfer will be described. As the starting point, a representative control volume like the one in figure 2.8 will be taken in consideration. For instance, the heat flow across dx direction is described as

$$q_{x,in} = -\lambda_x \frac{\partial \mathrm{T}}{\partial \mathrm{x}} \mathrm{dydz} \tag{2.14}$$

Where T is temperature, λ_x is the thermal conductivity for the direction dx and dydz is the cross section. On the other hand, the rate of heat flow out of the control volume will be

$$q_{x,out} = q_{x,in} + \frac{\partial q}{\partial x} dx \tag{2.15}$$

The variation of the heat flow rate within the control volume in the xx direction is written as

$$q_{x,in} - q_{x,out} = \frac{\partial}{\partial x}\left(\lambda_x \frac{\mathrm{dT}}{\mathrm{dx}}\right) dxdydz \tag{2.16}$$

The same deduction can be made for the remaining directions yy and zz which results in

$$q_{total,in} - q_{total,out} = \left[\frac{\partial}{\partial x}\left(\lambda_x \frac{\partial \mathrm{T}}{\partial \mathrm{x}}\right) + \frac{\partial}{\partial y}\left(\lambda_y \frac{\partial \mathrm{T}}{\partial \mathrm{y}}\right) + \frac{\partial}{\partial z}\left(\lambda_z \frac{\partial \mathrm{T}}{\partial \mathrm{z}}\right)\right] dxdydz \tag{2.17}$$

The internal energy storage U inside the control volume by unit volume V and unit temperature T depends on the material's density and heat capacity. The equation is given by

$$U = \rho cVT = \rho cTdxdydz \tag{2.18}$$

Which becomes a differential equation when derived by time. Assuming that the specific heat and density are constant for a certain material, the equation becomes

$$\frac{\partial U}{\partial t} = \rho c \frac{\partial T}{\partial t} dxdydz \tag{2.19}$$

Heat generation Q inside the control volume depends on the type of source, but in generic terms, it will be a function of the type

$$Q = Q(x, y, z) \tag{2.20}$$

Replacing equations (2.5), (2.6) and (2.7) in equation (2.0) it will end up as

$$\left[\frac{\partial}{\partial x}\left(\lambda_x \frac{\partial \mathrm{T}}{\partial \mathrm{x}}\right) + \frac{\partial}{\partial y}\left(\lambda_x \frac{\partial \mathrm{T}}{\partial \mathrm{y}}\right) + \frac{\partial}{\partial z}\left(\lambda_x \frac{\partial \mathrm{T}}{\partial \mathrm{z}}\right) + Q(x, y, z)\right] dxdydz = \rho c \frac{\partial T}{\partial t} dxdydz \tag{2.21}$$

Dividing both sides by $dxdydz$ and considering that heat generation mechanisms in soils are usually insignificant, the so called heat equation can be written as

$$\frac{\partial}{\partial x}\left(\lambda_x \frac{\partial \mathrm{T}}{\partial \mathrm{x}}\right) + \frac{\partial}{\partial y}\left(\lambda_x \frac{\partial \mathrm{T}}{\partial \mathrm{y}}\right) + \frac{\partial}{\partial z}\left(\lambda_x \frac{\partial \mathrm{T}}{\partial \mathrm{z}}\right) = \rho c \frac{\partial T}{\partial t} \tag{2.22}$$

Using the gradient operator (2.9) becomes

$$\nabla \cdot (\lambda \nabla T) = \rho c \frac{\partial T}{\partial t} \tag{2.23}$$

Finally, assuming thermal conductivity is the same in all three directions, equation (2.23) takes the shape

$$\nabla^2 T = \frac{\rho c}{\lambda} \frac{\partial T}{\partial t} \quad or \quad \nabla^2 T = \frac{1}{\alpha} \frac{\partial T}{\partial t} \tag{2.24}$$

$$where\ \nabla^2\ is\ the\ Laplacian\ operator\ \frac{\partial^2}{\partial x^2} + \frac{\partial^2}{\partial y^2} + \frac{\partial^2}{\partial z^2}$$

If the control volume in figure 2.8 is filled with a liquid material (water e.g.), then convective heat transfer also takes place. In such cases, material enters the control volume at a rate $u\ (m.s^{-1})$, transporting with it thermal energy. Such phenomenon has been called in the previous chapter as advection. If the effect of advection is included, equation 2.1 becomes

$$q_{x,in} = -\underbrace{\lambda_x \frac{\partial \mathrm{T}}{\partial \mathrm{x}} dydz}_{diffusion} + \underbrace{\rho c u_x T dydz}_{advection} \tag{2.25}$$

Overall, in three dimensional problems the heat equation changes from the one shown in 2.10 to the following:

$$\nabla \cdot (\lambda \nabla T) + \nabla \cdot (\rho c u T) = \rho c \frac{\partial T}{\partial t} \tag{2.26}$$

If fluid motion in the control volume is not permitted, i.e. by imposing a solid boundary, a new parcel of heat transfer is defined by the contact between a convective material and a conductive material. This occurrence is explained by Newton's Law of cooling in the form

$$q = h(T_s - T_f) \tag{2.27}$$

Where T_s and T_f are the solid's temperature and the fluid's temperature, respectively, and h is the convective heat transfer coefficient ($W/m^2.K$). This variable depends on the properties of both contact materials and also the flow regimen (turbulent or laminar).

This mathematical formulation is applicable to all situations. However, due to their morphology and *modus operandis,* a more complex formulation is required in GSHP systems. In the following chapters, these systems will be properly presented, including the simplified way of solving the heat transfer problem numerically.

2.3. Shallow geothermal heat transfer systems

2.3.1. System components

Shallow geothermal energy existing naturally in the ground soil may be harnessed and transferred for inside use. Unlike the typical HVAC systems, where heat is generated through combustion or electricity, with SGHTS heat is simply moved from one placed to another. Not only ground soil works has a heat source, but it may also be used has a heat sink. Therefore, a SGHTS is able to provide heating or cooling for buildings depending on its energy needs (Omer, 2008). The first records about using soil as an energy source for heating purposes goes back to 1912, in a registered Swiss patent. From that point, the concept of geothermal heat pump (GHP) or Ground Source Heat Pump (GSHP) was born (Sarbu & Sebarchievici, 2014). Since then the technology has been investigated mainly in the early 50's after the second world war and during the 70's after the first oil crisis. Since 2004, it is estimated that the number of GSHP installed is growing 10% every year (Self et al, 2013). As of today, there are two main approaches to effectively use low enthalpy thermal energy. One of them gathers heat from a heat wasting source and stores it underground in an underground thermal energy store (UTES) for further use. The second method utilizes the already mentioned ground source heat pumps (GSHP) to transfer heat from a source to a usable space (Mands & Sanner, 2007). Although both systems are similar in many concepts, for the purpose of this thesis heat transfer systems refer to the applications using GSHP.

A ground source heat pump system can be decomposed in three global components: primary circuit, heat pumps and secondary circuit, as shown in figure 2.9. (Brandl, 2006) (Omer, 2008)

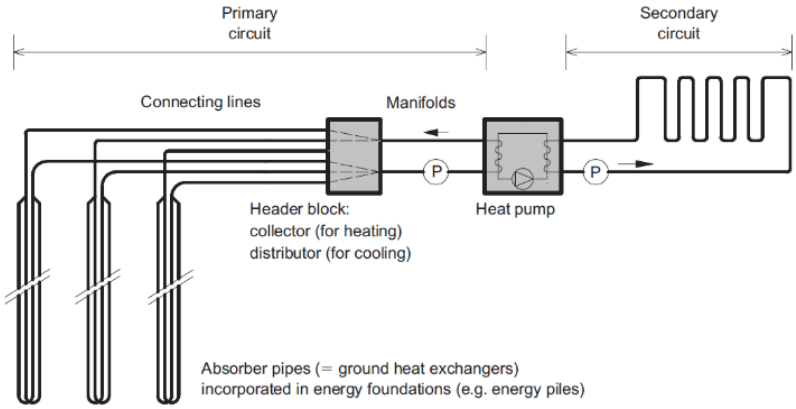

Figure 2.9. Representation of a geothermal energy system (Brandl,2006)

A primary circuit is comprised of lengths of heat exchanger pipe buried in the ground, either in a borehole, horizontal trench or a concrete foundation. The heat exchanger (also called absorber pipe)

has a heat carrier fluid inside, usually water or water with antifreeze. This fluid carries the heat from the soil to the heat pump, or the other way around if the system is working in cooling mode.

A heat pump is a cold vapor machine, which circulates a low evaporation point fluid to generate pressure. Then, the pressure will generate heat that will be transferred to the external sink by conduction. After the heat is transferred, the gas goes through a condensation process, returning to the liquid state that connects to both primary and secondary circuits. In this process, the refrigerating fluid only transports heat from one source to one sink. For instance, heat pumps are used in refrigerators all over the world, and if someone puts their hands on the back of the appliance, it will be considerably hot. That is because the heat pump is moving thermal energy from inside the refrigerator to the outside. The basic structure of a geothermal heat pump can be seen in figure 2.10. The cycle of a heat pump may be reversed, depending if the purpose is to heat or to cool a space. A more complete scheme of the heat pump can be found in annex A.

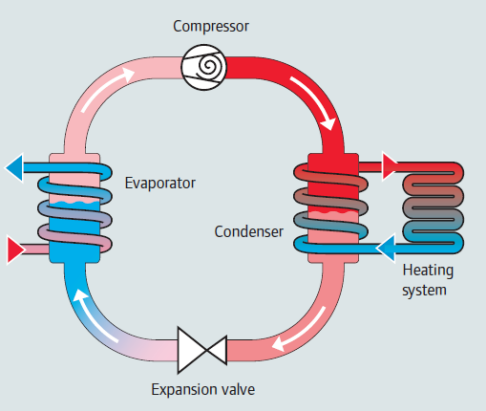

Figure 2.10. Simplified structure of a heat pump, connected to the primary and secondary system

The secondary circuit is a secondary set of pipework, consisting of a closed loop network embedded in the floors and walls of the above structure, responsible for allocating heat to the needed purpose. The heat carrier fluid may remain always inside slabs or walls (providing space heating), or it may be used indirectly for ventilation purposes by heating conditioning air. In some cases, it may also be used for heating water for domestic uses. (Brandl, 2006)

2.3.2. Open and Closed Systems

Shallow Geothermal systems may be classified as open or closed systems. Open systems are based on pumping ground water from a natural aquifer directly into the heat pump. In closed systems there is no exchange of matter between the heat exchanger and the outside. Therefore, the heat carrier fluid remains the same during the lifetime of the Geothermal System. Usually this fluid is water, or water with antifreeze and it circulates inside one or more closed loops (Brandl, 2006).

Open systems are not always possible to install because aquifers don't exist everywhere and even when they do, its size and location may not be viable. Also, water chemistry, hydraulic properties and aquifer yield (well capacity) are all limiting factors (Brandl, 2006). On the other hand, open systems are proven to be more efficient. For example, a vertical closed loop system can usually supply a few hundred thermal kW and it may easily cost more than 1200 €/Kw to execute, weather an open loop system can provide a few thermal MW and its cost is around 100 €/Kw. However, these values don't take into account the maintenance costs of open systems, which are much higher than those of closed systems (McCorry & Jones, 2011).

2.3.3. Geotechnical applications

There are many Geotechnical applications of ground source heat exchangers. Some of them are open systems and others closed systems. A few of them are exclusively purposed for working has shallow geothermal systems while others are also structural elements of buildings. All of the geotechnical works in GSHP are related to how the primary circuit is used. The most common applications are presented next, and illustrated in figure 2.11:

- Borehole Heat Exchangers may be installed individually or as an array of exchangers, right beside or below the building with depths ranging from 20 to 150 meters. They consist of inserting lengths of pipe inside one or more boreholes and filling it with fluid material (Omer, 2008). The boreholes may be done virtually in any material, including rock. In order to mobilize the required heat transfer, a minimum spacing of 6 meters in southern European climates is recommended. One of the advantages this technique provides is the fact there is no need for a large ground area when compared with other systems. The second advantage is that the seasonal temperature fluctuations have little influence on the system's efficiency. Finally, this method requires little to no maintenance.

- Horizontal Heat Exchangers obey the same principle of the boreholes described above, but instead they are installed horizontally on the shallow ground on a dense pattern of heat exchanger loops. The fact that the pipes are installed near the surface take a toll on the system's efficiency due to the seasonal variation of the soil temperature in the first 10 meters. Besides, solar irradiation of the surface soil has to be assured. On the other hand, the installation costs are cheaper than drilling a borehole well. (McCorry & Jones, 2011)

- Energy Foundations are the denomination given to structural foundations equipped with heat exchanger pipes integrated into its steel mesh. The geometry of such piles is determined by structural requirements and not by energy demands. In fact, the installation of the heat

exchanger pipes should not reduce the design bearing capacity prescribed. Static testing of the foundations are recommended to exclude any possible doubts. It is possible to install the system with bored piles or pre-fabricated press piles. (UPONOR catalogue, 2012) Using the piles as a heat exchanger takes advantage of its high thermal conductivity, which enhances heat transfer underground and, therefore, the system's efficiency (Brandl, 2006). Besides, this technique avoids excavating extra soils, which represents an initial cost advantage when comparing to other systems.

- Ground water wells are the typical open loop system, where water is pumped from a natural aquifer through heat exchanger pipes and later is returned to the aquifer by an injection well. This is a very efficient system because the heat carrier fluid is the ground water itself, meaning that the water reaches the heat pump exactly at ground temperature. Besides, there is no need for great lengths of pipework. However, pumping power for water extraction/injection is a downside and the sustainability of the ground aquifer must be guaranteed. Maintenance of such systems are also higher than any closed systems. In this case, GSHP may be also known as GWHP (Ground Water Heat Pumps)

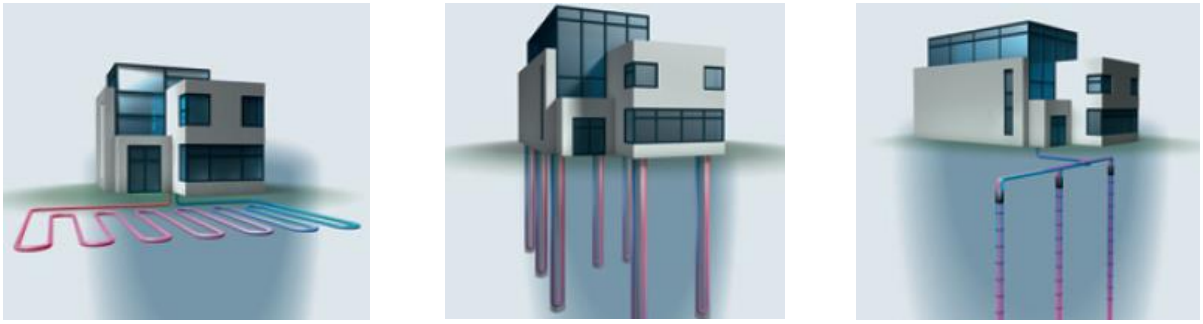

Figure 2.11. Horizontal heat exchangers (left); Energy Piles (center); Borehole Heat Exchangers (right) (images taken from Uponor catalogue)

The pipework involved in the mentioned solutions are usually made from polyethylene due to its flexibility and durability. Diameters range from 25mm to 60mm.These pipes may also take several configurations, and are classified based on their cross-sectional geometry and/or type of flow. Two basic configurations are the fundamental designs for all the other types: the coaxial and the U-tube.

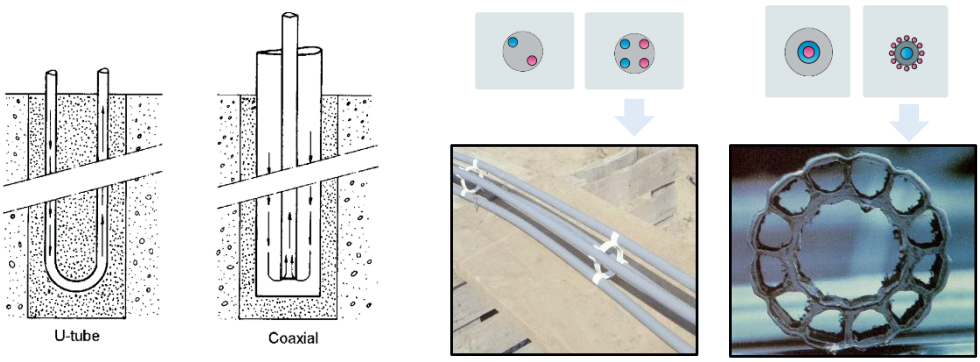

Figure 2.12. The fundamental piping designs schematics (left) and other variations (right). Images taken from (McCorry & Jones, 2011) and (UPONOR catalogue, 2012) respectively

The dimensioning of coaxial and U-tube collectors depends on the balance between heat demand and heat capacity needed for each collector. Several factors like ground conditions, pile/borehole diameter, workload hours and heat pump capacity are taken in consideration. However, it is clear that for U-tube collectors, the further apart the inlet tube is from the outlet (shaft distance), better the performance.

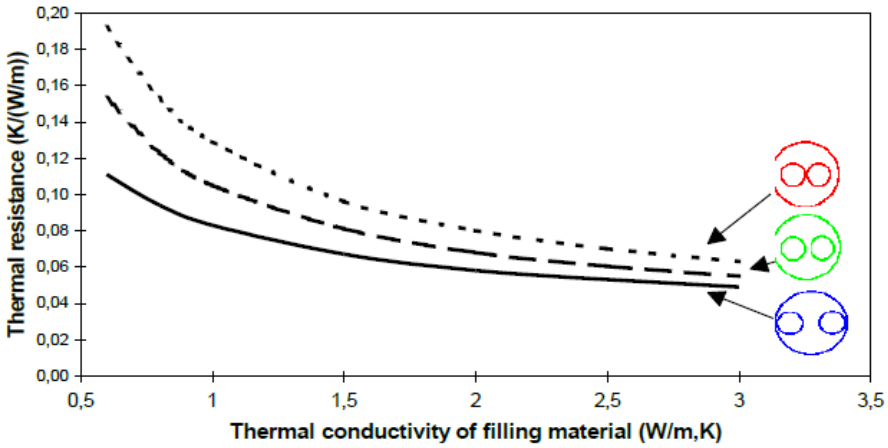

Figure 2.13. Shaft distance influence on a borehole's thermal resistivity (McCorry & Jones, 2011)

As previously mentioned, energy piles reduce land use area and drilling costs when compared to other GHP systems. The heat transfer problem obeys the same principles as other systems, with exception made to the mechanical effect of temperature variations on the foundation piles. So, instead of a thermo-hydrological interaction, a thermo-hydro-mechanical interaction may be considered. In this thesis, only the thermal interaction is studied.

This master thesis focuses on a case study of a building that includes, in its design, more than 80 energy piles. When modelling heat transfer in shallow geothermal systems, two distinct situations may occur: The first situation is related to the heat transfer between plane surfaces, for instance, between the soil and the atmosphere. In this case, heat propagates only in one direction, according to a temperature gradient imposed at the surface. This problem was solved for different boundary conditions and heat supply (Adam & Markiewicz 2002, Hofinger 2002). The second situation describes heat propagation from the vertical borehole to the surrounding soil. In this case, the energy foundation is modelled by a cylinder, hence propagating heat radially from its centre

Both cases are easily deduced from equation (2.24), either by considering only direction xx or by changing the referential from Cartesian to cylindrical coordinates:

$$Heat\ Conduction\ Law: \nabla^2 T = \frac{1}{\alpha}\frac{\partial T}{\partial t} \tag{2.28}$$

$$Case\ 1: \frac{\partial^2}{\partial x^2} T(x,t) = \frac{1}{\alpha}\frac{\partial}{\partial t} T(x,t) \tag{2.29}$$

$$\text{Case } 2: \frac{\partial^2}{\partial r^2} T(r,t) + \frac{1}{r}\frac{\partial}{\partial r} T(r,t) = \frac{1}{\alpha}\frac{\partial}{\partial t} T(r,t) \tag{2.30}$$

The previous cases only consider the conduction mechanism. That means that no water flow is assumed, and no advection from ascending vapour is also assumed. Furthermore, more complex models that simulate heat transfer inside the borehole have been described. For instance, the governing heat transfer equations for a U-tube heat exchanger, may be described considering the interactions inside a control volume with three components: The pipe-in (i), the pipe-out (o) and the grout (g) (Al-Khoury R, 2011). In this formulation, the coefficient b represents the thermal resistence between the different elements and u is the Darcy's velocity of the circulating fluid.

$$\text{Pipes} - \text{in}: \quad \frac{\partial T_i}{\partial t} \rho c - \lambda \frac{\partial^2 T_i}{\partial z^2} + \rho c u \frac{\partial T_i}{\partial z} = b_{ig}(T_i - T_g) \tag{2.31}$$

$$\text{Pipes} - \text{out}: \quad \frac{\partial T_o}{\partial t} \rho c - \lambda \frac{\partial^2 T_o}{\partial z^2} + \rho c u \frac{\partial T_o}{\partial z} = b_{ig}(T_o - T_g) \tag{2.32}$$

$$\text{Grout}: \quad \frac{\partial T_g}{\partial t} \rho c - \lambda \frac{\partial^2 T_g}{\partial z^2} = b_{ig}(T_g - T_i) + b_{og}(T_g - T_o) \tag{2.33}$$

The real thermal behaviour of GSHP is very complex to describe and the computation of all its variables represents a heavy calculation effort. Even the U-tube model presented above neglects a few aspects like: The temperature gradient between the pipe's inner and the outer wall; The variation of the thermal conductivities as the material's temperatures change; The fluid's velocity should not remain constant for different temperatures.

As this thesis is a preliminary analysis of an energy pile, only conduction will be considered, as a simplification. Therefore, case 1 and case 2 previously mentioned, in combination with each other, should suffice for a simplified approach.

2.3.4. System efficiency

According to SGHP systems designing manuals (McCorry M & Jones G, 2011) there are three terms upon which the efficiency of a SGHP systems depends on. The first one is the efficiency of the heat pump as a cold vapor machine. This depends mainly on the quality of the components used in the heat pump. Secondly, global efficiency depends on the heated or cooled water produced by the heat pump, which usually ranges from 30ºC to 60ºC depending on user's end use. Finally, efficiency depends on the temperature of the incoming heat exchanger pipes, buried in the ground. This last term is essential for the sustainability of the GSHP because, ultimately, if the soil cannot provide or dissipate the incoming heat, the heat pump might shut down in overheat.

Energy efficiency relates the input of primary energy used with the useful heat output for heating purposes, in percentage. Geothermal heat pumps have efficiencies larger than 100% both in heating and cooling. To avoid the awkwardness of these values, performance coefficients are usually used to characterize the performance of GSHP. For heating, a coefficient of performance (COP) is used, while for cooling an energy efficiency ratio (EER) is used. In theory these parameters are defined as follows (Monroe B. et al, 2014):

$$Energy\ output\ from\ Heat\ Pump = Energy\ input\ for\ operation + Energy\ trades\ with\ the\ soil \quad (2.34)$$

$$COP = \frac{Energy\ output\ from\ Heat\ Pump\ (kW)}{Energy\ input\ for\ operation\ (kW)} \quad (2.35)$$

$$EER = \frac{Energy\ trades\ with\ the\ soil\ (Btu/h)}{Energy\ input\ for\ operation\ (kW)} \quad (2.36)$$

In literature, EER is often mentioned as a cooling efficiency ratio measured in Btu/h per Watts. This approach intends to compare the heat pump in the reverse cooling mode, with the heat pump of a central air conditioner. Therefore, discretion is advised when reading such values. The difference between EER and $COP_{cooling}$ is a simple unit conversion

$$COP_{cooling} = \frac{EER}{3.413} \quad (2.37)$$

Theoretically, the COP of a heat pump is restricted by the second law of thermodynamics, where the efficiency depends on the temperature of the cold source (T_c) and hot source (T_h) in Kelvin. (Sarbu I & Sebarchievici C, 2014)

$$COP_{heating} \leq \mathrm{COP}_{theoretical} = \frac{T_h}{T_h - T_c} \tag{2.38}$$

$$COP_{cooling} \leq \mathrm{COP}_{theoretical} = \frac{T_c}{T_h - T_c} \tag{2.39}$$

It is easy to realize that the larger the difference between T_h and T_c, the smaller is the efficiency. In figure 2.14, the relationship between COP and the source temperature (soil) for a heat pump in heating mode can be seen.

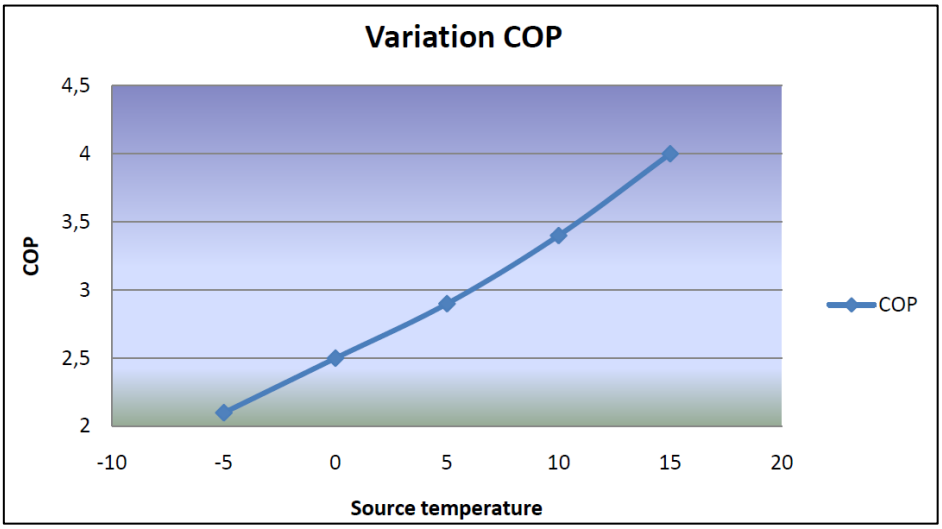

Figure 2.14. Values of COP for a heat pump producing hot water at 45ºC (McCorry M & Jones G, 2011)

As mentioned in previous chapters, GSHP are seasonal adaptive technologies. Therefore, it is possible to measure different efficiencies for the same heat pump, in different time frames. If the COP is measured for the whole duration of the heating or the cooling season, then its value represents the *seasonal performance factor.* Besides, the SPF measures the actual *Usable Energy Output*, instead of the *Heat Pump Output* which accounts for the energy losses of other energy consuming elements (e.g. circulation pumps) (Brandl H, 2006)

$$SPF = \frac{Usable\ energy\ output\ from\ System\ (kW)}{Energy\ input\ for\ operation\ (kW)} \tag{2.40}$$

When designing a GSHPS or any other kind of HP, the energy demands of the building should be taken into account. For instance, a heat pump that consumes 100kW.h and produces 600kW.h has COP=6. However, the total heating demand of a building is 10MW.h, meaning that the HP only accounts for 6%

of the energy demand. The sizing factor (SF) is often mentioned in literature to evaluate how efficient the system is, regarding the building's demands (Sarbu I & Sebarchievici C, 2014)

$$SF = \frac{Energy\ output\ from\ Heat\ Pump\ (kW)}{Energy\ Demand\ (kW)} \tag{2.41}$$

Sometimes it may not be economically feasible to rely on GSHP for acclimatization if these installations don't account for a large percentage of the energy demand. Large GSHP installations include the Dock Midfield Zurich airport, which has over 300 energy piles, accounting for 85% of the annual heating demand. In Germany, Berlin's International Solar Center relies on 200 energy piles to achieve 20% of heating and 100% of cooling demands. (Monroe B. et al, 2014)

All the efficiency factors mentioned above may be used to evaluate the performance, but usually the COP is the most common, because it's the easiest to measure. The higher the COP, the more efficient is the system. For instance, a COP = 4 means that for each unit of energy used to power the heat pump, there are 4 units of energy that are put back into the secondary heating system. For economic reasons, the recommended COP of a heat transfer system should be larger than 4, however, values between 3 and 4 are not uncommon. When comparing the energy efficiency of other heating systems with the GSHP there is no doubt which ones performs better. (Sanner B, 2006)

Table 3. Typical Values of COP for different heating equipment

Comparison of the efficiency of Heating Systems (Self S. et al, 2013)	
Ground source heat pumps	3-6
Air source heat pumps	2.3-3.5
Electric baseboard heaters	1
High-efficiency natural gas furnaces	0.88-0.97

The COP of a GSHP depends on several factors including: the local method of electricity generation; climate; refrigerant used; size of the heat pump; thermostat controls; quality of the installation (Sarbu I and Sebarchievici C, 2014). However, those are all "*above the ground*" factors. Other factors that may be called "*geotechnical"* factors play an important role (Brandl H, 2006): Thermal properties of the soil; difference between the cold source and the hot source temperatures; length of the thermo-active foundations; heat extraction rate; Hydrological conditions of the soil.

3. Case Study: the CICFANO university building

3.1. Building overview

The purpose of this master thesis is to investigate the performance of the shallow geothermal heat pump system as part of a building's acclimatization installation. In Portugal, there are currently some academic buildings under study named as CICFANO and CCI, where this technology is being used and both are located in Aveiro's University (UA). The building evaluated in this investigation is designated by CICFANO (Complexo Interdisciplinar de Ciências Físicas Aplicadas à Nanotecnologia e Oceanografia). CICFANO consists of a building built in 2012 in between two other existing buildings. The GSHP was integrated in the project from the beginning, but it has only been functional since mid-2013. The second building equipped with this technology is named CCCI (Complexo das Ciências de Comunicação e Imagem) and it was inaugurated December 15th 2016. The Geothermal System is not yet operational and hence this building will not be analysed in the thesis. The UA is located close to the Atlantic Coast, about 10Km into the mainland, in the central north region of Portugal. Figure 3.1 shows the location and shape of these buildings.

Figure 3.1. Location of CICFANO and CCCI buildings at Aveiro University campus and close-up of the CICFANO building.

On February 10th 2017 a field trip took place to visit both buildings and the geothermal command centre, which covered the entry/exit heat exchanger pipes, heat pumps, instrumentation and the controller software. Several disturbed soil samples were recovered from field surrounding CICFANO.

The CICFANO building has a rectangular shape, comprising a deployment area of 1600m^2. The gross building area is 4514m^2 including three floors (2 elevated). It is founded on a total of 110 piles (ϕ600mm,

L=10m and ϕ400mm, L=10m), distributed as shown in figure 3.2. From those piles, only 85 are thermally activated with heat exchanger pipes (PEXa100). However, each primary heat exchanger circuit is coupled to more than one pile (series display). Therefore, there are only 30 primary circuits coupled to the foundations.

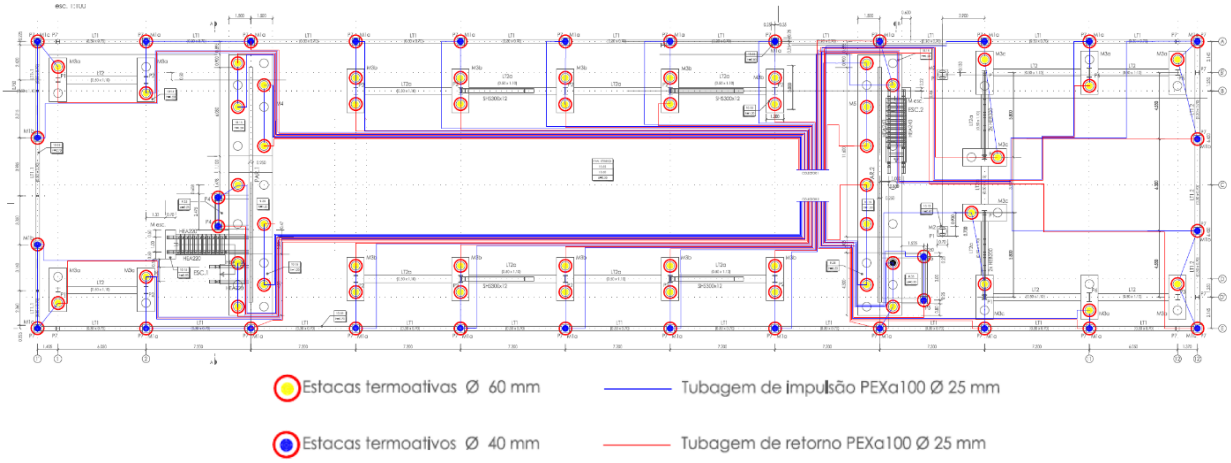

Figure 3.2. CICFANO's building foundation and hydraulic network schematics (no scale)

The acclimatization of the building results of a combination of techniques, including a GSHP and a Biothermal Heat Pump System (BHPS) as heat sources. These underground systems provide thermal energy to a secondary pipe system. The secondary system directly provides heat to the walls and slabs of the building, by means of extensive pipework embedded in the concrete. Alternatively, it may also trade head with several ventilation units (UTAN's), responsible for the air conditioning of the building. These acclimatization systems are continuously adapting to the user's needs, according to the monitoring devices strategically placed in the classrooms, hallways and corridors. The geothermal system is controlled in real-time by a software, from which an image is shown in figure 3.3. It is this software that determines whether the heat pumps should be turned on or off. Regarding the heat pump equipment, the condensation-evaporation cycle works with a COP of 4.1.

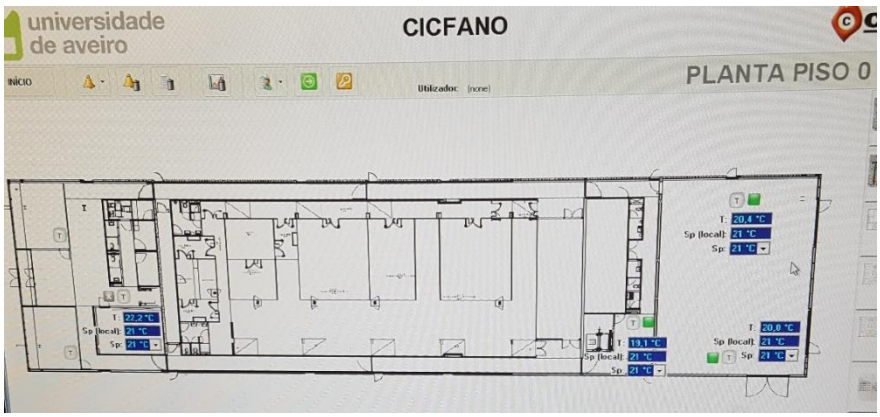

Figure 3.3. Controller software: representative information output from "floor 0"

In order to study the thermal behaviour of the soil underneath the CICFANO building, when subject to the thermal loads of the GSHP, three elements must be assessed:

- Climate of the Aveiro region: it plays a major part in this analysis because not only it directly influences the natural temperature of the soil, but it is also a decisive factor when determining the energy demands of the building.
- Energy demands of the building: they must be analysed because they determine what kind of energy trades will be solicited from each thermos-active pile
- Soil characterization: it is an obligatory part of this study, in particular the quantification of the hydro-geological and thermal properties and the definition of the geotechnical model.

3.2. Climate analysis

The climate data used in the analysis was retrieved from two different sources. The first source was an online database called *worldweatheronline.* This database provides historical information about the climate around Aveiro's city from as early as 1986 and up to (and including) 2016. However, for a more accurate evaluation of the building's thermal performance, another climatic station was also used. This second station is located closer to the UA campus, no more than 200 meters from the building. From this source, temperature readings taken every 10 minutes, referring to the period between October of 2013 and September of 2014 (365 days), were analysed. Regarding the hourly variation of the temperature, only one source was used and a constant temperature oscillation was considered throughout the year.

The methodology for the climate data retrieved from *worldweatheronline* was simple, since the database only provides monthly temperature values for the average, maximum and minimum readings. The UA campus data required further treatment, since the reading had to be transformed in daily and monthly averages. All data was then fit of a harmonic equation:

$$T = A + B.sen\left(\frac{2\pi t}{365} + C\right) \tag{3.1}$$

By using the *solve* tool in *Excel*, which changes the parameters A, B and C to minimize the measurement of the error, which was estimated using the squad error formula given by

$$Error = \sum (T_i - \overline{T}_i)^2 \tag{3.2}$$

Figure 3.4 shows the result determined by the *solve* tool for data retrieved from the UA campus. Nevertheless, all the remaining graphics from the other sources can be found in annex C. Condensed

in figure 3.5 are the analytical estimations for all the data sources and timeframes that were found. All the presented analytical curves exhibit a R^2 larger than 98% related to the real data.

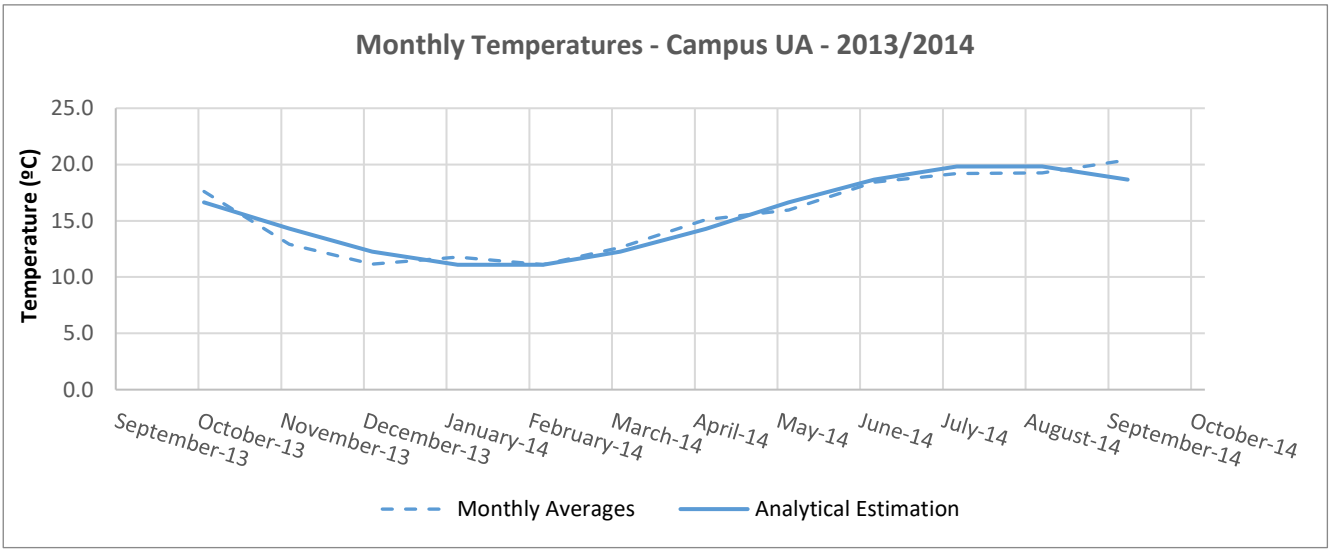

Figure 3.4. Outdoor temperature data for the UA during 2013/2014

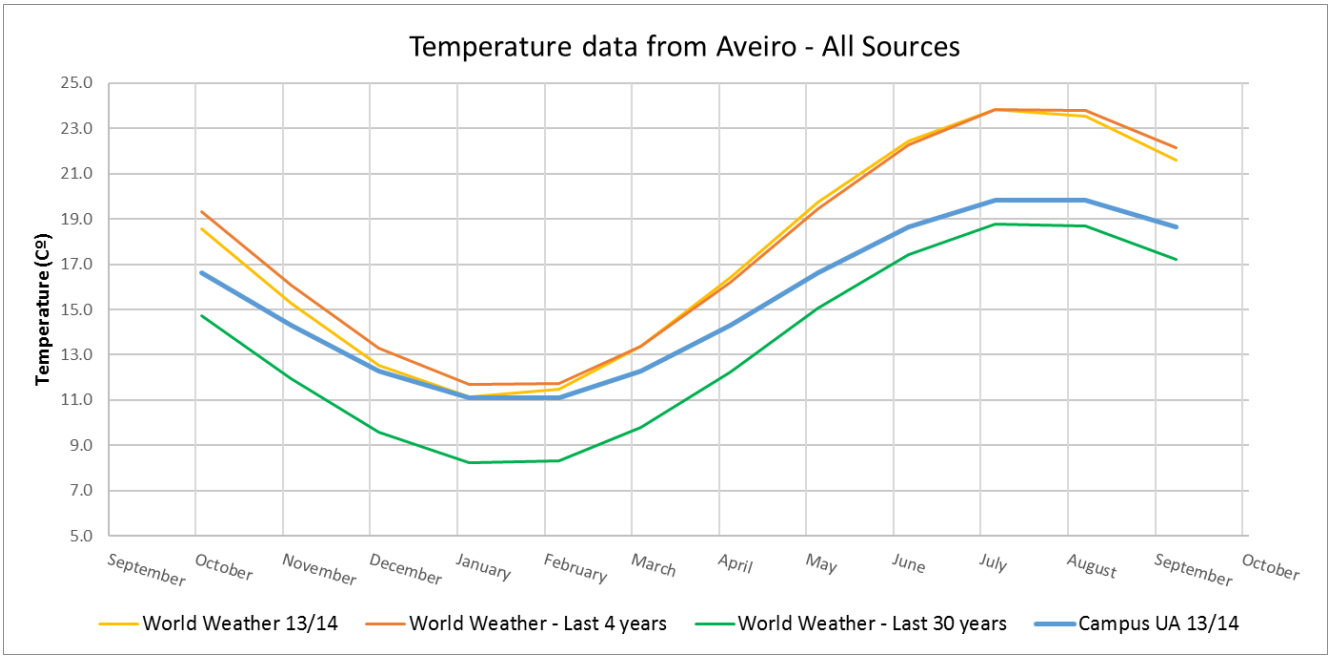

Figure 3.5. Analytical sinusoidal fits for all data sources

By comparing the *Worldweatheronline* data for different timeframes, the difference is quite obvious. In the last 4 years, average monthly temperatures are considerably higher than the ones registered during the 30-year time spam, in an yearly average of 4.3ºC. This is an indicator that yearly average temperatures are rising in Aveiro. The same conclusion can be taken when looking specifically to the year of 2013/2014. However, for this 12 months' period, it may also be seen that temperature is source

dependant. The two stations are separated only by approximately 6 kilometres, and yet the measurements show some differences. Globally, temperature data retrieved from the lighthouse is higher than the one taken from the University Campus, especially in the summer. This differences between the two measurements was not investigated, but the wind exposure is a well-known factor that influences temperature readings. As it can be seen in table 4, the locations of the reading equipment are quite different.

Table 4. Description of both weather data sources from Aveiro

Source	Location	Coordinates
WorldWeather Data	Lighthouse close to the sea	40°38’35"N 8°44'50"W
UA Campus Data	Close to the University	40°38'07"N 8°39'35"W

As previously mentioned, the weather action to consider is an important parameter when investigating the behaviour of a GSHPS. From the climate assessment performed above, it is clear that different sources of information may play an important role when simulating the behaviour of such systems. CICFANO geothermal system has been operating since 2013, hence being subject to the temperatures analysed in this chapter. Furthermore, it makes sense to consider a source as close as possible from the building. Hence, the blue curve “Campus UA 13/14” from figure 3.5 will be the one considered in future simulations. The analytical equation for that curve was found to be:

$$T = 15.46 + 4.52 * sin(t * 2\pi/31536000 + 2.36) \quad (3.3)$$

3.3. Energy demand analysis

This assessment of energy demand focuses on two aspects: what are the building requirements and what trades are expected from the thermo-active piles. Due to the limited depth of the energy piles, the system is only expected to satisfy 75% of heating demand and 65% of cooling demand. In accordance with the data provided by the University of Aveiro, the building’s requirements for heating are 96.1 MWh/year for heating and 62.3 MWh/year for cooling. However, this data must be subject to treatment, in order to fit the analytical temperature equation determined in the previous chapter. According to the climate data, the average annual temperature was estimated to be 15.45ºC. As a simplification, it is assumed that building only requires heating if temperatures drop below that value and, similarly, it only requires cooling if temperatures rise higher than the average temperature. In that regard, the months that will require cooling are: May, June July, August, September and October. On the other hand, heating loads will be applied only in: November, December, January, February, March and April. Figure 3.6 shows which periods are subject to cooling loads or heating loads, based on the deviation from the average temperature.

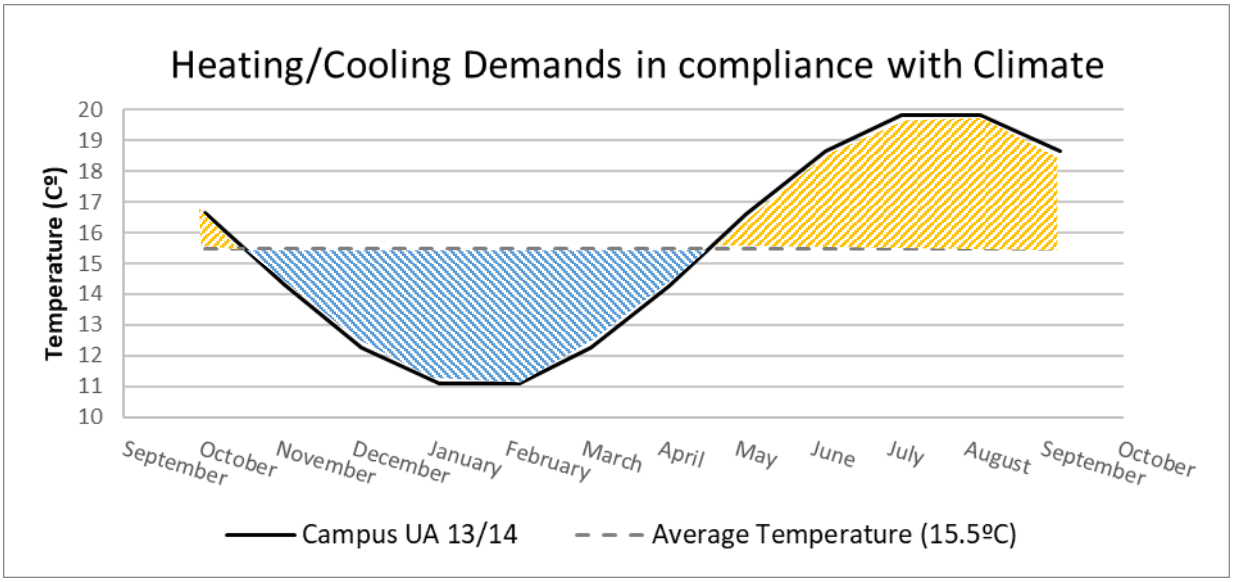

Figure **3.6**. Heating and cooling periods based on average annual temperature

This hypothesis ensures that in heating season, the heat pump works only in heating mode, disregarding any short periods where cooling would be necessary. The same assumption is made for the cooling season. The second assumption from this hypothesis assumes that the heat pump works constantly, on a 24-hour basis. This simplification implies that no peak load will be imposed to the soil, therefore the analysis is based on an average continuous load. The raw data available, was processed in order to comply with the GSHP design, resulting in a maximum limit of 24 W/m in heating mode and 13W/m in cooling mode. This values already consider a heat pump efficiency of 4.1 and assume a uniform heat load distribution among all 85 energy piles. Figure 3.7 shows the final energy load for each pile.

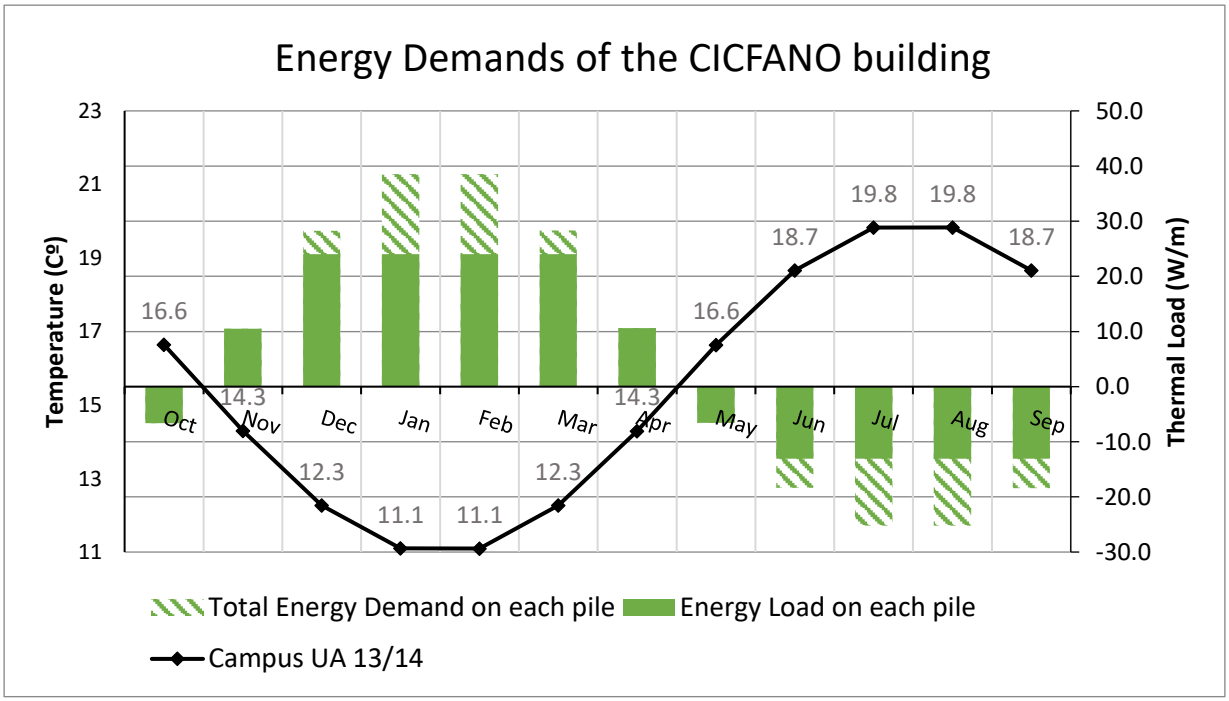

Figure 3.7. Energy monthly requirements for a single thermo-active pile

As mentioned before, in the months where the energy demand is too high, the system cannot provide the total amount necessary. Hence the differences in the bars shown in figure 3.7. In borehole heat exchangers, values of 50W/m-100 W/m are considered rule of thumb values for the specific heat extraction rate (McCorry & Jones, 2011). The values required from the heat exchangers in this analysis will be considerably lower (from 6.6 W/m to 24 W/m) simply because it is considered that this heat pump's work load is spread out through approximately 730 hours every month, while in reality they won't surpass the 150 hour/month.

3.4. Soil analysis

The information available about the existing soil of the Santiago Campus consists of a geotechnical study performed in 2009 by the company GSG Lda (Gabinete de Serviços Geotécnicos). This study comprehended four boreholes drilled using a rotary drilling technique. Standard Penetration Tests (SPT) was performed on each of the boreholes, with readings done every 1,5 meters. Also, some disturbed samples were extracted.

From that study it was clear that two different layers could be identified in the first 7.5 meters. The first one, consisting of old beach/river sand deposits, could be found up to at least 4.2 meters of depth. The second layer, consisting of claystones and siltstones typical from the city of Aveiro, could be found at depths larger than 4.2 meters.

Based on this information, already available on the geotechnical report, further analysis need to be conducted in order to access the thermal parameters necessary to an accurate simulation. Hence, two samples were used for such purpose:

- Undisturbed sample recovered in February 2017, from the siltstone/claystone stratum, stored in a wet chamber located at LNEC (sample 5422)
- Disturbed sample recovered in February 2017, from the upper layer made mainly of sand, stored in the geotechnical department's facilities in LNEC (sample 5447)

The author followed and participated in all the laboratory works, under supervision of an experienced technician. Laboratory testing was performed in accordance to the Portuguese official procedures in the National Laboratory of Civil Engineering (LNEC). The works included the determination of the granulometric composition of both soils, the determination of the void ratio (e_0) and Atterberg Limits of the undisturbed sample. The grading size distribution analysis resulted in the curves shown in figure 3.8.

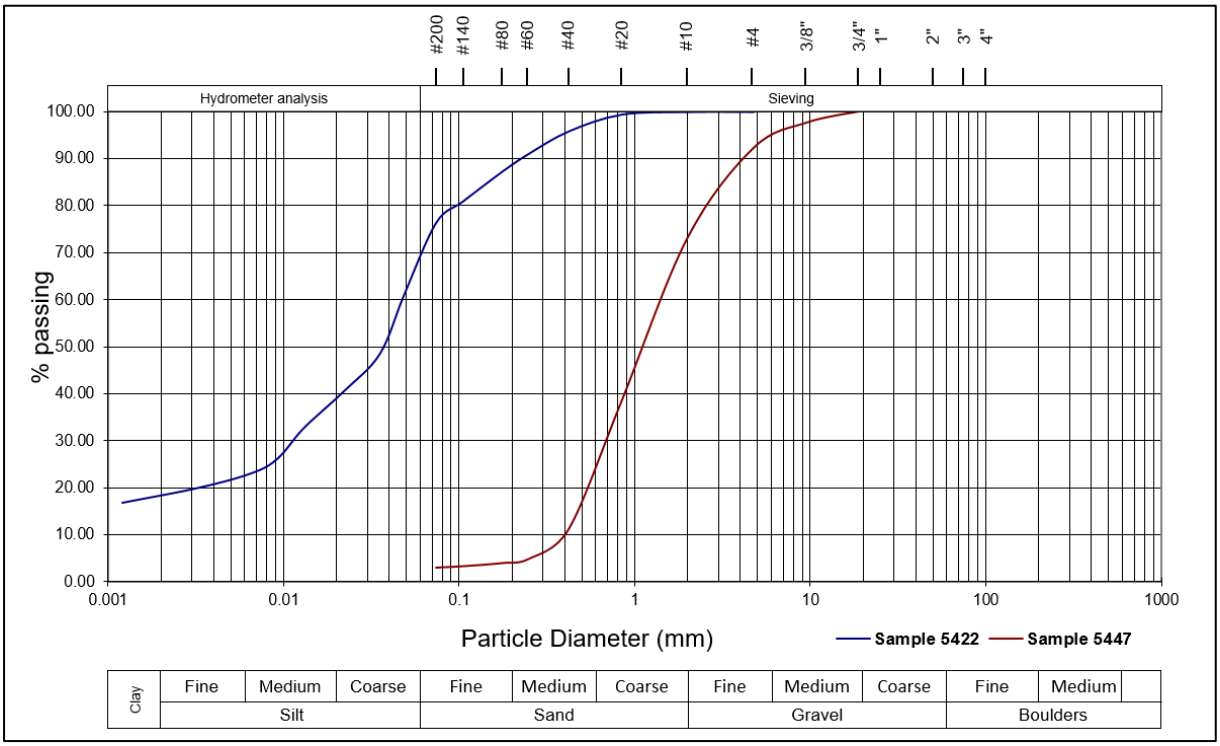

Figure 3.8. Particle size distribution of sample number 5422 (silty soil) and sample 5447 (sand soil)

The Atterberg Limits of sample 5422 were determined according to the international norm ISO/TS 17892-12. For the liquid limit (LL) the chosen method was the Casagrande test. On the other hand, for the plasticity limit (LP), crackling formation on drying soil filaments was the chosen method.

Using the particle size distribution curves together with the Atterberg limits it was possible to classify the soils according to Unified Soil Classification System (USCS) from the ASTM, and the results can be seen in table 5, for both the upper and lower layers.

Table 5. USC of sample 5422 (left) and 5447 (right), together with the relevant information

SP : Poorly Graduated Sand				ML-CL : Silty Clay with sand			
Cc	Cu	%Gravel	%Sand	LL	PL	PI	%fines
0.82	3.75	27	71	22.9	17.8	5.1	75

Furthermore, the determination of the initial void ratio (e_0) is a crucial step in order to acquire the required information for empirical determination of the thermal conductivity. As previously shown in chapter 2 all empirical methods are based on the porosity (χ) of a given soil. Porosity relates the void ratio in the from

$$\chi = \frac{e_0}{1 + e_0} \tag{3.4}$$

In the process of determining e_0, other relevant information was acquired about the CICFANO claystone. All the important data is presented in table 6.

Table 6. Soil characterization results obtained for the CICFANO's lower layer soil

w (%)	G_S	γ_{dry} $(g.cm^{-3})$	γ_{sat} $(g.cm^{-3})$	S (%)	e_0	χ (%)
18.2	2.70	1.82	2.15	100	0.483	0.326

The lack of undisturbed samples from the upper layer of sand, hinders the investigations regarding its natural state. However, laboratory work has been performed in Instituto Superior Técnico (IST) using the disturbed samples, in order to determine the void ratio values envelope for this soil (Cruz,2017). Vibro-compaction of the sample showed that minimum void ratio of this material was 0.334, while the disturbed sample exhibits a void ratio of 0.729. Natural soil will obviously have e_0 values between those two extremes. Therefore, for simulation purposes, it is assumed that an average value of 0.532 for the void ratio, which implies a porosity of 34.7%. In his thesis, Cruz also measured the thermal conductivity of the disturbed sand samples, which were dried in a controlled humidity chamber for a week. Using a thermal needle, he determined the thermal conductivity to be 0.44 W/Mk for a sample with average void ratio and dry conditions. The measured value refers to the effective thermal conductivity λ_{eff} of a dry sample.

At this point the information about the dry sand soil layer consists of the porosity (34.7%) and the λ_{eff} (0.44W/mK), which is enough to perform a back analysis in order to determine the solid phase thermal conductivity (λ_s). As mentioned in chapter 2, one of the most common empirical relations to determine effective thermal conductivity is the geometric average, where

$$\lambda_{eff} = \lambda_s^{\chi_s}.\lambda_w^{\chi_w}.\lambda_a^{\chi_a} \tag{3.5}$$

Cruz M. measured the dry effective conductivity, where $\chi_w = 0$ and hence the equation may be simplified to the multiplication of only two factors. Considering that simplification, a geometric back analysis of the thermal conductivity reveals that $\lambda_s = 3.56\, W/mK$. Therefore, the resulting effective conductivity of the saturated sand obtained from equation 3.4 is $\lambda_{eff} = 1.89\, W/mK$.

Despite all the laboratory investigations, direct measurement of the thermal conductivity for the silty layer was not possible. The option was to perform mineralogy analysis for both soils, in order to assess the thermal conductivity based on the soil's constituents. The analysis was performed in LNEC, by means of the reference intensity ratio method (RIR). Both samples 5422 and 5447 were subject of the analysis. Results can be seen in table 8. The RIR method was based on the X-Ray diffraction test performed on both samples.

Surprisingly, these tests show that both the sandy soil and the silty soil have extremely similar compositions. Based on that fact, it may be assumed that empirically, both soils will have similar λ_s, if

the same arrangement of the soil is assumed. Since sample 5422 displays a porosity of 0.326, effective thermal conductivity may be calculated according to equation 3.4 to be $\lambda_{eff} = 1.96\, W/mK$ considering saturated state.

Table 7. Mineralogical composition semi quantitative of sample 1 (silty soil) and 2 (sandy soil)

	Compostos cristalinos*						
Amostras	Quartzo	Moscovite	Albite	Microclina	Ortoclase	Clorite	Caulinite
58/2017/1	92	1	1	3	1	1	1
58/2017/2	93	1	1	4	1	-	-

The location of the water table was first mentioned in the geotechnical report using the information of the four prospection boreholes. All of the borehole logs report the water table as being at a depth of 2 meters depth into the sandy layer. Nevertheless, other monitoring devices located in the University of Aveiro have shown that this reading changes seasonally. In fact, Summer season might reveal that the sandy layer is completely dry, as well as flooded in the rainy winter season. Considering that the city of Aveiro is located at the surroundings of a river mouth, the seasonal changes are to be expected. For the two extreme situations (totally dry and totally wet) there will be dramatically different thermal conductivities. Many examples of laboratory measurements of thermal conductivity of sands can be found in literature. For instance, Mitchel et. al (1978) measured thermal conductivity of several SP and SW sand samples using the transient thermal needle method. For dry sands, thermal conductivity falls between 0.2 and 0.5 W/mK. On the other hand, for saturated sands, λ varies between 1.5 and 3.0 W/mK. The measured values vary greatly because void ratio has an important impact on this parameter. Besides, the values determined empirically and by laboratory testing are compatible with those from VDI shown in annex B.

Taking into consideration all the information gathered, the geotechnical model that will be used in the numerical analysis is shown in figure 3.10. The remaining relevant features about the GSHP system can also be consulted in table 8.

Table 8. Information on the GSHP system to take into consideration in the simulation

Thermally Activated Piles	
Material	C30/37
ϕ600 (number of piles)	50
ϕ400 (number of piles)	35
Pile Lenght (m)	10.0
Thermal Cond. (W/mK)	2.0
Heat Exchangers	
Material	PEXa 100
Number of circuits	30
Thermal Cond. (W/mK)	0.35
Diameter (mm)	25
Building's Floor Slab	
Thickness (m)	0.2
Thermal conductivity	2.0

Thermal conductivity of the heat exchanger (pile + pipes) was arithmetically determined, assuming that heat propagates perpendicularly from the pile axis and all materials are disposed in a parallel distribution for a pile with a diameter of 0.6 meters. Such hypothesis is represented in figure 3.9, which results in an equivalent saturated conductivity of 1.61W/Mk, or1.33W/mK if the concrete is dry.

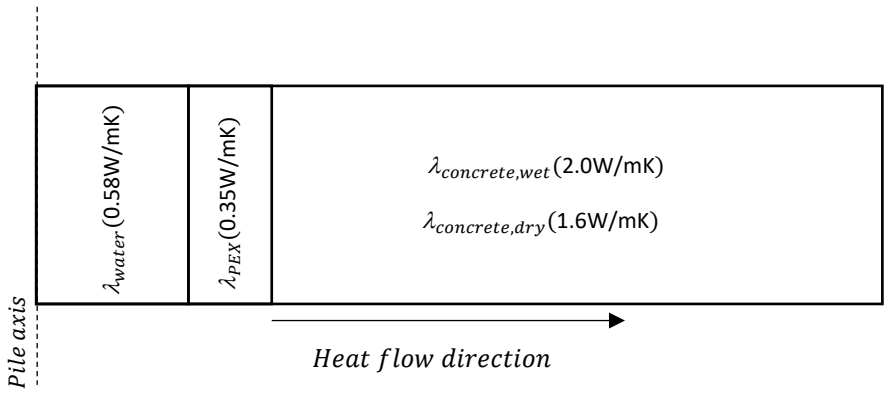

Figure 3.9. Scheme of the thermo-active pile model used to determine equivalent thermal conductivity

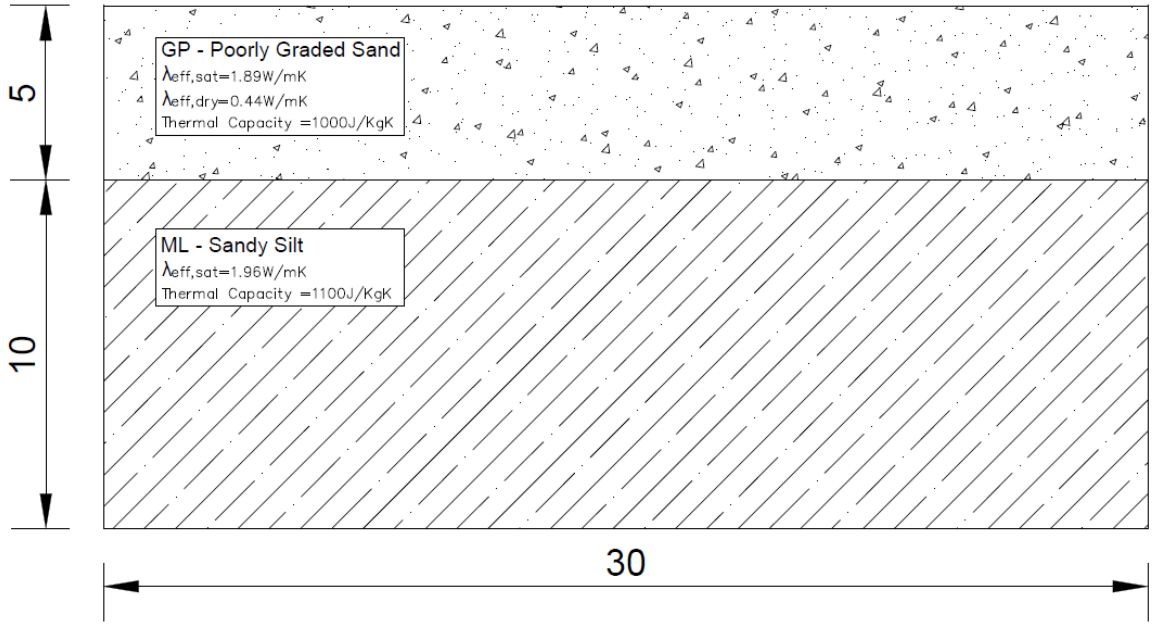

Figure 3.10. Geotechnical model of the foundation soil of the CICFANO building

4. Numerical Modeling

4.1. Preliminary numerical verifications

A numerical analysis was performed using software FLAC (*Fast Lagrangian Analysis of Continua*) from ITASCA Consulting Group, which is a tool for solving mechanical/thermal/hydraulic engineering problems. FLAC solves linear or non-linear problems using the finite differences iterative method. FLAC uses a programing language called FISH. All the code for the simulations was written in that language.

Prior to the development of the case study model using this numeric tool, a few summary verification problems are solved in order to demonstrate the reliability of upcoming results. The goal is to compare the results obtained using FLAC with well described analytical solutions. In section 4.2, a thermo-active pile will be simulated in an axisymmetric space to allow studying heat propagation perpendicularly to the pile, considering the thermal load applied along its axis, and also heat propagation occurring vertically across the half-space due to the climate wave imposed. Therefore, these two situations will be isolated, simplified and tested against analytical models. The summary of all verifications performed can be seen in table 8.

Table 9. Verifications performed using FLAC software

Model	Configuration	Verification	Analytical Solution	Grid Tested [m x m]
Infinite Line Source	Axysimetric state	Steady state conduction	Nowacki (1962)	20x20 and 40x40
		Transient state conduction	Nowacki (1962)	40x40
Infinite Half Space		Steady state conduction	Fourier Law of Conduction	40x40
		Transient state conduction	Wealthy (1974)	40x40

4.1.1. Infinite Line Source Verifications

A “Conduction Only” analysis in axisymmetric state was performed on a homogeneous soil, considering isotropic heat conduction model. A constant heat load was applied on the symmetry axis (i=1). The results were then compared against the analytical solution provided by Nowacki (1962), as shown in equation 4.1. The coefficient E_i represents the exponential integration operation, r is the radial distance from the line source, λ is the thermal conductivity and α the thermal diffusivity.

$$T = \frac{-Q}{4\pi\lambda} E_i\left(\frac{-r^2}{4\alpha t}\right) \tag{4.1}$$

The input data for the soil and for heat load are generic values and are representative of typical values found in GSHP problems. At the time of these verifications, investigations on the CICFANO case study were yet to be completed. Table 9 shows the relevant inputs for this simulation and figure 4.1 illustrates the model and one of the grid analyzed.

Table 10. Summary of the input data to the FLAC simulation

Simulation Data	
Thermal Step	1 hour
Simulation Time	5.71 years
Grid	40m x 20m
Thermal Cond.	1.25 (W/m.K)
Heat Capacity	900 (J/Kg.K)
Bulk Density	1900 (Kg/m^3)
Heat Load	50(W/m)

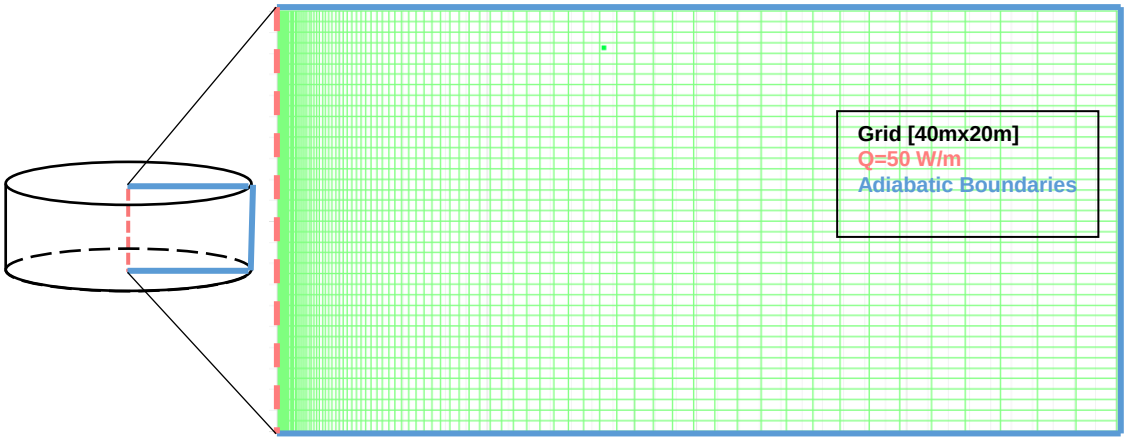

Figure 4.1. Actions and boundary conditions for the Infinite Line Source Model

The analytical representation shown in equation 4.1 solves the heat transfer problem for an infinite line source propagating thermal energy radially from its core. It considers both transient and stationary stages of heat conduction. In stationary state, temperature is time independent and the system is in thermal equilibrium. However, until stationary state is reached, transient conduction occurs and temperature changes with time. Nowacki's solution is able to account for both states by using the exponential integer function (E_i), which depends on the time elapsed (t). In this simulation, both the heat source and the soil properties are time and temperature independent.

Temperatures in the soil were computed for a constant heat load of 50W/m applied in the axis. Two grids were tested regarding their size: a squared grid with 20 meters of width, and a rectangular grid of 40x20 meters (width x height). The dimensions of the elements were kept equal. Therefore, the 40x20 grid had twice as many elements as the 20x20 grid. The two grids were tested in order to assess

minimum dimensions for problems of this nature. The absolute error calculated is the difference between analytical and numerical values for the same point, while relative error is the absolute error divided by the analytical value, in percentage. The results of the simulation can be seen in figures 4.2 and 4.3. It becomes quite clear that the quality of FLAC's estimations become less precise when the edge of the cylinder becomes closer (at 20.05m and 40.05) Both relative and absolute errors were considerably reduced after doubling the width of the grid. Furthermore, the 40x20 grid provided near perfect results up to a distance of 25.5 meters from the line source. For these reasons, future simulations will be based on a model with a length factor of at least 2:1 instead of 1:1 (width:height).

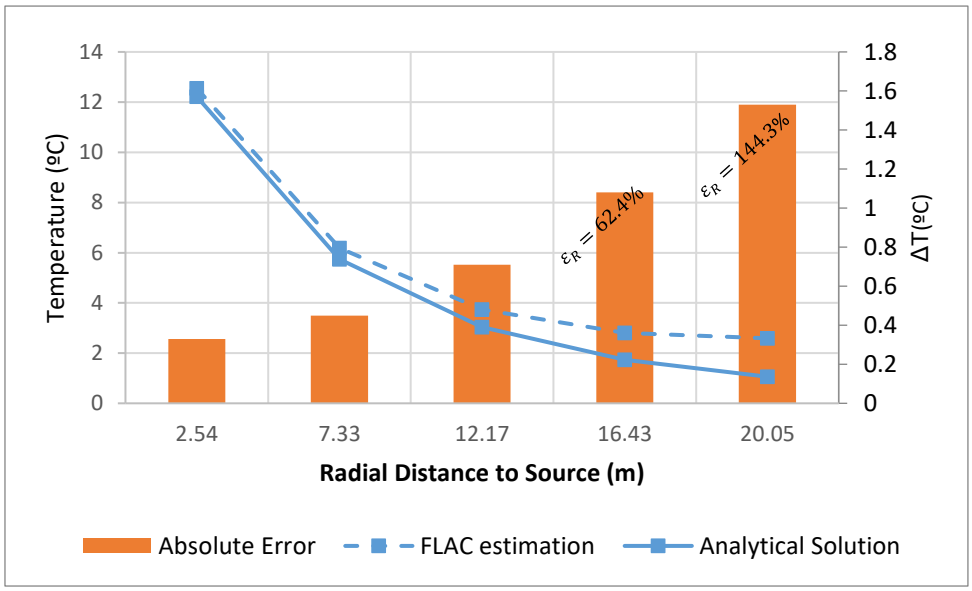

Figure 4.2. Temperature profile after 5.21 years of elapsed time. Absolute and relative errors ε_A and ε_R, respectively (20x20 grid)

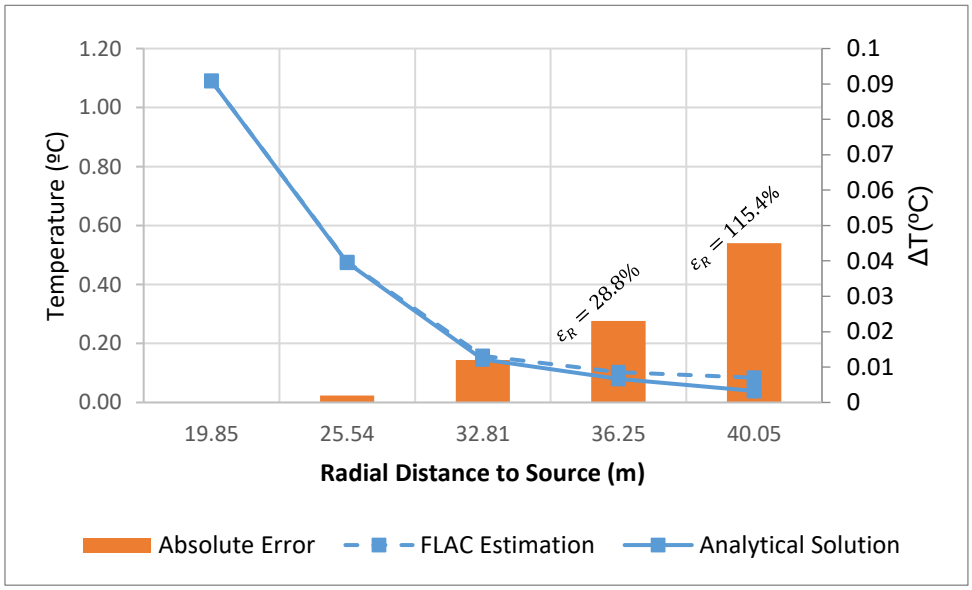

Figure 4.3. Temperature profile after 5.21 years of elapsed time. Absolute and relative errors ε_A and ε_R, respectively (40x20 grid)

The previous verification was developed to assess temperature distribution after a large duration of time, while the following verification takes in consideration early temperature changes along time, which tests heat transfer from the scope of transient response. Equation 4.1 can also be used to find the transient analytical solution. Three different points, ranging between 1 and 3 meters from the line source, were monitored every 1000 steps, registering its own temperature changes. Results can be seen in figure 4.4. The FLAC input is the same as in table 9, while the 40x20 grid was used since it was proven that it can provide more accurate results. Dashed lines correspond to FLAC calculations while solid lines are the analytical solution.

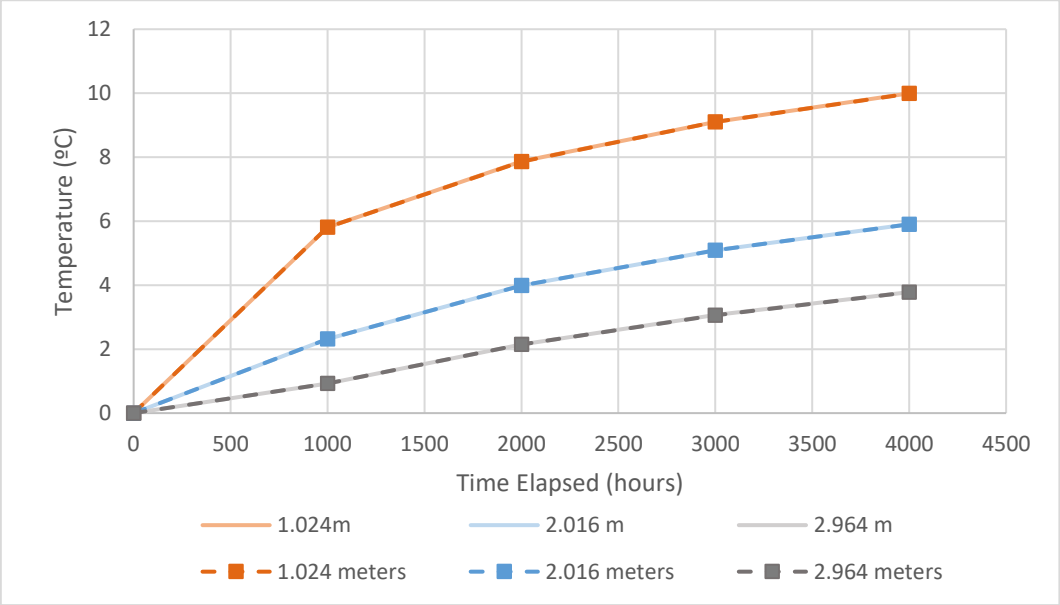

Figure 4.4. Results for transient heat conduction with infinite line source model, calculated on 3 points, during the first 4000 hours

As it is clear, estimations are very accurate in transient state, since differences are negligible and no further adjustments are needed. With this, all verifications regarding the infinite line source were performed and checked.

4.1.2. Heat Conduction in an Infinite Half Space

In the situation of an infinite half space, there are several analytical models to describe the conduction problem. The following verification is valid for transient state only, and it is based on equation 4.2 (Wealthy, 1974):

$$\frac{T_{(x,t)} - T_i}{T_s - T_i} = erfc\left(\frac{x}{\sqrt{\alpha t}}\right) \tag{4.2}$$

where *erfc* is the complementary error function, T_i is the initial temperature of the half-space and T_s is the surface temperature, fixed at a constant value.

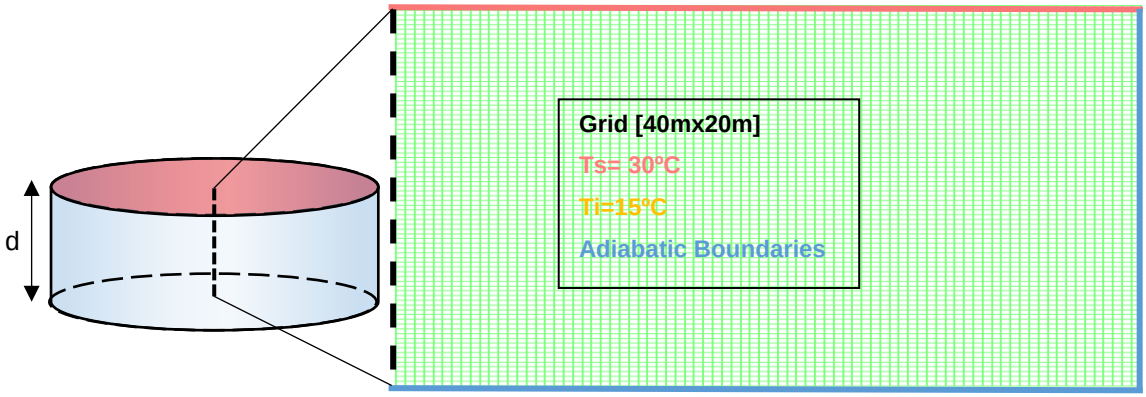

Figure 4.5. Actions and boundary conditions for the Infinite half-space model (transient state conduction)

Using the input data shown in figure 4.5, and a homogeneous soil with thermal conductivity of 1.25 W/Mk, transient heat transfer was measured in 4 points of the domain in the first 50 hours of simulation time. The grid used has the same number of elements as the 40x20 grid used in section 4.1.1. The elements are all equally dimensioned with 0.5m of width and 0.25m of height. Results can be found in figure 4.6, where dashed lines are the FLAC estimations and continuous lines are analytical results.

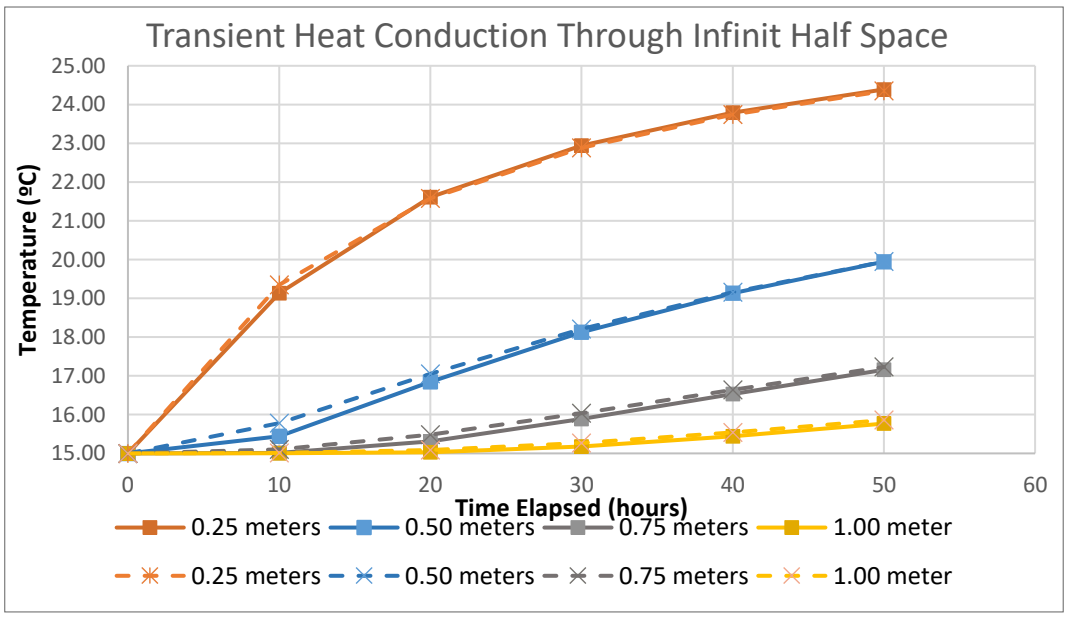

Figure 4.6. Transient heat conduction through infinite half space, measured in 4 points during the first 50 hours of the simulation (dashed lines are FLAC estimations)

The difference between analytical and estimated calculations is visible, mainly in the first 20 hours. However, not only those differences are independent from the location of the measured point, but also its absolute value never exceeds 0.34ºC (at 0.5 meters and 10 hours elapsed time). That value

represents no more than a 2.2% difference in relative proportions. Overall results have a high reliability and may be trusted in further analysis.

For the steady state verification, the same type of simulation was performed, exception made to the boundary conditions. In this case, different temperatures are applied to the top and bottom boundaries of the model, which will eventually cause a stationary conduction state across the 20 meters' cylindrical section.

The analytical solution for this conduction problem is described by the Fourier law of conduction in the form:

$$T_i = T_1 - \frac{q}{A} \times \frac{\Delta y}{\lambda} \tag{4.3}$$

Where the equilibrium heat flow is given by

$$\frac{q}{A} = \frac{\lambda}{d} \times (T_1 - T_2) \tag{4.4}$$

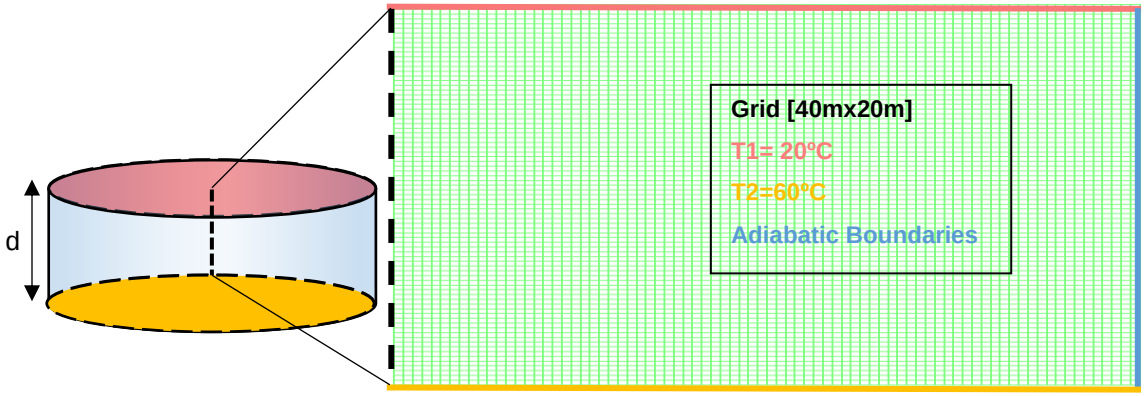

Figure 4.7. Actions and boundary conditions for the Infinite half-space model (steady state conduction)

FLAC accurately estimates temperatures across the grid, as can be seen in table 10. The results are not presented in a figure because the results overlap completely. Absolute errors never exceed 0.04ºC which corresponds to a relative error of 0.1%.

Table 11. Results obtained from the steady state heat conduction verification

Equilibrium Thermal Conduction [40mx20m]					
Vertical distance from the base (m)	0	5	10	15	20
Analytical Solution (ºC)	20	30	40	50	60
FLAC estimation (ºC)	20	29.97	39.96	49.97	60
Relative Error (%)	0	0.1	0.1	0.06	0

Overall with these verifications, it became proven that results obtained in further simulation will be trustworthy in the mathematical sense. Both transient and steady state conduction have been verified for two different kinds of heat source: a temperature boundary and a heat flux boundary.

4.2. Numerical modeling of a single thermo-active pile

The thermal behavior of a single thermo-active pile and its impact on the surrounding soil is investigated in this chapter. According to the investigations carried out in chapter 3 for the CICFANO building, three cases will be evaluated in terms of heat transfer in the soil for the durations of 365 days and after 5 years. In chapter 3 it was mentioned that the water table changes its position frequently. For instance, it might be located at the surface due to heavy rains or if the river reaches its flood level (usually in winter), but it may also be down to 5 meters of depth, which means that the sand layer is completely depleted of water (usually in summer). The phenomena described above will be modelled by considered those two extreme positions of water level, which translate in Case 1 and 2. Case 3 studies the effect of the building's slab on the soil mass.

Case 1: Considers the sand layer fully saturated, which corresponds to the location of the water table at surface (typical in rainy periods).

Case 2: Considering the sand layer completely dry, which corresponds to the location of the water table at a depth of 5 meters (typical in draught periods).

Case 3: Based on the summer case model (case 1) a second simulation will be performed taking in consideration the existence of a slab on the surface of the model, surrounding the head of the pile. This slab is a realistic boundary condition modeled as an applied temperature (constant indoor temperature)

Climate action considered was the average profile computed considering the data from Aveiro campus, previously presented in figure 3.4 and 3.5. This temperature wave was applied as a variable boundary condition on the surface of the model, changing its value each step of the simulation.

The influence of the thermo-active pile was modeled by a variable heat flux, applied as a boundary condition. This heat flux corresponds to a step function which reflects the analysis already presented in figure 3.6.

The soil input data will differ from case to case, as it will be explained later in this section. However, all the thermal parameters correspond to the ones presented in figure 3.10 (geotechnical model). Physical properties are the ones that were already presented in section 3.4.

As a summary of the three cases described above, table 12 shows the relevant input data:

Table 12. Model Cases Condition

	Water table	Slab boundary	Thermal conductivity	Climate Action	Thrmal Pile load
Case 1	At surface	Non existing	Sand: (1.89 W/mK) Silt: (1.96 W/mK)	Equation (3.3)	Step function (fig.23)
Case 2	At 5 meters depth	Non existing	Sand: (0.44 W/mK) Silt: (1.96 W/mK)		
Case 3	At 5 meters depth	Constant indoor temperature			

These models are defined considering the axisymmetric state previously described, which means that the domain revolves around the vertical axis of the thermo-active pile. Because of software constrictions, heat flux actions cannot be applied directly on the axis. To overcome this situation, the model's left boundary begins at x=0.05m. Isotropic conduction was the chosen thermal model for all simulations. Mechanical stress-strain implications induced by temperature changes are not computed. All the input parameters are considered to be temperature independent. The simulated pile is 10 meters long and has radius of 600 mm, according to the structural design. The size of the simulated space was defined based on pile length. Hence, 5 times the length of the pile in terms of horizontal dimension and 2 times in terms of the vertical dimensions. This size allows the user to assume adiabatic boundaries on the proper boundaries, where heat trades are not allowed. The grid obeys to a 0.75 densification ratio towards the pile axis and is then refined within the pile's radius. The grid adopted for both cases 1 and 2 can be seen in figure 4.8. As mentioned before, in case 1 the water table will be at the surface and, in case 2, at the bottom of the sand layer. Figure 4.8 also shows the location of the building's slab modeled in case 3. A detail taken from the upper left corner of the grid is shown in figure 4.9, showing the refinement done inside the element of the pile.

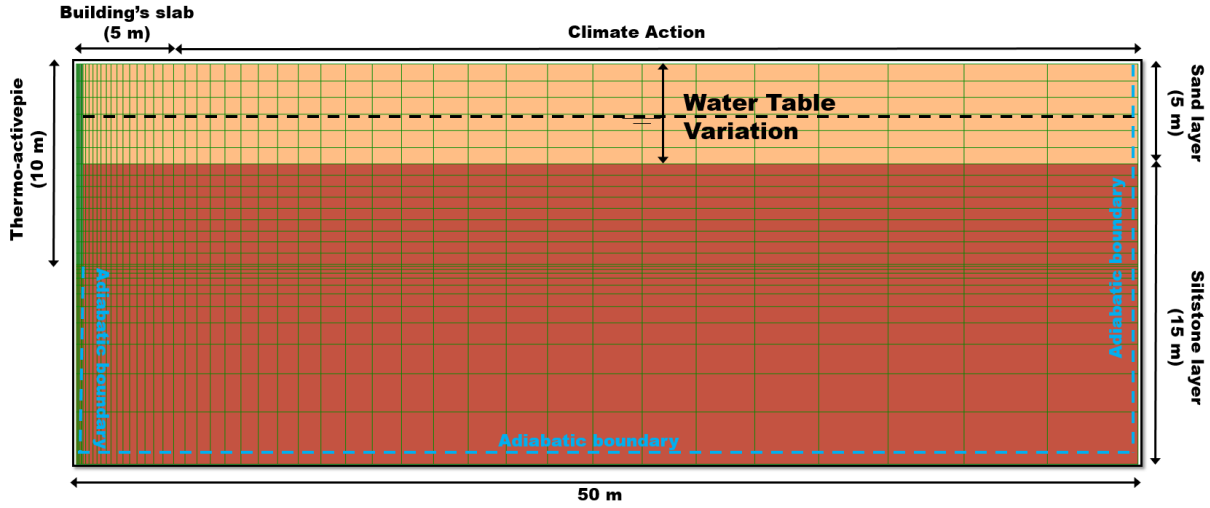

Figure 4.8. Model used in the numerical simulation with the relevant boundaries, inputs and dimensions

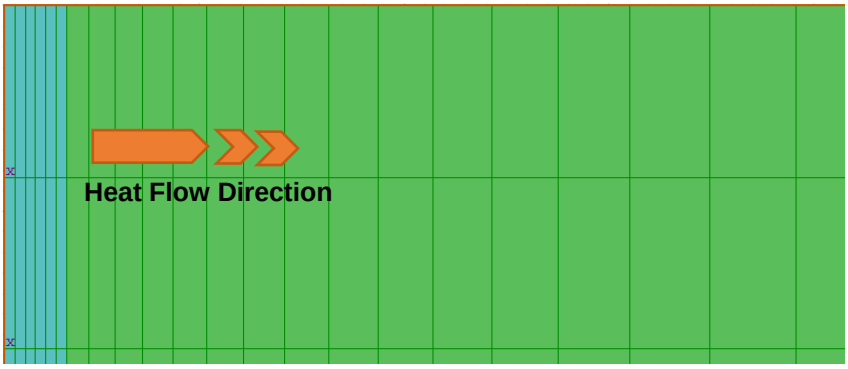

Figure 4.9. Detail taken from the upper left corner of the grid

The simulation performed computes temperature variations in the soil mass. However, different kinds of temperature data can be extracted from models such as the one shown in figure 4.10:

- Vertical temperature profiles: Values of the temperature registered on every grid point located at a certain distance x from the axis.
- Extreme temperature profiles: For the total duration of the simulation, these profiles specifically register the highest and lowest values of temperature computed on each grid point located at a certain distance x from the axis.
- Temperature histories: For a certain grid point with coordinates (x, y), a history registers the values of temperature computed on each time step.
- Temperature average (T_{avg}): Variable formulated to determine the average temperature felt among a certain number of grid points of the model. This calculation was done considering each point's area of influence (A_{ij}) as shown in the following equations:

$$T_{avg} = \frac{\sum_{j=a}^{N}\left[\sum_{i=b}^{M}\left(T_{i,j} * A_{ij}\right)\right]}{(N-a) * (M-b) * A_{total}} \tag{4.5}$$

$$A_{ij} = \left[x_{(i+1)} - x_{(i)}\right] * \left[y_{(j+1)} - y_{(j)}\right] \tag{4.6}$$

$$A_{total} = (x_N - x_a) * (y_M - y_b) \tag{4.7}$$

In order to make a comparative analysis, identical data analysis was performed for the three cases analyzed, namely:

- Extreme temperature profiles from 4 different sections (figure 4.10), located at consecutively larger distances from the axis (0.0m; 0.7m; 3.1m; 9.0m)
- The average temperature (T_{avg}) of the soil calculated for a representative area of 5mx15m, counted vertically from the pile axis and horizontally from the soil surface.

- Temperature histories registered as time elapsed, taken from 4 points located exactly in the middle of the sand layer, at 2.5 meters of depth. Much like the extreme temperature profiles, the points are positioned at consecutively larger distances from the axis (0.0m; 0.7m; 3.1m; 9.0m).

The reason behind the locations chosen is simple. At 9.0 meters from the axis, temperatures suffer negligible influence from the thermos-active pile. This was verified by running the model with and without the pile action, and it was concluded the results were coincident. Therefore, this location (9.0m) serves as the reference information. The remaining three locations are positioned to measure temperatures at: the axis of the model (0.0m), approximately one diameter ($\phi\, 0.6$ m) away from the axis of the pile (in order to facilitate the definition of boundaries, note that the model's left boundary is located at $x = 0.05m$); and five times the diameter of the pile located at (3.1 m). The area of influence of 5m by 15m (width by height) was chosen because it comprises the length of the slab, as can be seen in figure 4.8. A schematic of the information can be seen in figure 4.10.

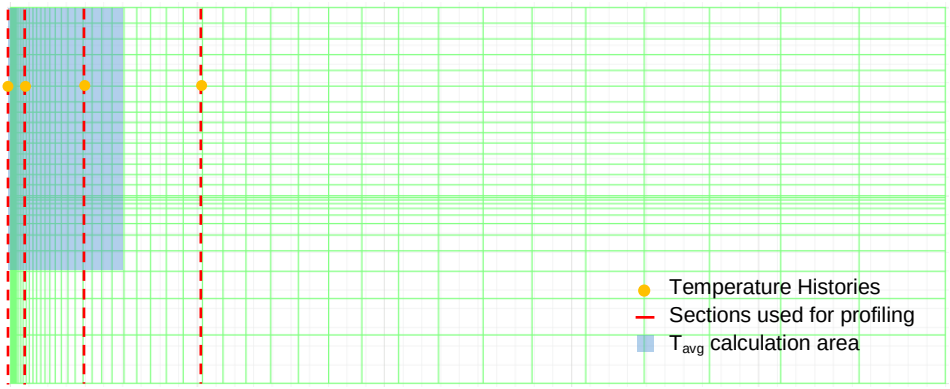

Figure 4.10. Detail of the different measurements performed in this chapter

4.2.1. Cases 1 & 2

When modeling the soil as fully saturated or completely dried, the only difference is in the values of the effective thermal conductivities adopted for the layer of sand. For the dry model, a value of $\lambda_{eff,dry} = 0.44$ W/mK is used, contrasting with the saturated conductivity, which is more than 4 times higher $\lambda_{eff,sat} = 1.89$ W/mK. For a simulation lasting 365 days, the vertical profiles with the maximum and minimum temperatures are presented in figure 4.11.

In both cases the influence of the thermo-active pile on the extreme temperatures felt in the soil can be seen by the separation of the three curves (blue, orange and green) among each other. In case 2 (dry sand), this separation is more accentuated than in case 1 (wet sand). At 0.7 meters from the pile axis and 3 meters of depth, dry sand exhibits temperature amplitudes of 6ºC, while without the thermo-active pile, amplitudes are smaller than 1.5ºC. With the wet sand, at 0.7 meters from the pile and 3 meters of depth, amplitudes reach 5ºC and without the pile, amplitudes reach 4 ºC. In the case of the dry soil,

there is a clear contrast between temperatures below and above 5 meters, which is expected, due to the larger contrast in thermal conductivity below and above the water level. On the other hand, the model for the fully saturated material shows smoother temperature lines in all profiles. Globally, the saturated soil shows a larger amplitude of extreme temperatures, except for the minimum temperature at the profile closest to the axis (blue line). In this case, the dry soil exhibits, at times, colder temperatures than the saturated layer (difference of about 1 degree Celsius).

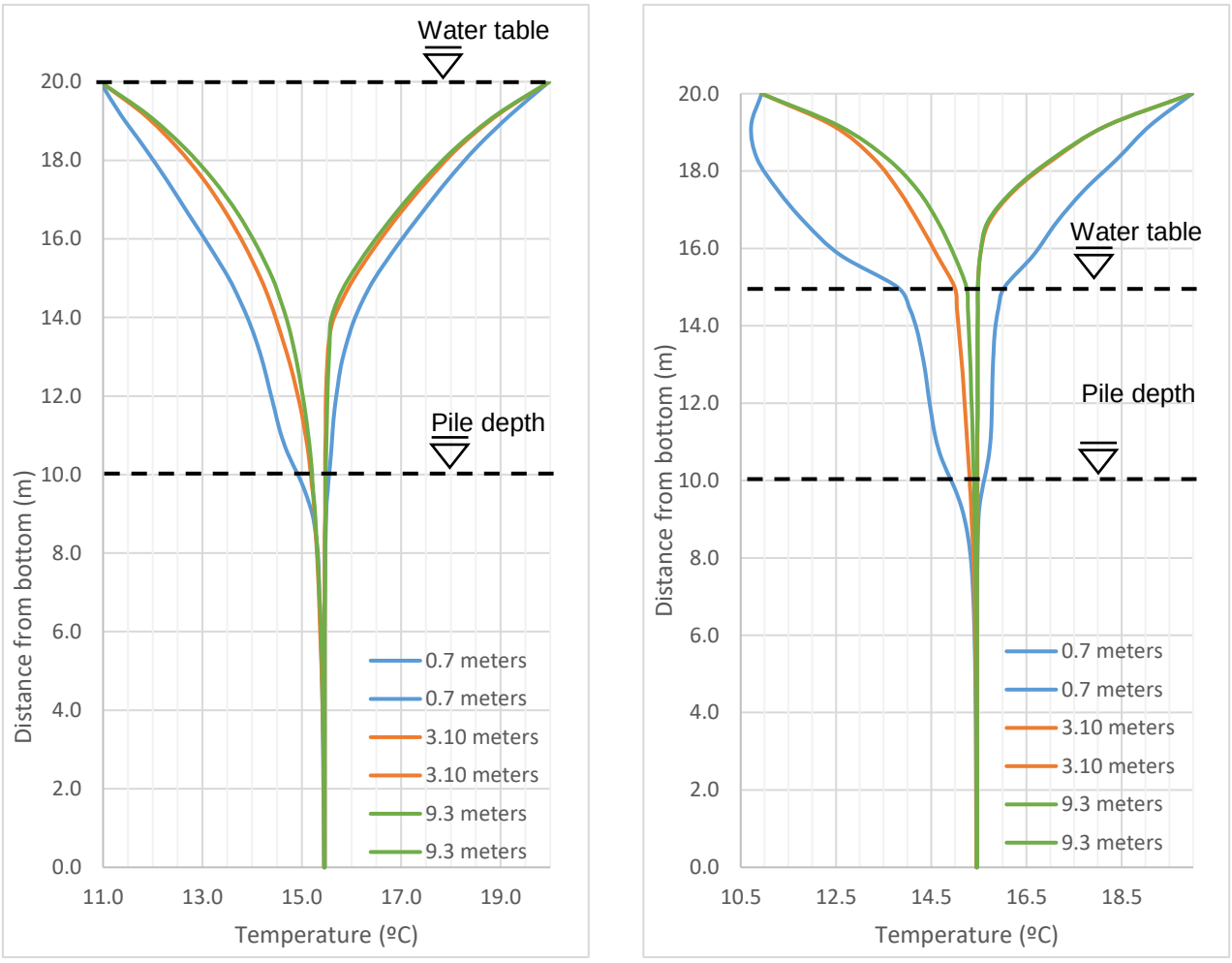

Figure 4.11. Maximum and minimum temperatures computed for case 1 (left) and case 2 (right)

Temperature records were registered on four different points, located at different distances from the pile's axis and at a depth of 2.5 meters. This depth corresponds to the middle of the sand layer. The plots can be seen in figures 4.12 and 4.13. From their analysis, a few statements can be made:

- Considering history 4 as a reference wave for that depth (9.3 meters away from the source), the influence of the thermo-active pile is quite clear, mostly in the records for history 1 and history 2.
- Minimum temperatures are 42% lower in history 1 than in history 4. Minimum temperatures are 22% lower in history 2 than in history 4.

- Maximum temperatures cannot be quantified because of the delay in the soil's response to the thermal actions. After 365 days, the maximum values are yet to be reached on all histories
- Dry sand (case 2) cannot transfer heat as fast as wet sand (case 1). In fact, after comparing history 4 (reference wave) for both cases, the delay of the heat wave is more accentuated in case 2, than in case 1. More specifically, the minimum temperature on dry sand was registered 53 days later than in the wet sand.
- The curves found in figure 4.11 are consistent with the profiles presented in figure 4.12 and 4.13. Maximum and minimum values found on history 2, history 3 and history 4 are identical to temperatures registered in the vertical profiles, at that depth (2.5 meters).

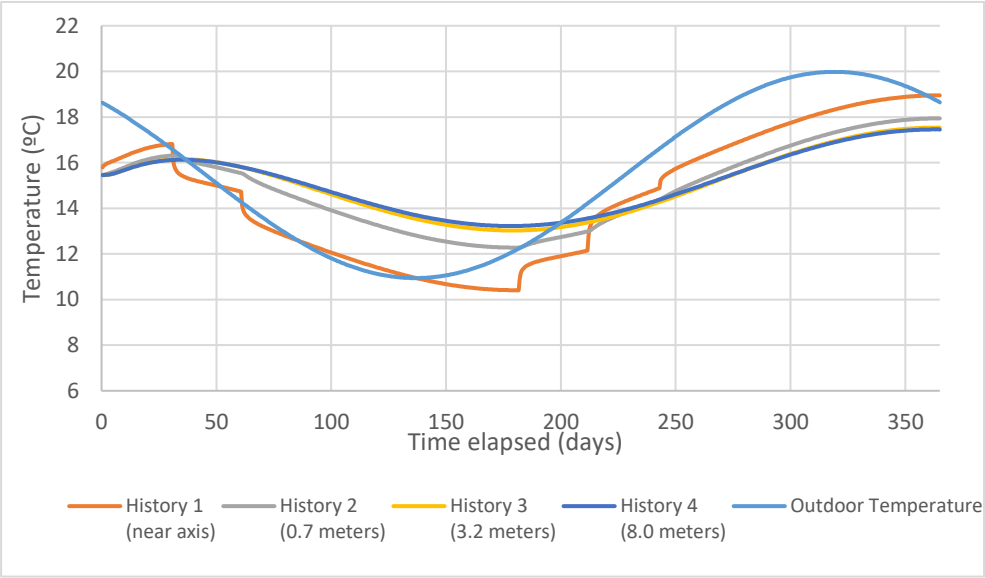

Figure 4.12. Temperature histories taken at a depth of 2.5 meters, at four different distances from the pile, regarding Case 1

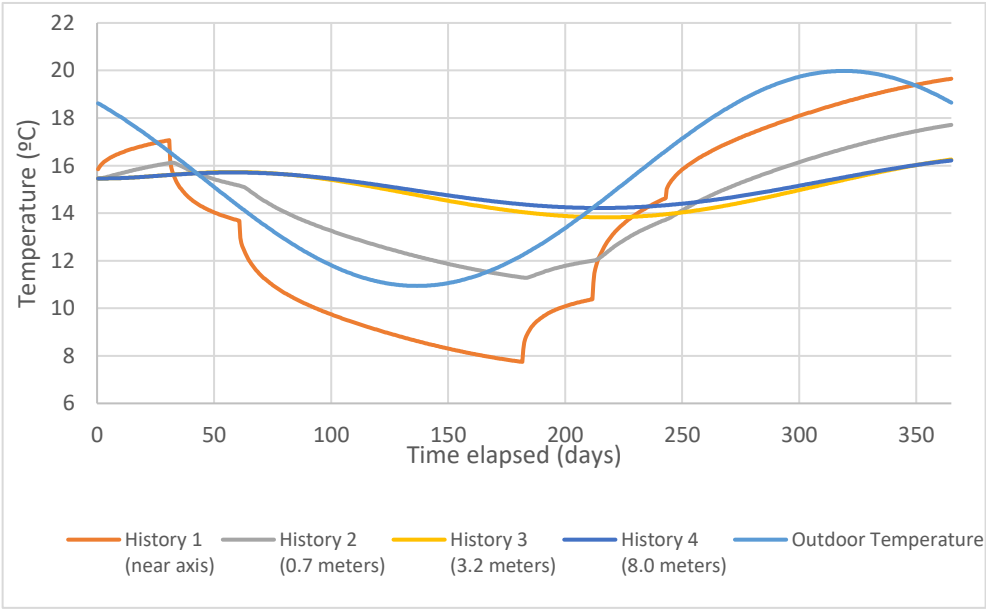

Figure 4.13 Temperature histories taken at a depth of 2.5 meters, at four different distances from the pile, in case 2

As mentioned in section 4.2, the average temperature (T_{avg}) was calculated for a partial area of the model, which was chosen to include the areas that are subjected to larger temperature gradients. Figure 4.14 presents the maximum and minimum temperatures computed for the dry model at the end of 5 years of simulation. In this case, temperatures vary mostly in the first 5 meters horizontally from the pile axis. Also, the values vary considerably in the first few meters into the ground, due to solar irradiation. Hence, it was found adequate to analyze the average temperature of a 5x15 grid, trimmed from the total 50x20 original one. The calculation was performed through simple arithmetic average included in the code, already explained in the section 4.2

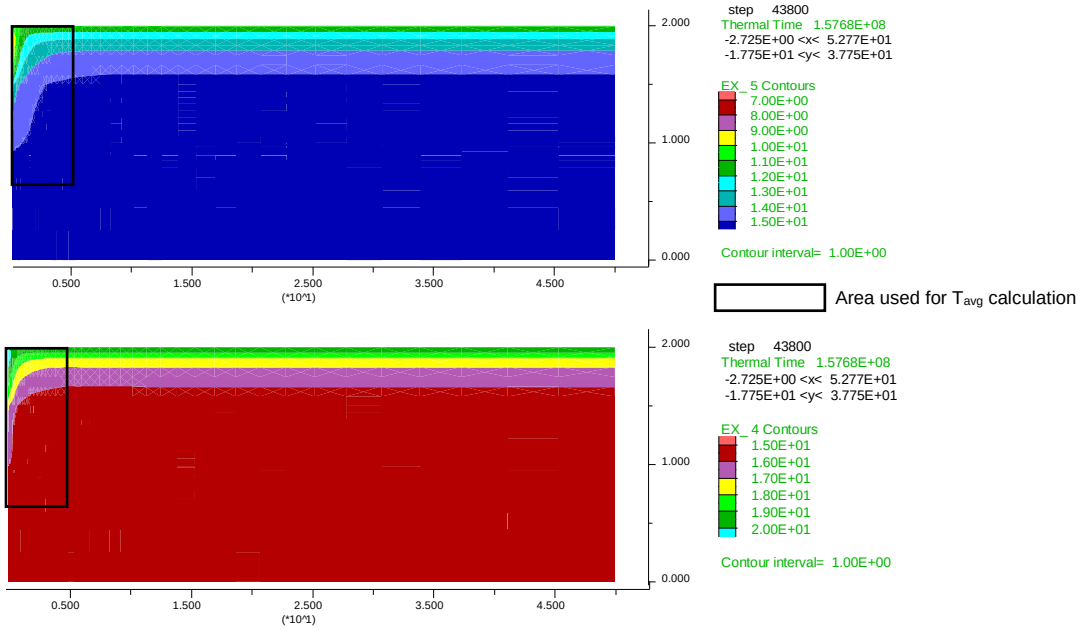

Figure 4.14. Maximum (bottom) and minimum (top) temperatures computed for the dry model, at the end of 5 years of simulations

The average temperature calculated for both case 1 (saturated) and case 2 (dry) is presented in figure 4.15. From a global point of view, it becomes clear that both the saturated and dry soils provide similar results. Both cases register a slight increase in the average temperature, after the 365 days of simulation. This value corresponds to an average temperature increment of 0.5ºC, after such elapsed time. Earlier in this section, extreme temperatures and histories were analyzed, resulting in considerable differences between saturated sand and dry sand. However, regarding the average temperature analysis, the differences are insignificant between the two cases, after a 365-day period.

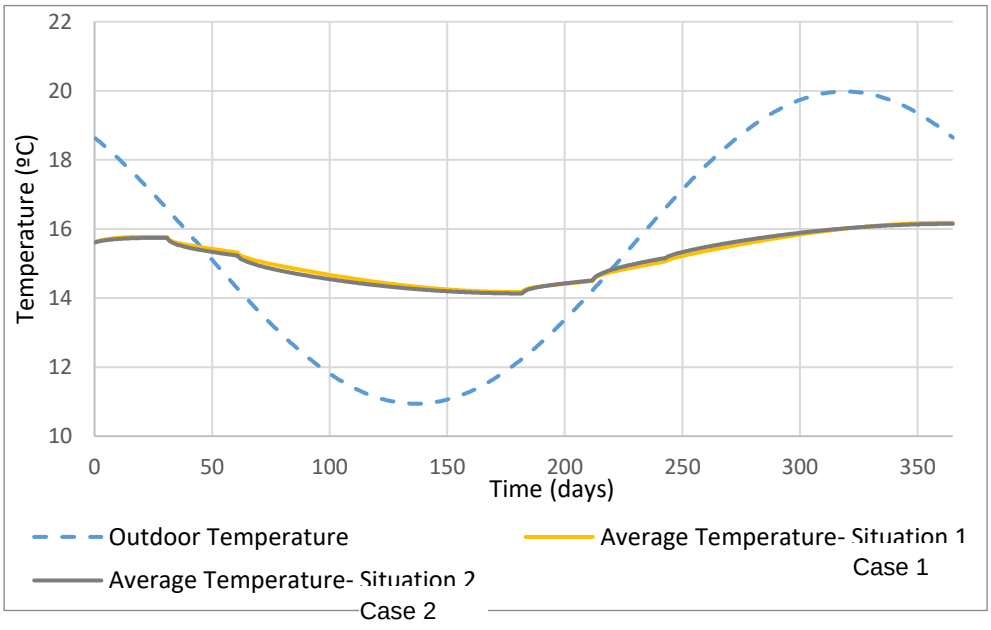

Figure 4.15. Average temperature evolution for cases 1 and 2

4.2.2. Case 3: Slab Influence on the SGHP's efficiency

The inclusion of a slab above the pile axis is a simple attempt to replicate the existence of the CICFANO building on top of the foundation soil. As previously stated, most of the 85 thermo-active piles are enclosed by at least 5 meters of floor slab, in all directions. This simulation assumes that the floor slab showcases a constant temperature equal to the indoor room temperature of 22ºC. The simulation was performed only considering the dry soil conductivity, because the results presented in section 4.2.1 are indicative that case 2 (dry sand) is the worst scenario. Therefore, the following results will be compared with those of case 2, mentioned in the previous section.

The extreme temperatures computed by FLAC show an expected elevation of the maximum and minimum values, comparing to case 2. Such results may be seen in figure 4.16 and compared with those from the dry simulation.

- Profiles of the minimum temperature at 0.8 and 3.1 meters from the axis are partially or even totally coincident with a vertical line at the temperature 15.45ºC. This value is the initial starting temperature at step=0.
- At 3.1 meters, maximum temperatures from case 2 are similar to the control profile (9.3m). However, with the slab installed, maximum temperatures are 1.7ºC higher than the control

profile, along the first 5 meters (sand layer). Below the water table (siltstone), the difference is no longer significant

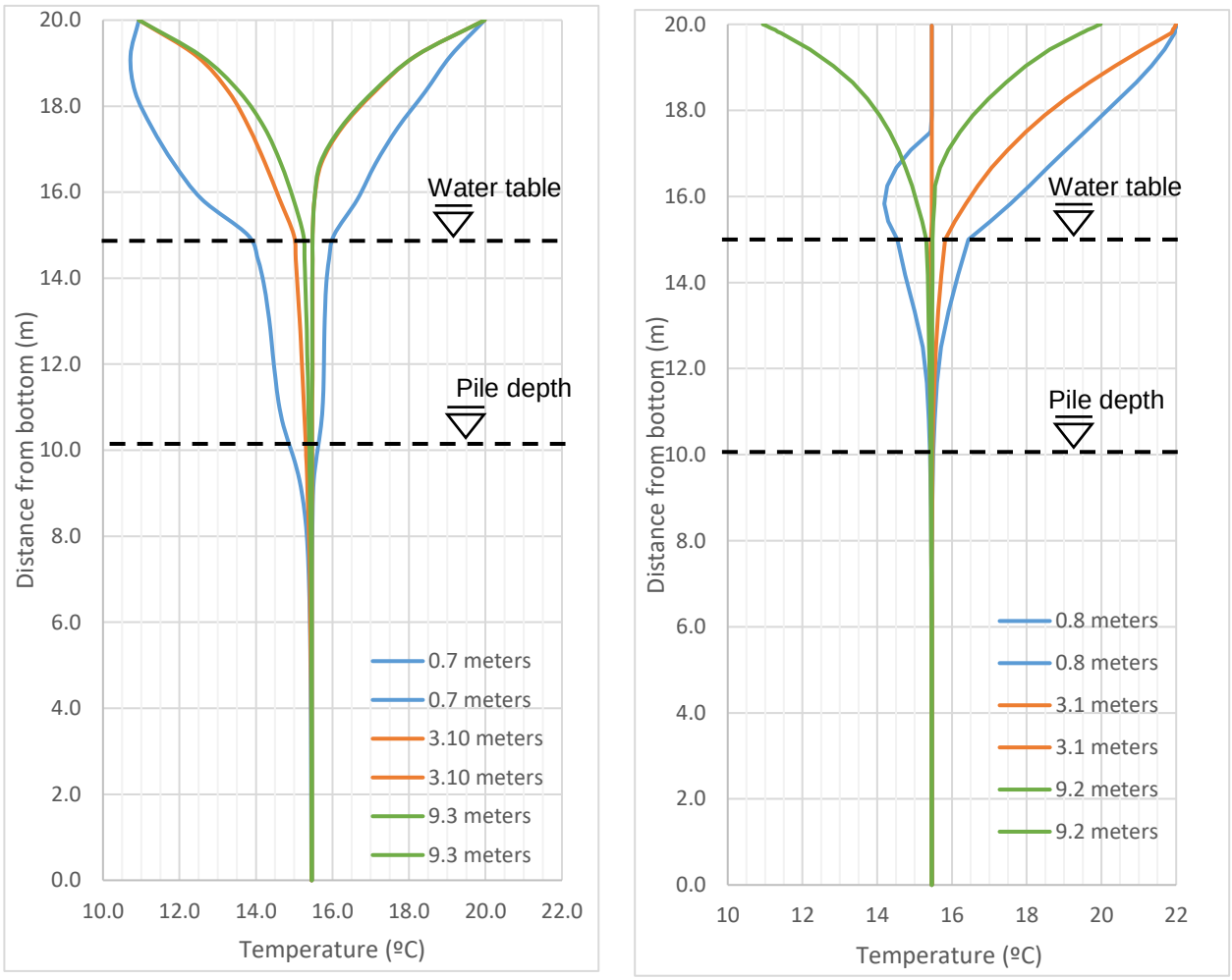

Figure 4.16. Maximum and minimum temperatures computed for case 2 (left) and case 3 (right)

- Considering a slab in case 3 increases maximum temperatures on the profiles analysed between 0.5ºC and 1.7ºC in comparison with case 2, for the sand layer.
- Considering a slab in case 3 increases minimum temperatures on the profiles analysed between 0.7ºC and 4.8ºC in comparison with case 2, for the sand layer.

In the claystone layer, the only relevant difference from case 2 to case 3 is the profile at 0.8 meters, regarding the minimum records, which are slightly higher until the end of the pile.

Figure 4.17 shows a plot of the minimum temperatures for case 3. As it can be seen, the slab is a very influent boundary, because it forces the soil close to the pile never to attain temperatures below 15.45ºC. This could be a major setback when the heat pump works in cooling mode.

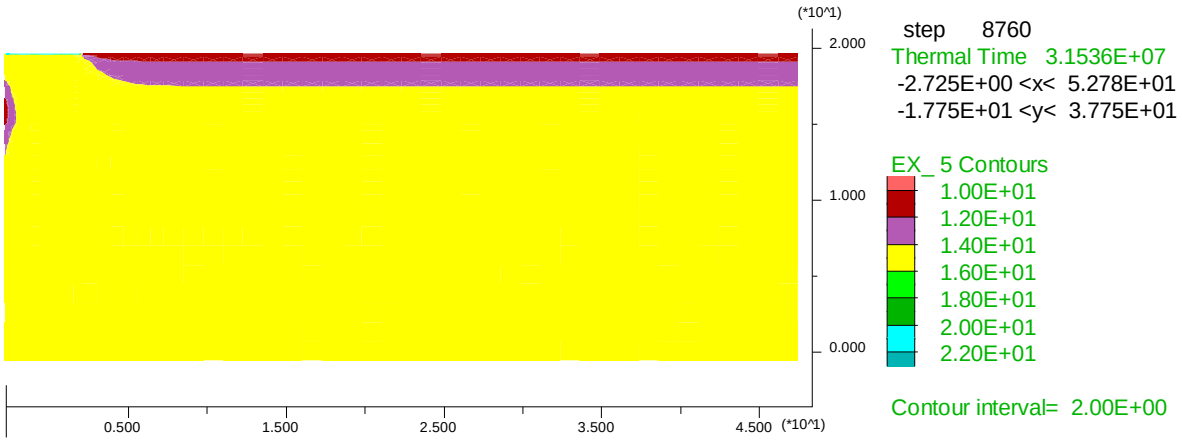

Figure 4.17 Minimum temperatures recorded across the domain in case 3

The data related to the temperatures evolution along time can be found in figure 4.18. Once again the points studied were located at a depth of 2.5 meters. These four histories differ completely from the ones without the slab included in the model previously shown in figure 4.13. The following information was retrieved:

- When the slab is considered, temperatures start rising from the beginning of the simulation and, in some areas, they never stop raising.
- History 3 has a behaviour which is dominated by the presence of floor slab, because its coordinates are too far away from the place where the thermal load is applied. Closer than that, and the axial thermal load still has a dominating role, forcing the surrounding soil mass to follow its demands.

History 4 reveals that even at a greater distance from the pile axis (8 meters), the curve remains the same as in case 2

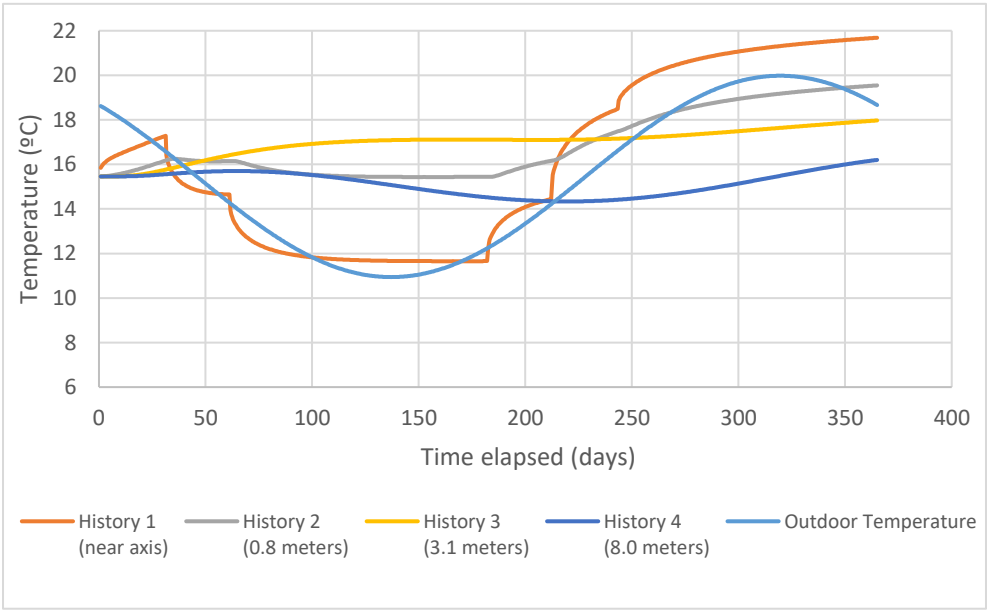

Figure 4.18. Temperature histories taken from four different positions, in case 3 and at a depth of 2.5 meters

The area used for T_{avg} is the same as case 1 and 2. Average temperatures from case 3 (slab model) are considerably higher than in cases 1 and 2, which were already presented in figure 4.19. In fact, after one cycle of 365 days of elapsed time, temperature raises 3.2 ºC (figure 4.19), which is more than 600% the value in the previous cases. Besides, average temperature in the studied area is never lower than the initial value.

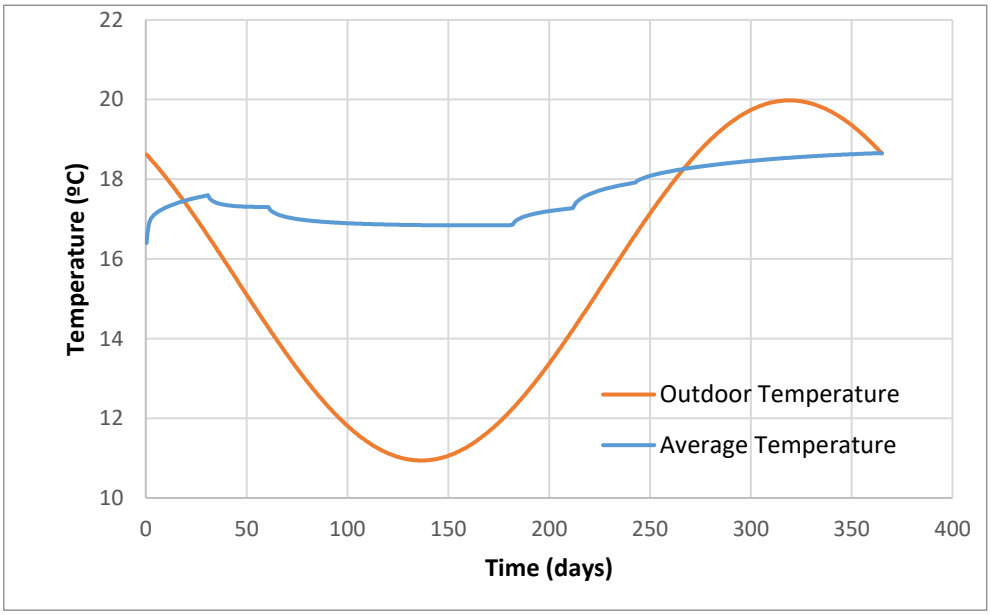

Figure 4.19. Average temperature evolution for case 3 at depth of 2.5 meters

Heat Flux Evaluation

From the data acquired in the previous simulations, it is possible to elaborate a calculation of the heat flux passing through the soil, perpendicularly to the pile axis (direction x). Since this analysis is purely conductive, the heat flux on each point was calculated by using Fourier's law of conduction in the form

$$q = \lambda \frac{\Delta \mathrm{T}}{\Delta \mathrm{x}} \qquad (W/m^2) \tag{4.8}$$

Considering an grid point of coordinates (i, j) and also that i is constant for a vertical profile, the heat flux passing from point i to point $i + 1$ becomes:

$$q_{i,j} = \lambda \frac{T_{i+1,j} - T_{i,j}}{x_{i+1,j} - x_{i,j}} \tag{4.9}$$

After calculating the heat flow for each point of a profile was calculated, they were integrated in the cylindrical area respective to each profile, becoming a measurement of the energy per second (Watt) transferred by the soil at a certain distance from the source. The geometrical translation of this integrated

heat flux, is a combination of concentric cylinders, each of them corresponding to a different profile. Figure 4.20 is a scheme of what was done:

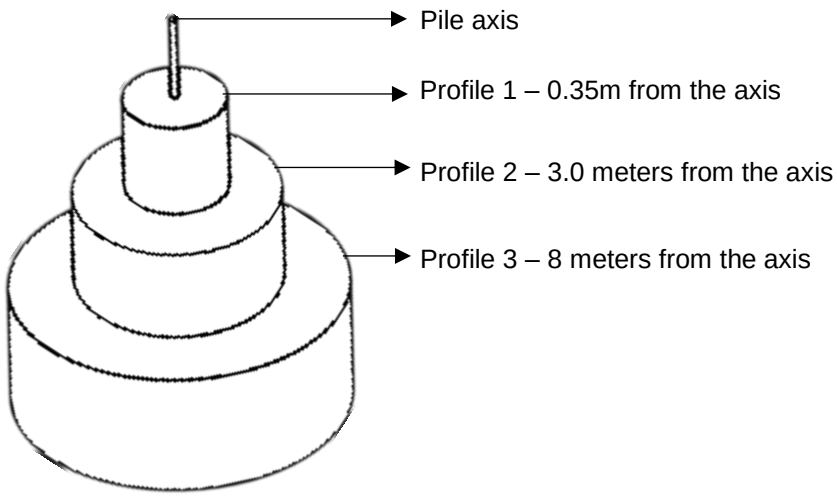

Figure 4.20. Schematic representation of the three profiles calculated with Fourier's Law of Conduction

According to the model's axis orientation, a positive value of heat flux means that energy is being transferred from left to right, and *vice versa*. FLAC does not allow the direct measurement of the variable heat flux in other places than the boundaries, so this process had to be coded in a separate set of FISH file, put together with the remaining code.

In figure 4.21, 4.22, and 4.23 the thermal power computed for each profile of the model can be found. Note that the *imposed action* line found in the figures is not calculated with equation 4.6, because it is located at a boundary. As mentioned above, FLAC directly calculates heat flux at the boundaries and, as such, there was no need to calculate it manually.

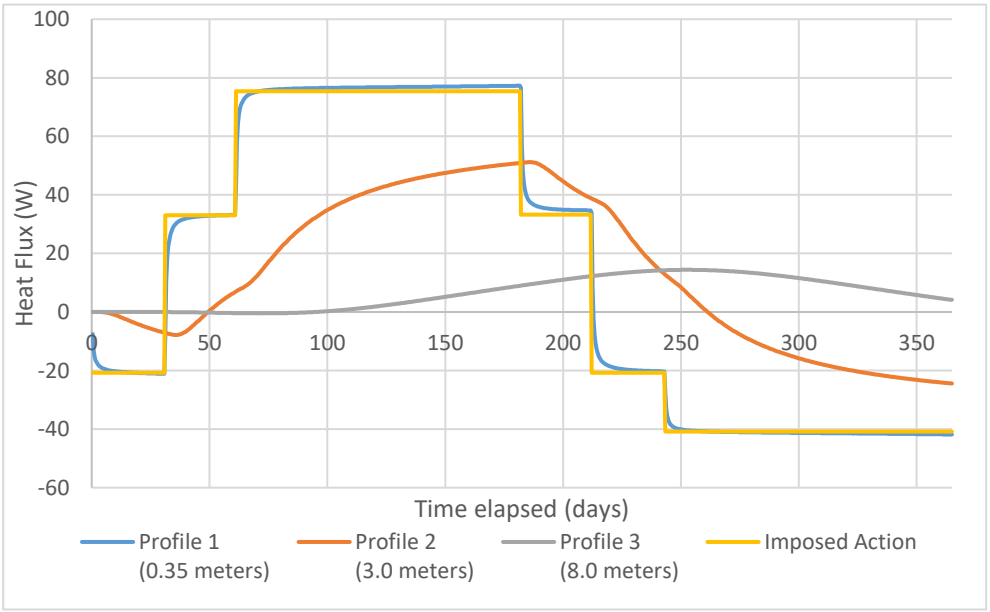

Figure 4.21. Thermal power held by the soil mass in three different areas for case 1

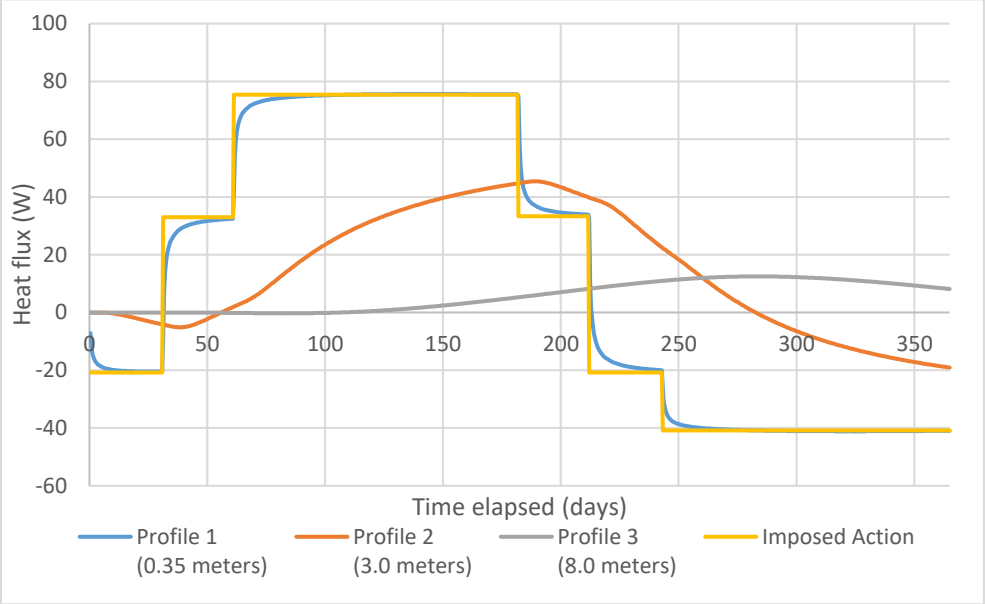

Figure 4.22. Thermal power held by the soil mass in 3 different areas for case 2

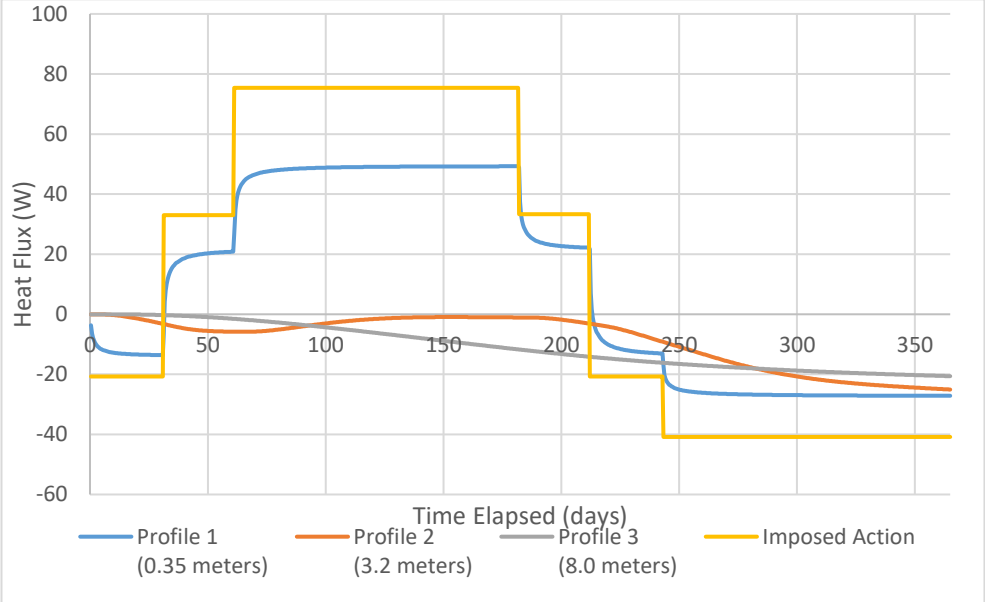

Figure 3. Thermal power held by the soil mass in three different areas for case 3

Case 1 presents more promising results in comparison to those from case 2. In fact, not only the saturated model can transfer more heat, but it will also do it faster. This was expected due to the higher thermal conductivity of the saturated soil compared to when it is dry. The difference in the amount of heat is more visible at 3 meters from the pile's axis. At that distance, the peak thermal power computed

is 50.4 Watts for case 1, and 45.3 Watts for case 2, which is equivalent to a 10% decline in the dry model. Regarding the thermal inertia of the soil, the trend is similar to the one mentioned in figure 4.12 and 4.13, which means that saturated soil is quicker to transfer heat than dry soil (note the results from "profile 3" for both cases). However, specifically for profile 2, peak thermal power occurs at the same time for both cases, despite what happens with peak temperature

Following up what was done with cases 1 and 2, a take on the thermal power transferred in the soil was attempted. Figure 4.23 reveals a totally different reality than the one from previous results. Profile 2 and 3 show negative values for the complete simulation. Profile 1, which is located in the interface between pile and soil, presents a significant loss in the amount of heat transferred. For instance, at the 100th day of simulation, the input thermal power is 75.4 watts, while 35 centimeters away, this value drops to 48.8 watts, which corresponds to a loss of 35.3%.

4.2.3. Prolonged exposition to the annual cycle

In the previous sections, the analysis of the CICFANO case study was performed for the duration of one year, beginning and finishing in October 1st. However, a set of annual cyclical action might not produce the same results when repeated for several years. In this chapter, the results for a 5-year span analysis is presented. As mentioned before, identical climate data was considered for the five years.

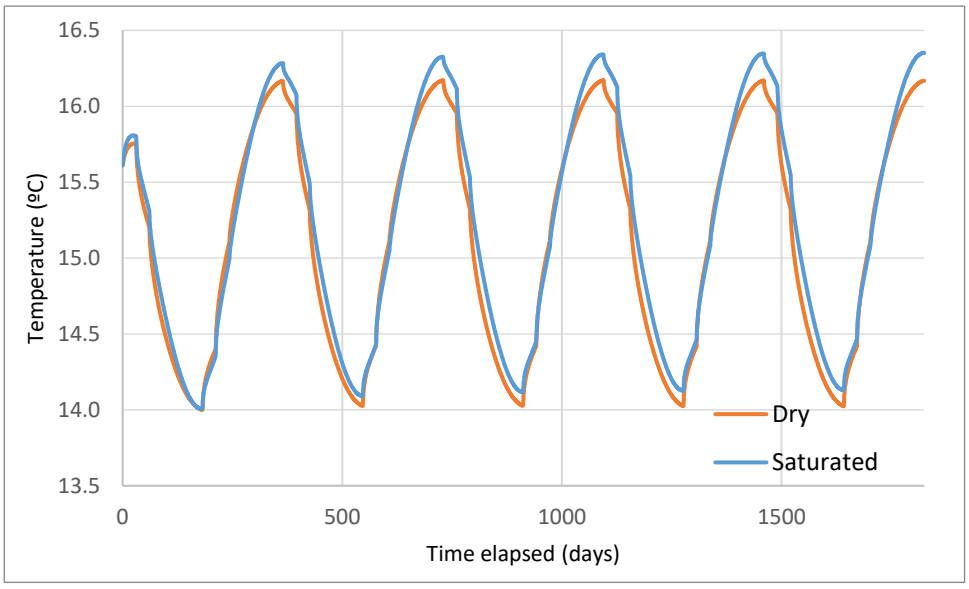

Figure 4.24. Average temperature evolution for cases 1 and 2, over 5 years.

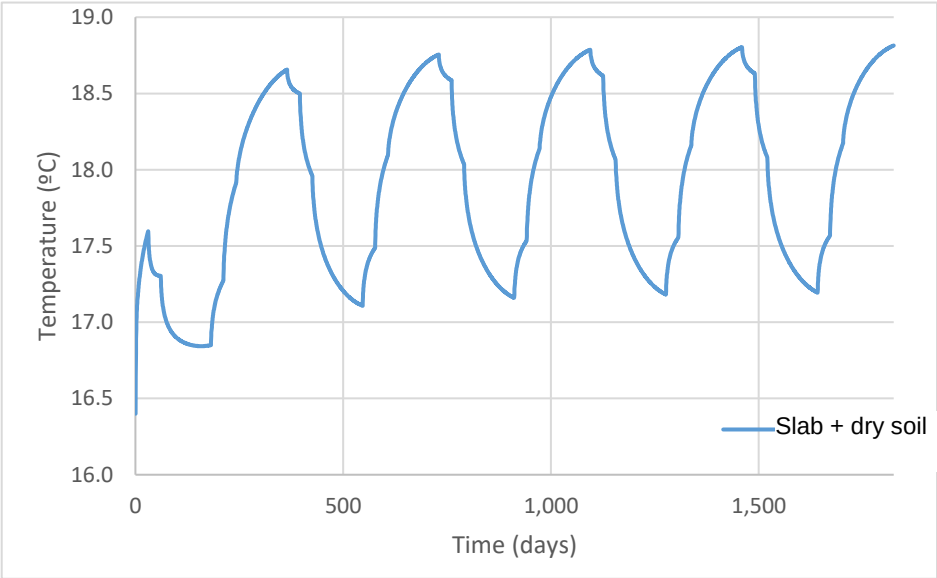

Figure 4.25. Average temperature evolution for case 3, over 5 years

The average temperatures from cases 1 and 2 are plotted in figure 4.24. While the dry scenario exhibits a near- constant wave over time (orange line), the saturated soil translates in a constant, mild increase in the extreme temperatures (blue line). In the end of the 5th year, the soil average temperature is 16.4ºC in the saturated scenario and 16.2ºC in the dry scenario. The average soil temperature without the building would be 15.5ºC. For both situations, the largest leap of average temperature occurs during the first year (90%of total), stabilizing later in the simulation.

Case 3 has a similar pattern. In the end of the 5th year, average temperatures under the building's slab are 18.8ºC, contrasting with 18.6ºC in the end of the first year and 15.45ºC in the beginning of the simulation, as can be seen in figure 4.25.

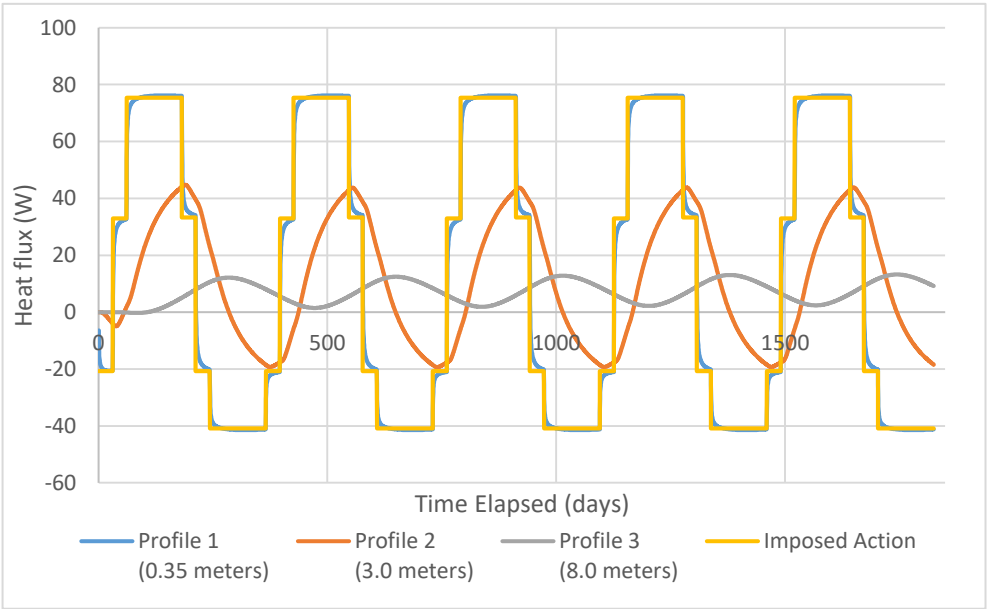

Figure 4.26. Thermal power held by the soil mass in 3 different areas for case 2, over 5 years

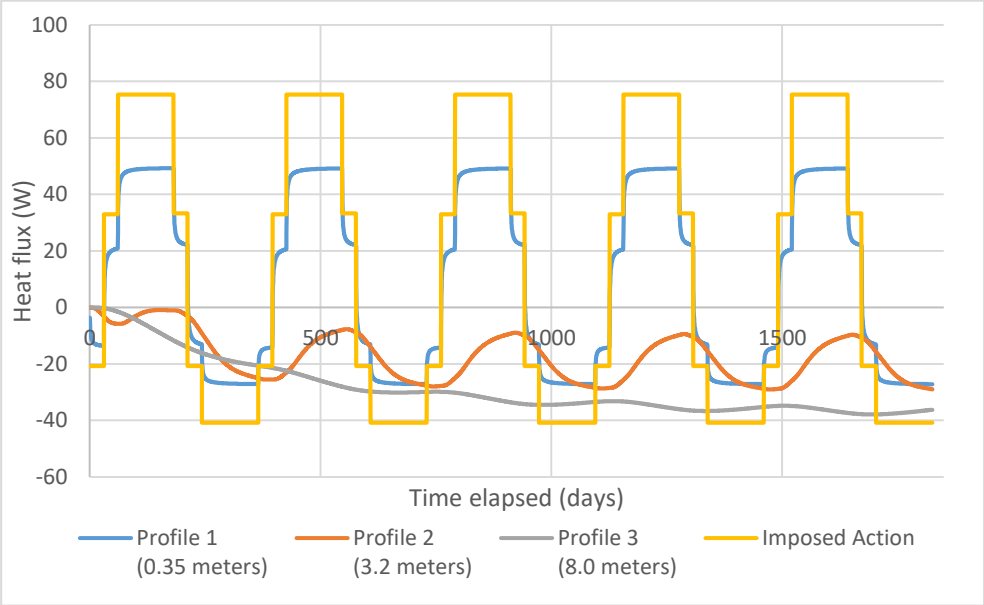

Figure 4.27. Thermal power held by the soil mass in 3 different areas for case 3, over 5 years

Figure 4.26 and 4.27 present the computation results for the thermal power from the four profiles in situation 2 and 3. The main thing to note, is the constant decay of heat flux in the soil for situation 3, unlike what happens in situation 2. After the 4th year of simulation, this trend seems to disappear, since the values decay much less than in the first 3 years.

Considering a slab's temperature as a boundary condition above the pile has an effect on the direction of the heat flux vector. The analysis presented only considers heat flux perpendicularly to the pile's axis and that justifies the amount of heat loss seen in figure 4.27.

5. Conclusion and future work

5.1. Conclusions

This thesis focused on two main themes: the numerical simulation of the heat transfer of a thermo-active pile located in a building in Aveiro University Campus and the evaluation of its energy efficiency. Chapter 3 presents the GSHP solution used by the CICFANO building as part of the dynamic energy system, focusing on the four main aspects that influence the energy trades within the system: climate action; thermal properties of the soil; building's energy demand; system configurations. All these aspects were considered in the numerical model either as applied actions or as input for the soil model. Chapter 4 follows up on this investigation, using a numerical approach to understand the impact of the foundation soil and the presence of the building in the form of the of a foundation slab on the global thermal behavior of the system. The conclusions can be separated into those two different aspects.

Regarding the climate analysis, the choice of an adequate source of information is a sensitive subject. As it was observed, data available for the same city can provide very different temperature records, some of them presenting differences in average up to 4ºC, depending on the data's source and record's time span. Even records for the same year and the same city (i.e. different sources) can provide dissonant information. The use of an inadequate source may interfere greatly in numerical analysis like the one performed in chapter 4.

The soil underneath the CICFANO building was characterized through a preliminary laboratory investigation. Despite different soil types (ML silty layer and a SP sand layer), mineralogy is similar for the materials found in both layers. Empirically, soils with identical minerals will have equally identical thermal conductivities (granted similar hydrological conditions). Therefore, with the available elements, it is concluded that in the CICFANO case study, the different thermal parameters used will depend mostly on the hydrological conditions assumed for the soil. However, it should be confirmed by undisturbed samples

Numerical modelling focused on comparing the thermal response of the soil among three cases: considering that the upper layer is saturated, dry and, in the last case, including a slab encased pile. Even though the saturated scenario produces slightly higher temperatures in the soil over time, such overall warming doesn't translate in a loss of thermal efficiency. In fact, it is the other way around. The dry soil seems to be incapable of transferring heat as efficiently as the saturated. In the summer season, statistics show that Aveiro often suffers moderate draught levels, and rain is scarce. Usually, such periods are associated with high temperatures, which require extra acclimatization effort. Therefore, a reduction in the amount of heat transferred by dry soil has a real impact on the building's acclimatization process.

Among the three cases studied, temperatures either stabilize after the first year (case 2), or they rise at an average rate of 0.05ºC per year, over a time lapse of 5 years (case 1). After the 1-year period, the

soil mass is already adapted to the thermo-active pile action. It is unknown if temperature will ever stabilize for the saturated soil.

Including the presence of the slab into the simulation has produced major changes in the outcome. According to the thermal power computed throughout the soil mass, the GSHP should not be capable of following through with the building's demands. In fact, after 3 years, the pile is attempting to absorb heat from the soil, and instead, heat is moving away from the pile. This system is expected to work for decades and, as such, the effect of the slab cannot be underestimated.

Overall, using a conduction only analysis and assuming no water advection within the soil mass, the GSHP system seems to be sustainable over a 5-year span for cases 1 and 2. However, assuming that the building's slab is at a constant indoor temperature, the system will respond with much lower efficiency, at least in the long therm. As a reminder, it is important to note the most of the 85 thermo-active piles are surrounded by at least 5 meters of building slab. In some cases, that value might reach up to 10 meters. However, the GSHP was analysed as a separate part of the CICFANO building. In reality, the complementary biological source heat pump as proven effective in supplying thermal energy when the GSHP cannot. The building's acclimatization using renewable energy sources is always secured.

5.*2. Future Work*

The study presented was a preliminary assessment of the thermal behaviour and as such, a number of hypotheses were assumed along the way. In this chapter, a few suggestions will be made to improve and carry the investigation to further developments.

Including a coupled advection-conduction model in this simulation, which would allow heat to be transported by the moving water inside the sandy layer. This would be a step towards accuracy, since the CICFANO building is close to the river and the sea. Therefore, a strong underground water percolation is expected.

This thesis computed the thermal needs of the building as sequence of monthly averages, applied during the year. Therefore, the peak loads and the system's "down time" was not studied in this work. This is important because certain hydro-geological conditions may allow a typical amount of heat to pass through the soil, but a peak load might not have the same response.

The numerical approaches were done in axisymmetric state, using a single pile. However, the interaction among the 85 thermo-active piles should not be despised. That kind of analysis requires a three dimensional analysis of a small group of piles. Such studies can be performed using FLAC 3D, or another adequate software.

In this work, empirical relations were used to determine thermal properties of the soil. Therefore, many direct methods for measuring thermal conductivity are available. For validation purposes, it is recommended that the soil samples used for the laboratory testing are also subject to these tests. For instance, the transient thermal needle can provide values for the thermal conductivity of both saturated and dry samples.

While this thesis focuses on the thermal behaviour of the soil, a thermo-hydro-mechanical coupled analysis provides a complete understanding of the system. This analysis would include the effects of advection in the efficiency of the system, but also the structural consequences caused by the cyclical temperature changes on the CICFANO's piles.

References

Rubio-Maya C et al (2015), Cascade Utilization of low and medium enthalpy geothermal resources - A review, Renewable and Sustainable Energy 52, 689-716

Comission of the European Communities, COM 545, 2006, Action plan for energy efficiency - Realising the potencial.

Comission of the European Communities, COM 1, 2007, An energy policy for Europe

Omer AM (2008), Ground-Source heat pumps systems and applications, Renewable and Sustainable Energy Reviews 12, 344-371.

French-Brooks J (ed). Transition to Sustainable Buildings, International Energy Agency (2013), Paris. 290 pp.

Self S et al (2013), Geothermal heat pump systems: Status review and comparison with other heating options, Applied Energy 101, 341-348.

PORDATA, Energias Renováveis no balanço energético, DGEG/MAOTE, 2015

Hughes P, Geothermal (Ground-Source) Heat Pumps: Market Status, Barriers to Adoption, and Actions to Overcome Barriers, (2008). US Department of Energy Publications. Paper 15.

Brandl H (2006), Energy foundations and other thermo-active ground structures, Geotechnique 56, 281-122

Rybach L & Mongillo M (2006), Geothermal Sustainability – A Review with Identified Research Needs, GRC Transactions 30, 1083-1090

Mands E & Sanner B (2007), Shallow Geothermal Energy, UBeG Geothermal Geotechnic Services, Wetzlar, Germany

Sawin L & Sverrison F (leading authors), Renewables 2016 - Global Status Report, REN21 (2016), UNEP Paris

Vieira A & Figueira J (2017), Reflexão sobre mercado português da geotermia superficial – Enquadramento Europeu e paralelismo com outros países da UE, Relatório LNEC, Portugal

Al-Khoury R , Computational Modeling of Shallow Geothermal Systems-CRC Press (2011), 245 pp.

Rees SW et al (2000), Ground heat transfer effects on the thermal performance of earth contact strucures, Renewable and Sustainable Energy Reviews 4, 213-265

Farouki O, Thermal properties of soils, CRREL Monograph 81-1 (1981), United Stats Corps of Engineers, United States of America, 150 pp.

Lo Russo S et al (2009). Low-enthalpy geothermal energy-an opportunity to meet increasing energy needs and reduce CO2 and atmospheric pollutant emissions in Piemonte, Italy. Geothermics, 38

W Rohsenow, J Hartnett, Y Cho (editors), Handbook of Heat Transfer, 3rd edition, McGraw-Hill publishing (1998), 1501 pp.

Vieira A & Figueira J. (2017), Estudo da conductividade térmica de solos e os factores que a influenciam, Relatório LNEC, Portugal

Sanner B et al (2005), Thermal Response Test - Current Status and World-Wide Application, Proceedings World Geothermal Congress, Antalaya, Turkey

Sarbu I & Sebarchievici C (2014), General Review of ground-source heat pump systems for heating and cooling of buildings, Energy Buildings 70, 441-454

McCorry M & Jones G.Ll (eds) 2011. Geotrainet Training Manual for Designers of Shallow Geothermal Systems. Geotrainet, European Federation of Geologists, Brussels. 192pp

Ground Energy Technical Information, UPONOR catalogue, 2012

Morrone B et al (2014), Energy and economic savings using geothermal heat pumps in different climates, Energy Conversion and Management 88, 189-198

Figueiredo A (2016) Energy Efficiency and comfort strategies for southern european climate: Optimization of passive housing and PCM solutions (Doctoral dissertation), retrieved from University of Aveiro, Department of Civil Engineering, Portugal

Vieira A, Maranha J (2013), Numerical Study on the Behaviour of Thermoactive Foundation Structures, 2012

Lapa J & Cardoso C (2014), Casos de aplicação da geotermia superficial em sistemas de estruturas termo-activas em edifícios escolares da UA (Powerpoint Presentation), 2º Seminário da Plataforma Portuguesa de Geotermia Superficial, LNEG, Portugal

[28] FLAC Online Manual, version 5.0, 3058 pp.

Annex A –Detailed features of a heat pump in cooling mode (lower) and heating mode (upper)

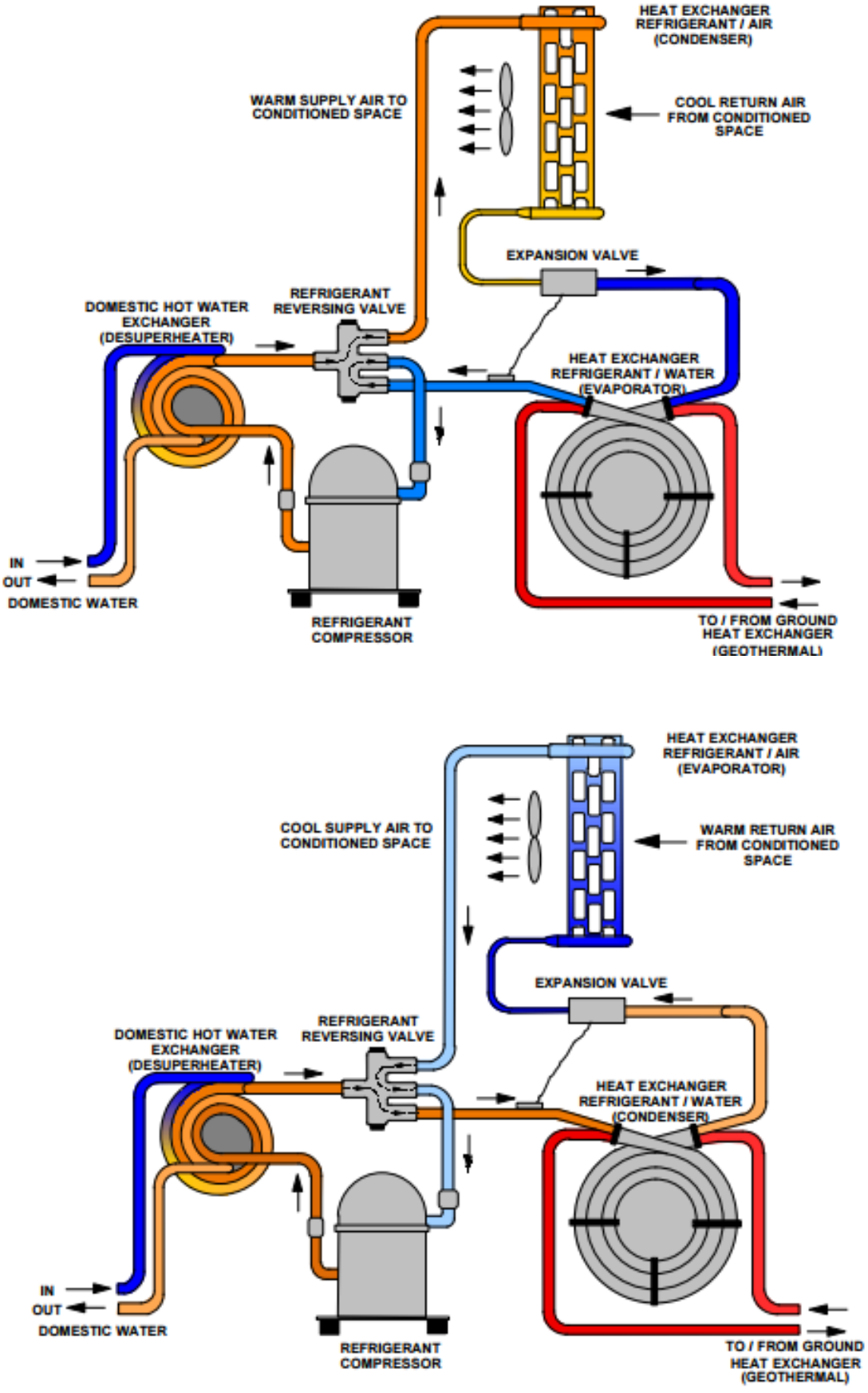

Annex B –VDI4640 – Typical Values for soil thermal properties

	Type of rock		Heat conductivity in W/(m · K)	Recommended value	Volume description special heat capacity in MJ/(m³ · K)	Density in 10^2 kg/m³
Unconsolidated rock	Clay/silt, dry		0.4 – 1.0	0.5	1.5 – 1.6	1.8 – 2.0
	Clay/silt, waterlogged		1.1 – 3.1	1.8	2.0 – 2.8	2.0 – 2.2
	Sand, dry		0.3 – 0.9	0.4	1.3 – 1.6	1.8 – 2.2
	Sand, moist		1.0 – 1.9	1.4	1.6 – 2.2	1.9 – 2.2
	Sand, waterlogged		2.0 – 3.0	2.4	2.2 – 2.8	1.8 – 2.3
	Gravel/stones, dry		0.4 – 0.9	0.4	1.3 – 1.6	1.8 – 2.2
	Gravel/stones, waterlogged		1.6 – 2.5	1.8	2.2 – 2.6	1.9 – 2.3
	Glacial drift		1.1– 2.9	2.4	1.5 – 2.5	1.8 – 2.3
	Peat, earthy brown coal		0.2 – 0.7	0.4	0.5 – 3.8	0.5 – 1.1
Sedimentary rocks	Mudstone/siltstone		1.1 – 3.4	2.2	2.1 – 2.4	2.4 – 2.6
	Sandstone		1.9 – 4.6	2.8	1.8 – 2.6	2.2 – 2.7
	Psephite/breccia		1.3 – 5.1	2.3	1.8 – 2.6	2.2 – 2.7
	Marlstone		1.8 – 2.9	2.3	2.2 – 2.3	2.3 – 2.6
	Limestone		2.0 – 3.9	2.7	2.1 – 2.4	2.4 – 2.7
	Dolomite brick		3.0 – 5.0	3.5	2.1 – 2.4	2.4 – 2.7
	Sulfate rocks (anhydrite)		1.5 – 7.7	4.1	2.0	2.8 – 3.0
	Sulfate rocks (gypsum)		1.3 – 2.8	1.6	2.0	2.2 – 2.4
	Chloride rocks (rock salt-/waste salt)		3.6 – 6.1	5.4	1.2	2.1 – 2.2
	Blue coal		0.3 – 0.6	0.4	1.3 – 1.8	1.3 – 1.6
Magmatic solid rock	Tuff		1.1	1.1		
	Volcanic rock, acid up to intermediary	e.g. rhyolite, trachyte	3.1 – 3.4	3.3	2.1	2.6
		e.g. trachybasalt, dacite	2.0 – 2.9	2.6	2.9	2.9 – 3.0
	Volcanic rock, basic up to ultrabasic	e.g. andesite, basalt	1.3 – 2.3	1.7	2.3 – 2.6	2.6 – 3.2
	Plutonite, acid to intermediary	Granite	2.1 – 4.1	3.2	2.1 – 3.0	2.4 – 3.0
		Syenite	1.7 – 3.5	2.6	2.4	2.5 – 3.0
	Plutonite, basic to ultrabasic	Diorit	2.0 – 2.9	2.5	2.9	2.9 – 3.0
		Gabbro	1.7 – 2.9	2.0	2.6	2.8 – 3.1
Metamorphic solid rocks	low metamorphic grade	Slate	1.5 – 2.6	2.1	2.2 – 2.5	2.4 – 2.7
		Silicous shale	4.5 – 5.0	4.5	2.2	2.5 – 2.7
	medium to high metamorphic grade	Marble	2.1 – 3.1	2.5	2.0	2.5 – 2.8
		Quartzite	5.0 – 6.0	5.5	2.1	2.5 – 2.7
		Mica slate	1.5 – 3.1	2.2	2.2 – 2.4	2.4 – 2.7
		Gneiss	1.9 – 4.0	2.9	1.8 – 2.4	2.4 – 2.7
		Amphibolite	2.1 – 3.6	2.9	2.0 – 2.3	2.6 – 2.9
Other materials	Bentonite		0.5 – 0.8	0.6	~3.9	
	Concrete		0.9 – 2.0	1.6	~1.8	~2.0
	Ice (-10°C)		2.32		1.89	0.919
	Plastic (HD-PE)		0.42		1.8	0.96
	Air (0°C to 20°C)		0.02		0.0012	0.0012
	Steel		60		3.12	7.8
	Water (+10°C)		0.56		4.15	0.999

Annex C – Climate Analysis

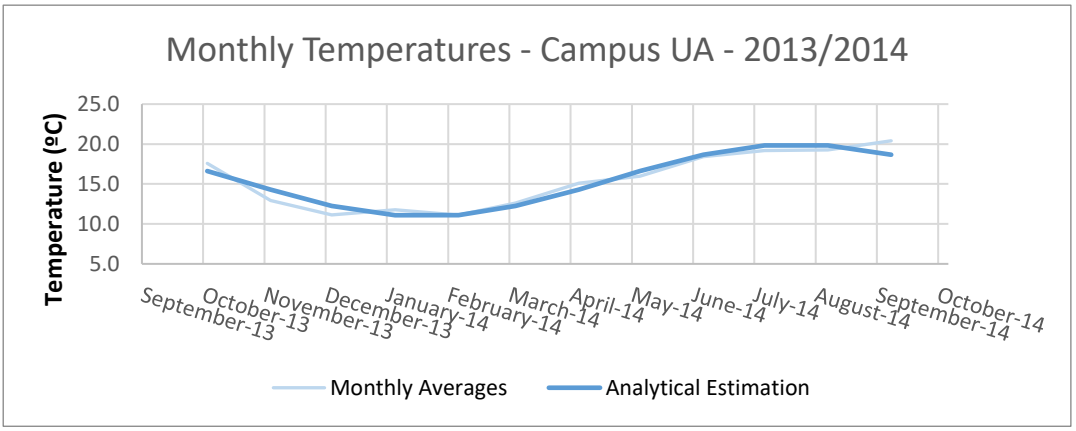

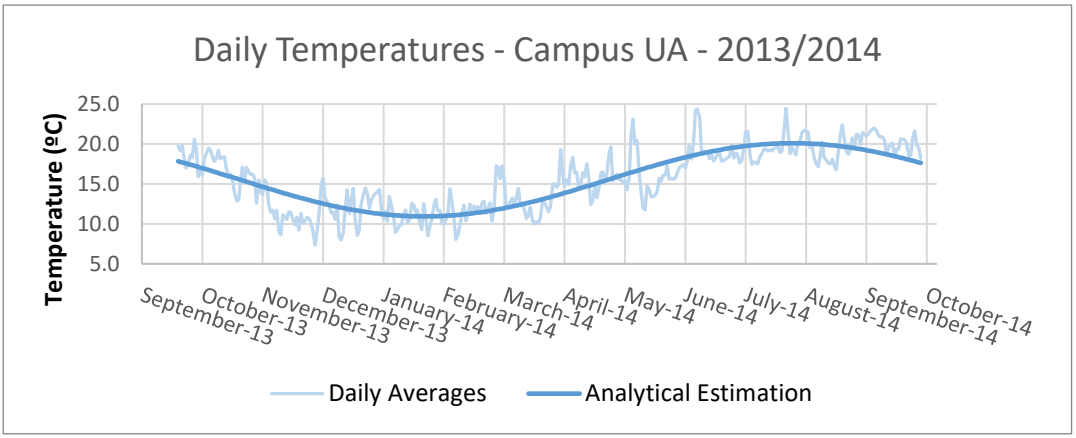

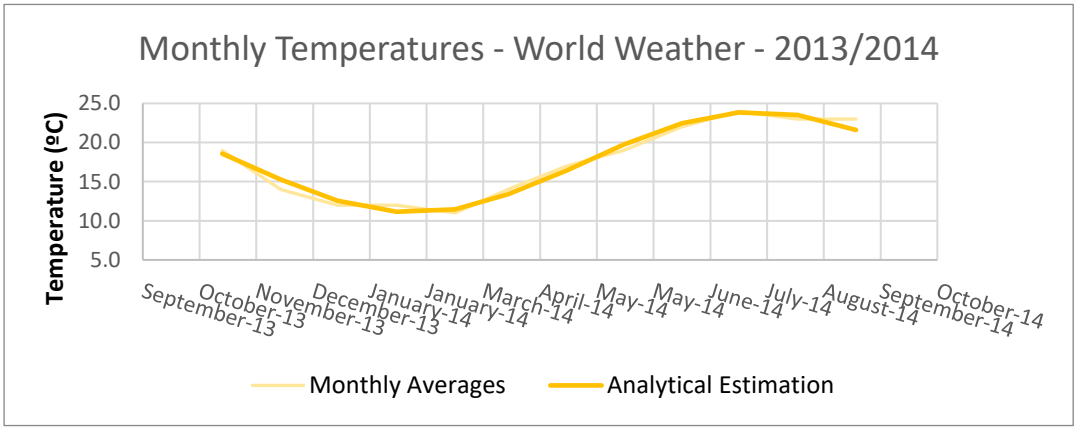

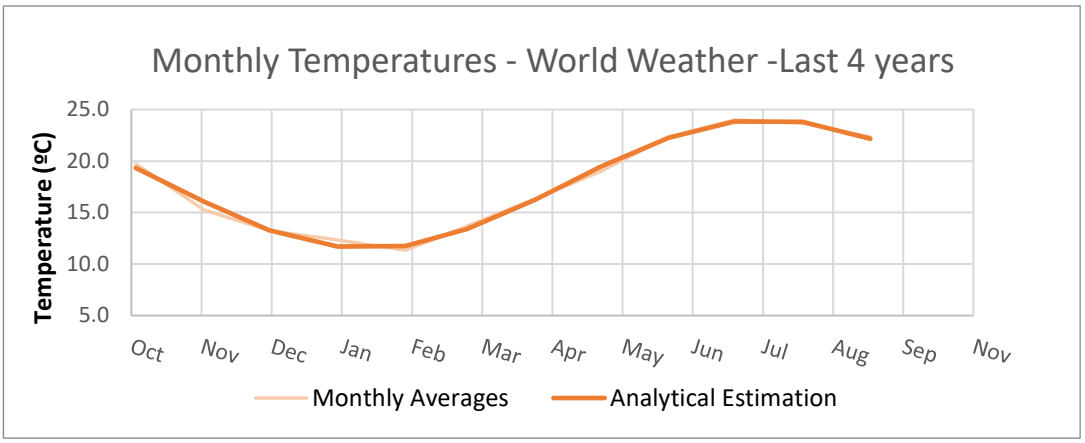
Monthly Temperatures - World Weather -Last 4 years
Temperature (ºC)
25.0
20.0
15.0
10.0
5.0
Oct
Nov
Dec
Jan
Feb
Mar
Apr
May
Jun
Jul
Aug
Sep
Nov
Monthly Averages
Analytical Estimation

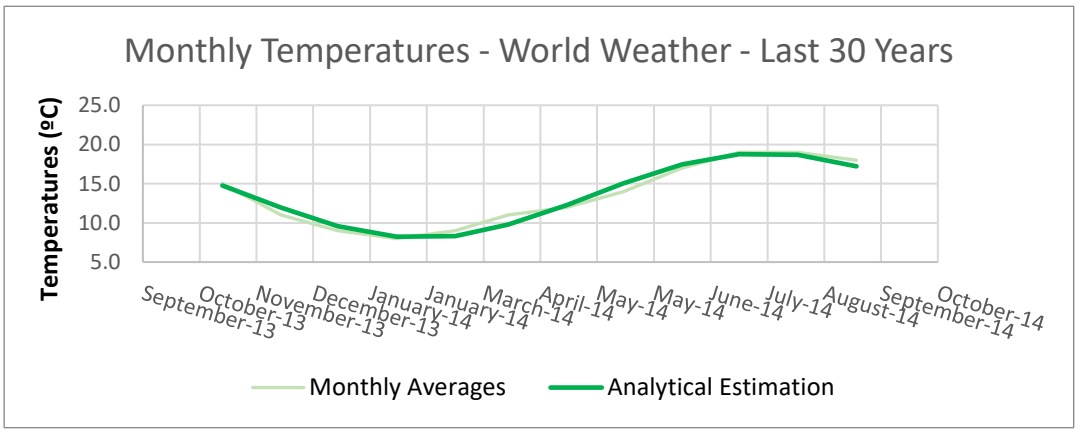
Monthly Temperatures - World Weather - Last 30 Years
Temperatures (ºC)
25.0
20.0
15.0
10.0
5.0
September-13
October-13
November-13
December-13
January-14
January-14
March-14
April-14
May-14
May-14
June-14
July-14
August-14
September-14
October-14
Monthly Averages
Analytical Estimation

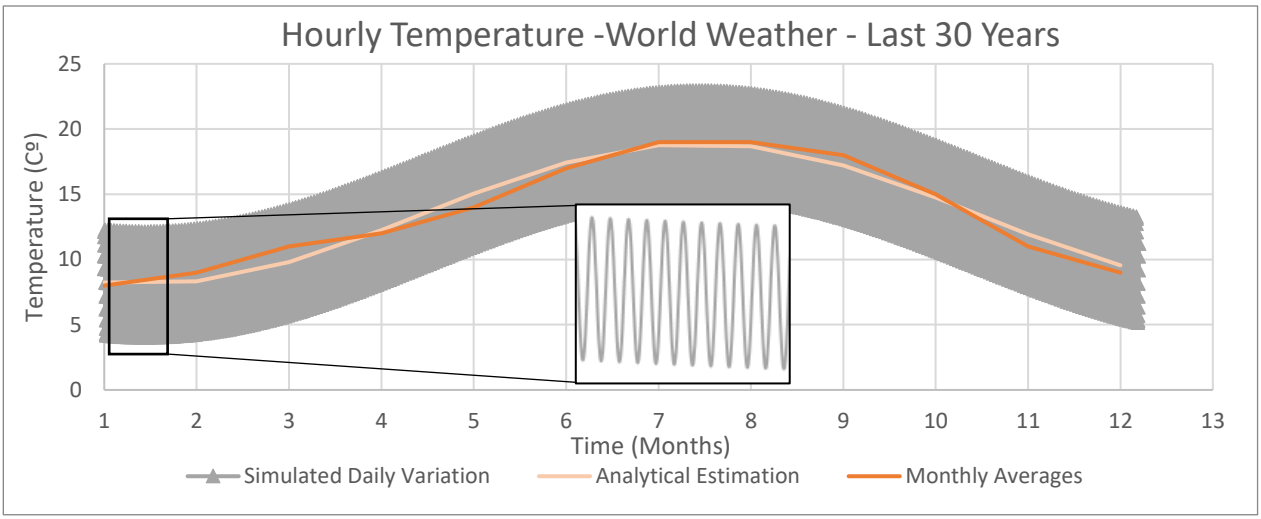
Hourly Temperature -World Weather - Last 30 Years
Temperature (Cº)
25
20
15
10
5
0
1
2
3
4
5
6
7
8
9
10
11
12
13
Time (Months)
Simulated Daily Variation
Analytical Estimation
Monthly Averages

Annex D- Grid used in situation 1 and 2 of the numerical analysis (bottom) and situation 3 (top)